AD-A169 788 MEDIUM-FREQUENCY DATA LINK FOR DIFFERENTIAL NAVSTAR/GPS 1/1
BROADCASTS(U) BOSTON UNIV MA DEPT OF ELECTRICAL
COMPUTER AND SYSTEMS ENGINE.. P K ENGE ET AL. JUN 86
UNCLASSIFIED DOT-TSC-CG-86-1 DTRS57-85-C-00091 F/G 17/7 NL

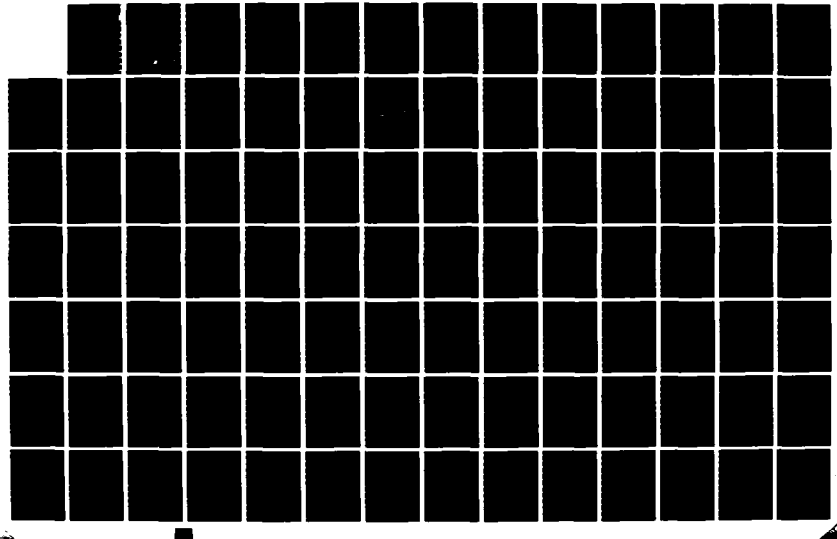

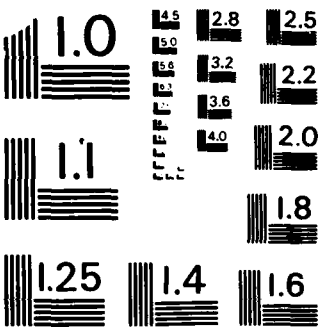

MICROCOPY RESOLUTION TEST CHART

NATIONAL BUREAU OF STANDARDS - 1963 - A

DOT-CG-N-02-86
DOT-TSC-CG-86-1

(12)

Medium-Frequency Data Link for Differential NAVSTAR/GPS Broadcasts

Boston University
Department of Electrical, Computer and
Systems Engineering
110 Cummington Street
Boston, MA 02215

June 1986
Final Report

U.S. Department
of Transportation
United States
Coast Guard

Office of Navigation
Radionavigation Division
Washington DC 20593

Technical Report Documentation Page

1. Report No.	2. Government Accession No.	3. Recipient's Catalog No.
DOT-CG-N-02-86		

4. Title and Subtitle	5. Report Date
MEDIUM-FREQUENCY DATA LINK FOR DIFFERENTIAL NAVSTAR/GPS BROADCASTS	June 1986
	6. Performing Organization Code: DTS-52
7. Author(s): Per K. Enge, Michael F. Ruane, and Lee Sheynblatt	8. Performing Organization Report No.: DOT-TSC-CG-86-1
9. Performing Organization Name and Address: Boston University* Department of Electrical, Computer and Systems Engineering 110 Cummington Street Boston, MA 02215	10. Work Unit No. (TRAIS): CG672/B6013
	11. Contract or Grant No.: DTRS-57-85-C-00091
12. Sponsoring Agency Name and Address: U.S Department of Transportation United States Coast Guard Office of Navigation Washington, DC 20593	13. Type of Report and Period Covered: Final Report September 1985 - April 1986
	14. Sponsoring Agency Code: NRN-2

15. Supplementary Notes

*Under contract to: U.S. Department of Transportation
Research and Special Programs Administration
Transportation Systems Center
Cambridge, MA 02142

16. Abstract

Differential GPS must communicate differential corrections to civilian users of the Global Positioning System. Modulation of existing marine radiobeacons can provide the needed communication link for DGPS, provided the operation of existing radiobeacon direction finding equipment is maintained and adequate DGPS range is provided in the presence of atmospheric noise and skywave fading. Existing DF and ADF units were studied through a manufacturers' survey, and a radiobeacon modulation scheme has been proposed that maintains reliable DF and ADF operation. MSK modulation with a frequency offset of 325 Hz is recommended, with a power offset of -3dB. This scheme limits ADF bearing errors to under 3° based on analysis of the modulation energy entering the effective passbands of the various ADF designs. CCIR data on atmospheric noise and multipath were studied and a rate 1/2 convolutional code with constraint length 6 is recommended to provide a DGPS bit error probability of less than 10^{-5}. Reliable DGPS range for 10 nautical mile beacons will be 100 km, and for 30 nm beacons, 195 km. Discussion of interleaving to control atmospheric burst noise is included.

17. Key Words	18. Distribution Statement
Data Link, Differential GPS, Global Positioning System (GPS), Ground Wave Propagation, Marine Navigation, Medium Frequency, Radiobeacon, Radio Direction-Finding, Sky Wave Propagation	DOCUMENT IS AVAILABLE TO THE PUBLIC THROUGH THE NATIONAL TECHNICAL INFORMATION SERVICE, SPRINGFIELD, VIRGINIA 22161

19. Security Classif. (of this report)	20. Security Classif. (of this page)	21. No. of Pages	22. Price
UNCLASSIFIED	UNCLASSIFIED	96	

Form DOT F 1700.7 (8-72) Reproduction of completed page authorized

PREFACE

The work described in this report was performed under the University Research Program of the U.S. Department of Transportation. The Center for Navigation of the Transportation Systems Center directed the work, which was performed at Boston University's Department of Electrical, Computer and Systems Engineering. Funds were provided by the Radionavigation Division of the Office of Navigation, USCG, under the direction of LCDR Eric Erickson. This is the final report on Technical Task 1.

The authors wish to thank Rudy Kalafus and John Kraemer of the Transportation Systems Center for their encouragement and guidance. John Quill of the USCG Office of Research and Development, and David Pietrazewski, of the USCG Research and Development Center, provided helpful comments and suggestions throughout this effort. We also appreciate the cooperation of the technical representatives of the many manufacturers who provided information on their ADF hardware.

METRIC CONVERSION FACTORS

Approximate Conversions to Metric Measures

Symbol	When You Know	Multiply by	To Find	Symbol
LENGTH				
in	inches	*2.5	centimeters	cm
ft	feet	30	centimeters	cm
yd	yards	0.9	meters	m
mi	miles	1.6	kilometers	km
AREA				
in^2	square inches	6.5	square centimeters	cm^2
ft^2	square feet	0.09	square meters	m^2
yd^2	square yards	0.8	square meters	m^2
mi^2	square miles	2.6	square kilometers	km^2
	acres	0.4	hectares	ha
MASS (weight)				
oz	ounces	28	grams	g
lb	pounds	0.45	kilograms	kg
	short tons (2000 lb)	0.9	tonnes	t
VOLUME				
tsp	teaspoons	5	milliliters	ml
Tbsp	tablespoons	15	milliliters	ml
fl oz	fluid ounces	30	milliliters	ml
c	cups	0.24	liters	l
pt	pints	0.47	liters	l
qt	quarts	0.96	liters	l
gal	gallons	3.8	liters	l
ft^3	cubic feet	0.03	cubic meters	m^3
yd^3	cubic yards	0.76	cubic meters	m^3
TEMPERATURE (exact)				
°F	Fahrenheit temperature	5/9 (after subtracting 32)	Celsius temperature	°C

*1 in. = 2.54 cm (exactly). For other exact conversions and more detail tables see NBS Misc. Publ. 286, Units of Weight and Measures. Price $2.25 SD Catalog No. C13 10 286.

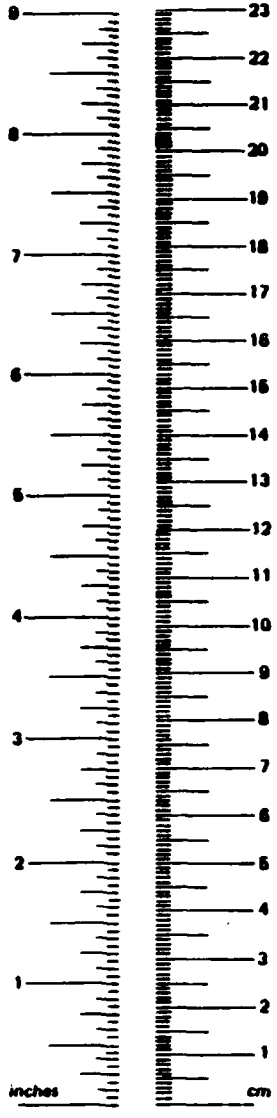

Approximate Conversions from Metric Measures

Symbol	When You Know	Multiply by	To Find	Symbol
LENGTH				
mm	millimeters	0.04	inches	in
cm	centimeters	0.4	inches	in
m	meters	3.3	feet	ft
m	meters	1.1	yards	yd
km	kilometers	0.6	miles	mi
AREA				
cm^2	square centimeters	0.16	square inches	in^2
m^2	square meters	1.2	square yards	yd^2
km^2	square kilometers	0.4	square miles	mi^2
ha	hectares (10,000 m^2)	2.5	acres	
MASS (weight)				
g	grams	0.035	ounces	oz
kg	kilograms	2.2	pounds	lb
t	tonnes (1000 kg)	1.1	short tons	
VOLUME				
ml	milliliters	0.03	fluid ounces	fl oz
l	liters	2.1	pints	pt
l	liters	1.06	quarts	qt
l	liters	0.26	gallons	gal
m^3	cubic meters	36	cubic feet	ft^3
m^3	cubic meters	1.3	cubic yards	yd^3
TEMPERATURE (exact)				
°C	Celsius temperature	9/5 (then add 32)	Fahrenheit temperature	°F

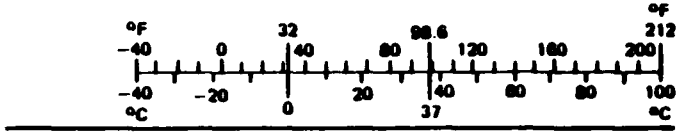

A1

Contents

List of Figures

List of Tables

Chapter 1

Introduction and Summary

The objective of Technical Task No. 1 is to develop a marine-beacon based network for the communication of navigation related data to civilian users of the Global Positioning System (GPS). GPS is a worldwide satellite-based navigation system, currently being developed by the U.S. Department of Defense. It will include at least 18 satellites, all of which will broadcast ranging signals for many user communities. The accuracy of any user's position determination will be limited by the various error mechanisms which limit the accuracy of the range measurement. Some of these errors vary very quickly with time or space and cannot be treated with "differential" techniques. However, some vary rather slowly with time and space and can therefore be reduced by using a technique known as differential GPS (DGPS). Such errors include unmodelled ionospheric delay and "selective availability", which is introduced intentionally for the purpose of national defense.

A DGPS system includes a local reference station which uses a high quality GPS receiver to continuously measure range to all satellites in view. Since the reference station is fixed and its location has been surveyed, all slowly varying errors can be measured. Corrections for these errors can then be communicated via some suitable link to local users and these users can remove the errors from their range estimates. This procedure will improve the position fixing accuracy of the public GPS service from 100 meters to better than 20 meters.

Several communication links have been considered for the DGPS data. One proposed link adds a digitally modulated subcarrier to existing transmitters in the marine radiobeacon network. The frequency of the subcarrier is 0 to 500 Hz above the beacon's main carrier and the DGPS information is applied using either MSK or FSK modulation. This approach is attractive for the following reasons:

- A well located and widespread radiobeacon network is already in place, which means substantial site and equipment costs can be avoided.

- The frequency of the radiobeacons is 285-300 kHz, which means user equipment is extremely inexpensive to realize.

- The radiobeacon transmitters will probably accept a subcarrier fairly readily.

The two most important questions concerning the proposed Radiobeacon-DGPS network are:

- Is it possible to digitally modulate a beacon subcarrier and cause no interference to the direction finding (DF) equipment, which currently uses the beacon signal?

- How will atmospheric noise and skywave limit the range to which the DGPS message can be reliably communicated?

These two questions are treated in the two subtasks, which comprise Technical Task No. 1. Subtask No. 1 is entitled *Modulation* and and Subtask No. 2 is entitled *Atmospheric Noise and Multipath Effects* and we now summarize the approach and results of these Subtasks.

Subtask No. 1 had the following components:

- Definition of candidate modulation schemes.

- Survey of manufacturers of direction finding equipment and development of interference models for a wide variety of direction finders.

- Interference analysis and recommendation of DGPS subcarrier modulation scheme.

The candidate modulation schemes have the following variables. The power in the DGPS subcarrier relative to the main carrier power can be varied and we consider power offsets of -3dB and -6dB. The frequency difference between the DGPS subcarrier and the main carrier can be varied and we consider "offsets" between 0 and 500 Hz. The DGPS modulation scheme can be optimized and we consider minimum shift keying (MSK) and frequency shift keying (FSK). More specifically, the candidate FSK scheme is continous phase FSK (CPFSK) with a modulation index of 1. Error detecting and correcting codes (EDAC) may be employed. We compare the interference performance of "rate 2/3" coding and "rate 1/2" coding. (The use of coding was originally motivated by the channel noise, but it also reduces interference.)

Over 110 manufacturers of direction finders were contacted. This effort revealed that the more complicated automatic direction finders (ADFs) are much more vulnerable to interference than the manual direction finders. Eventually, 16 different manufacturers responded with enough information to develop interference models for 20 ADFs.

Based on the analysis of these ADFs, MSK modulation with a frequency offset of 325 Hz is recommended. Additionally, a power offset of -3dB, a rate 1/2 error detecting and correction code are recommended.

A frequency offset of 325Hz is required to move the DGPS signal energy away from the "passbands" of the ADFs studied. A frequency offset of 0 Hz is not recommended for 3 reasons. First of all, some aviation ADFs use coherent detection and these detectors develop a coherent reference by phase tracking the radio beacon carrier. DGPS energy at 0 Hz could introduce unacceptably large levels of phase jitter at the phase lock loop output. Secondly, the DGPS bandwidth is relatively wide (even if MSK modulation is used) and could interfere with the operation of ADFs having small switching frequencies. (Switching signals are explained in Chapter 2.) Finally, the ADF switching signals will modulate DGPS at 0Hz directly into the passbands of the detectors. This will produce unacceptably large noise in the bearing estimates.

A frequency offset of 325Hz does not yield appreciable DGPS interference from the neighbor beacons, because of the 15 dB protection ratio. The rate 1/2 error correcting code "spreads" the spectrum of the DGPS signal relative to all ADF passbands and hence reduces interference effects. The error correcting code also greatly increases the DGPS range as discussed below. CPFSK cannot be used even though it spreads the DGPS energy over a wider spectrum. CPFSK has 2/3 of its energy at two discrete frequencies, and can produce severe bearing errors whenever the discrete frequencies enter an ADF passband.

Subtask No. 2 studies the effect of atmospheric noise and multipath on the performance of the DGPS link. Atmospheric noise and skywave (MF multipath) are described in CCIR Reports and this information was stored in a computer data base for use in analysis. Atmospheric noise is impulsive and therefore motivates the combined use of limiting or clipping in the receiver and error detecting and correcting (EDAC) codes. The probability of DGPS bit error ($Pr(\epsilon)$) is computed for such receivers and a variety of codes. These curves reveal that significant performance improvements are achieved if codes of moderate complexity are used. Specifically, convolutional codes of rates 1/2 and 2/3 are analyzed. These codes both have constraint lengths (v) of 6, where constraint length roughly measures decoder complexity and data latency. The signal to noise ratio required for $Pr(\epsilon) \leq 10^{-5}$ is 31, 12 and 6 dB for uncoded, rate 2/3-coded, and rate 1/2-coded systems, respectively.

Probability of link availability is defined as the probability that the SNR required for $Pr(\epsilon) \leq 10^{-5}$ will be achieved. The atmospheric noise and skywave data bases were used to compute $Pr(\textit{link available})$ as a function of range away from the beacon. The following results were obtained for the noisiest time block in Boston, Massachusetts. A link without coding and with a 30 nautical mile beacon will be available with probability .9 if the user

range is less than 15 kilometers. A link without coding and with a 10 nautical mile beacon will be available with probability .9 if the range is less than 10 kilometers. However, if the rate 1 2, v=6 code is used with the 30 nautical mile beacon, then the range will be 195 kilometers. If the same code is used with a 10 nautical mile beacon, then the range will be 100 kilometers. Clearly, EDAC codes not only reduce interference effects, but they also substantially increase the reliable DGPS signalling range.

The last part of Subtask 2 begins the study of channel memory effects. Atmospheric noise occurs in bursts and consequently the performance analysis described above is not valid unless interleaving is used. Interleaving prevents a single atmospheric burst from affecting more than one code symbol from any group of symbols, which are decoded together. However, it also introduces delay, and data latency greater than a few seconds cannot be tolerated in the DGPS link. The data latency is a function of code rate, code constraint length, decoder used, and the design value of atmospheric burst duration. If the rate $1/2$, $v = 6$ code described above is used with an interleaver and a Viterbi decoder, then the delay will be 12 seconds. Similarly, the rate $2/3$, $v = 6$ code suffers a delay of 14 seconds. Several alternatives exist to reduce delay. These will be investigated in Technical Task No. 2.

The remainder of this Report is organized as follows. Chapter 2 reports on Subtask 1: *Modulation* and Chapter 3 reports on Subtask 2: *Atmospheric Noise and Multipath Effects.*

Chapter 2

Modulation Scheme

2.1 Modulating Radiobeacons for DGPS

In this section, we evaluate the impact of various DGPS modulation schemes on the performance of existing DF equipment. Key assumptions underlying the analysis are presented first, followed by possible alternative modulation schemes. The status of DF and automatic direction finding (ADF) equipment will be considered next, based upon a survey of manufacturers of both marine and aeronautical units. It is argued that manual DF units are insensitive to DGPS modulation and we concentrate on a taxonomy of ADF technologies. Finally a general analysis method is described that yields the parameters required for DGPS modulation to ensure aceptable DF service by a given class of ADF receivers. Based on these requirements, the following recommendations are made:

- Modulation should be MSK.
- DGPS carrier offset should be 325 Hz.
- DGPS amplitude should be -3dB from the main carrier.
- A rate 1/2 error correcting code should be incorporated.

2.2 Key Assumptions

In the absence of a program of bench testing, and faced with limited details about many ADF units, a model-based analysis of interference effects was performed. To ensure that degradation of service would be detected in such an analysis, a number of conservative, worst-case assumptions were employed. This allowed recommedations to be based on ADF designs most sensitive to DGPS interference, even if the complete description of such units was unavailable.

Steady state linearized models were used, even though many ADFs are known to employ clippers and or limiters. Dynamic issues like acquisition and lock-in on beacons in the presence of DGPS noise were not treated quantitatively. Bearing error is assumed to be determined primarily by the average DGPS power entering the bearing detector of the ADF unit.

In order to maximize potential interference in our analysis, two assumptions concerning adjacent beacons are made. First of all, we assume that an adjacent beacon produces a received power 15dB below that of the beacon of interest. In the USA, where minimum spacing of radiobeacon frequency assignments is 1000Hz, physically adjacent beacons usually have more than 1000Hz spacing and are guaranteed to have at least 15dB of protection. The second assumption concerns the geometry of adjacent beacons. Bearing to an adjacent beacon is taken to be 90° from bearing to the desired beacon, because this gives worst case interference when the direction finder under consideration is near its correct orientation.

Most importantly, in the face of uncertainty about detailed nonlinear ADF operation, we seek a DGPS modulation scheme that minimizes interference by separating DGPS power from the ADF receiver passbands.

2.3 Candidate Modulation Schemes

DGPS modulation schemes can be described by specifying the method of modulation, the offset of the subcarrier frequency, the DGPS protection ratio, and the symbol rate of the channel. A typical candidate design might be Minimum Shift Keying (MSK) modulation, an offset of 100Hz, a DGPS protection ratio of 3 dB, and a channel rate of 75 symbols per second. Because of their spectral efficiency, two particular modulation methods were considered in detail, MSK and Continuous Phase Frequency Shift Keying (CPFSK).

MSK [15] [16] [17] is a subset of the class of digital modulation techniques called CPFSK. In simple Frequency Shift Keying (FSK), '1' and '0' are represented by frequencies $f_1 = f_c + \Delta f$ and $f_0 = f_c - \Delta f$. When, for B = symbol rate, the modulation ratio, $m = (f_1 - f_o)/B = 2\Delta f/B$ is integer, FSK makes smooth phase transitions at the bit edge and its spectrum becomes narrower. Cases with $m = integer$ are called CPFSK. The special case of $m = 0.5$ yields MSK which is the continuous phase FSK modulation scheme with minimum bandwidth. In MSK, signal phase motion describes the bit; forward motion by 90° in one bit duration is a '1' and 90° backward motion is a '0'.

Advantages of MSK include extremely low sidebands, constant signal power and compatibility with simple receivers. CPFSK(m=1) shares these characteristics but has a wider spectrum than MSK. CPFSK also contains two discrete frequency components at $\pm\Delta f$, each of which contains one-third of the total energy. [19] Other FSK schemes for higher

m or for non-integer m have even boader spectra than MSK or CPFSK(m=1) but offer possible receiver cost differentials. These cost advantages are already small in comparison with total unit costs, and are expected to disappear by the time GPS becomes operational. Other classes of modulation such as QPSK, or PSK have broader spectra as well. PSD's of MSK and CPFSK(m=1) are shown in Figures 2.1 and 2.2 for symbol rates of 75 and 100.

A bit rate of 50 bps is required for the DGPS signal, but error detection and correcting codes will increase the channel symbol rate to 75 or 100 symbols per second. The PSD's in Figures 2.1 and 2.2 are normalized to 1 to show the relative spreading of CPFSK compared to MSK, and to show the spreading due to increasing the symbol rate. In addition, note the discrete components in CPFSK at $f_d = B/2$.

The DGPS protection ratio is the ratio of radiated DGPS power compared to radiated beacon carrier power. DGPS protection ratios of -3dB and -6dB are considered.

An adjacent beacon having DGPS modulation is assumed, giving rise to Figure 2.3. As shown, the carriers are separated by 1000Hz, the minimum USA spacing, and the adjacent beacon is 15dB below the beacon being used for bearing. Each has an MSK modulated signal offset by the subcarrier and 3dB down from the carrier. The adjacent beacon DGPS is therefore at -18dB. In Europe, beacon spacing of 500Hz has been proposed.

The general nature of interference possibilities can be explained from Figure 2.3. There can be self-beacon or adjacent beacon interference. Self-beacon interference arises because ADF operation depends on detection of signals in sidebands located within a few hundred Hz of the beacon carrier. With small offset, f_{DGPS}, the DGPS spectrum overlaps and corrupts signals near the carrier. A narrower DGPS spectrum delays the onset of interference as f_{DGPS} decreases, but eventually some f_{DGPS} is reached with substantial DGPS energy reaching the ADF.

Increasing f_{DGPS} avoids these problems for self-beacon interference but simultaneously moves the DGPS spectrum of the adjacent beacon towards its higher frequency neighboring beacon. If f_{DGPS} becomes too large, adjacent beacon DGPS power will reach the ADF. The narrowness of the DGPS spectrum and the protection ratios for DGPS and adjacent beacons limit the interference effects.

Table 2.1 below summarizes the modulation scheme parameters that were analyzed.

2.4 Manual DF User Equipment

Manual DF equipment is quite similar to the ADF equipment described in the next section. Rather than automatically finding the bearing, manual DF equipment instead produces an audible tone or meter display whose magnitude indicates bearing error. The user manually

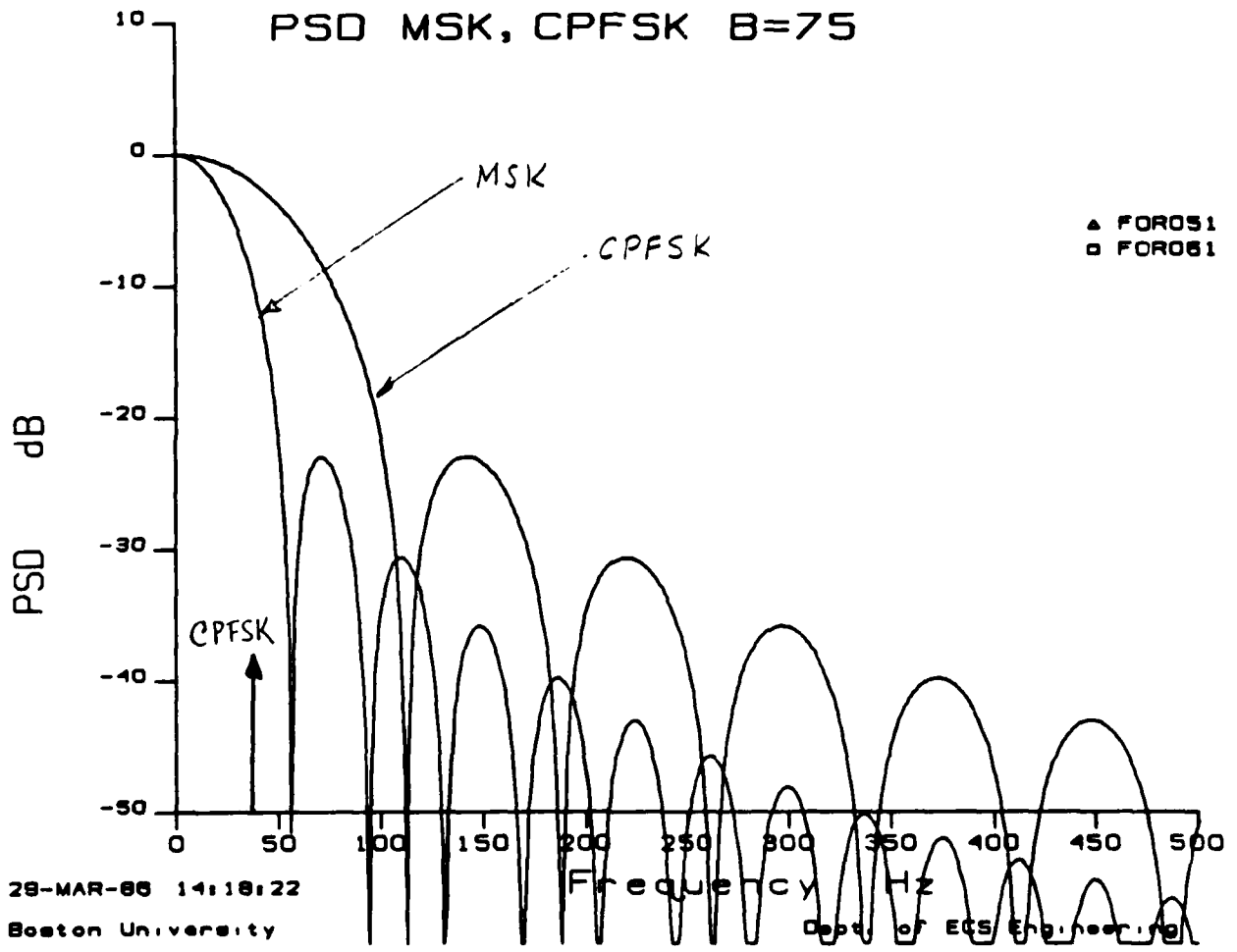

Figure 2.1: Power Spectral Densities at B=75

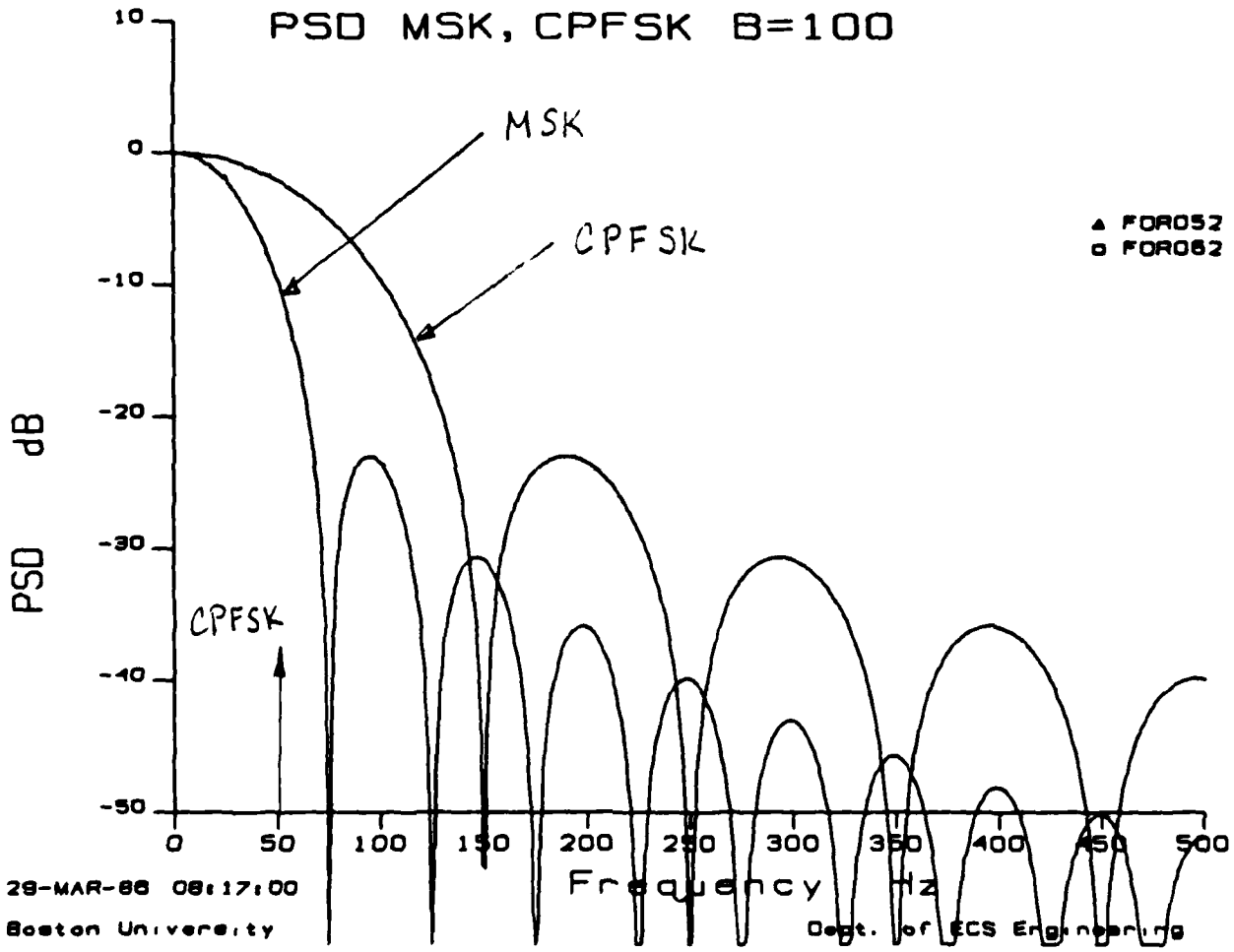

Figure 2.2: Power Spectral Densities at B=100

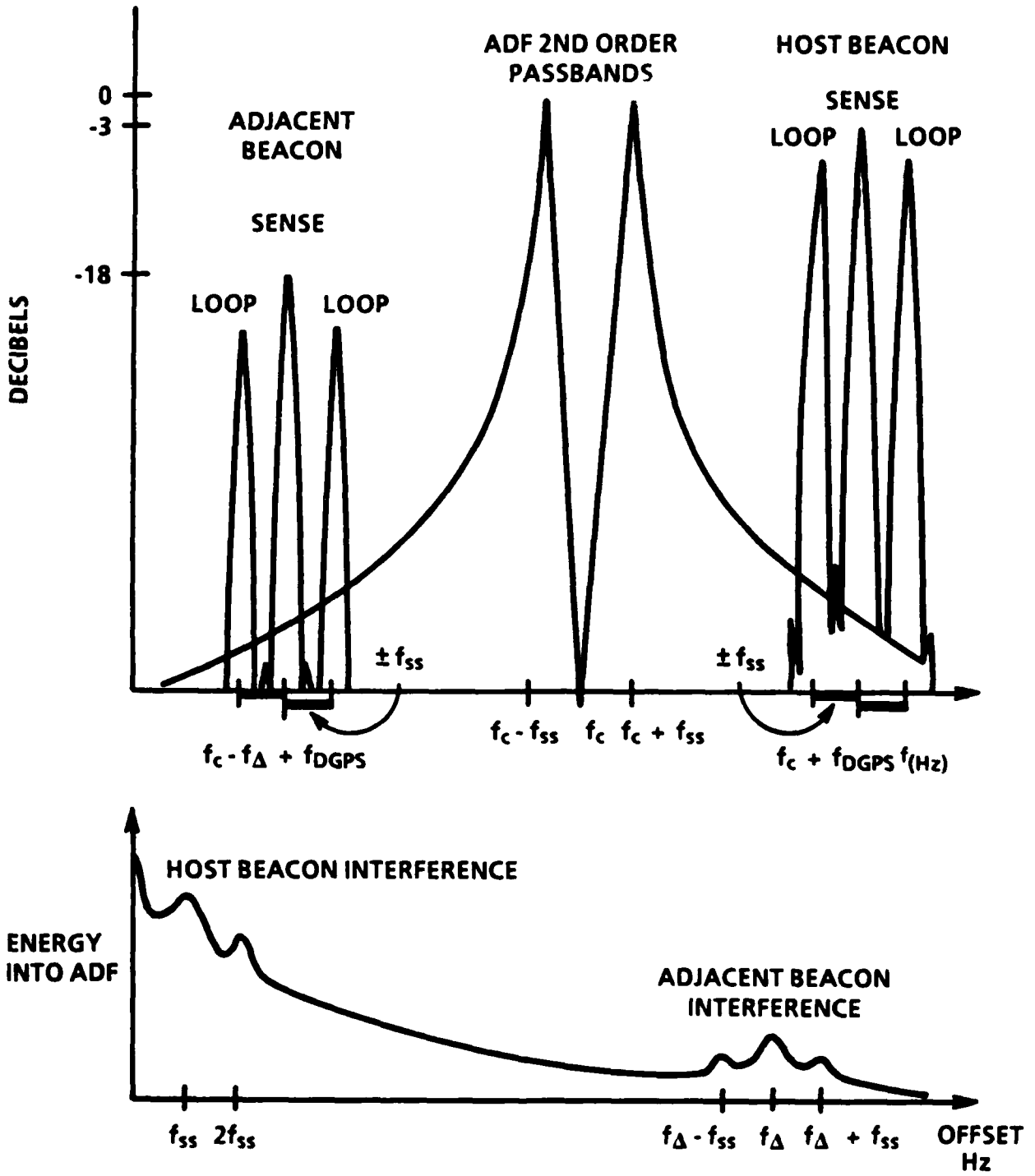

Figure 2.3: Beacon Carriers and DGPS

Table 2.1: Modulation Variables

DESIGN CHOICE	OPTIONS CONSIDERED
Type of Modulation	MSK or CPFSK(M=1)
DGPS Protection Ratio	-3dB
Adjacent Beacon Protection Ratio	-15dB
Adjacent DGPS Protection Ratio	-18dB
Adjacent Beacon Spacing	1000 and 500
Offset of DGPS (f_{DGPS})	0 to 500 Hz
Error Correcting Codes	rate 1/2 or rate 2/3

rotates the antenna until a null is reached and the tone disappears.

Interference from DGPS will appear in a manual DF unit as modulation of the tone or meter signal. The overall function of the unit will not change although a true aural null might be impossible with DGPS noise being present. While experienced users may notice the different sound of their DF, DGPS is not expected to contribute to bearing error except in weak signal regions where it might be difficult to detect the aural null of the beacon compared to the DGPS noise. Because of DGPS's expected minor impact on manual DF performance, and the difficulty of assessing that impact quantitatively in a technology strongly dependent on user experience, we conclude that manual DF interference will not determine the design of the DGPS *modulation scheme*. Manual DF's will not be considered further.

2.5 Characterization of ADF User Equipment

Over 110 companies that were possible marine or aeronautical ADF manufacturers and distributers were contacted. Of the original list, 16 companies claimed to be active independent suppliers of ADF equipment in the radiobeacon band. These were contacted a second time with a detailed request for information about their units. Only 14 offered ADFs (the other two had only manual units), and information was received for 20 different models. We estimate, from indirect references in sales materials, that at least another 5 or 6 models are offered by these companies, but no information was provided on those units.

The quality of the information varied greatly. Several companies provided technical manuals with block diagrams, theory of operation, and schematics. Others provided instuction booklets intended for non-technical users. A few supplied only data sheets and promotional descriptions. One company responded with a brief letter mentioning that they offer several ADFs, but provided no documentation or descriptions. Finally, a few companies forwarded our detailed requests to overseas engineering offices in Europe and

Japan and their replies have yet to arrive.

Despite this uneven response, a great deal of information was received on a variety of units, and it is still possible to characterize ADF technology in a conservative fashion and proceed with an interference analysis. The generic structure of ADFs will be described first, followed by a summary of the survey results.

2.5.1 ADF Generic Block Diagram

ADF characteristics that affect interference performance are shown in Figure 2.4 and can be listed as:

1. Loop and Sense Antennas
2. RF/IF Stages
3. Detector
4. Switching Filter
5. Servo or Display Filter

2.5.2 Antenna Configuration

The antenna block usually contains a directional antenna (Loop), an omnidirectional antenna (Sense), and a switching signal circuit at switching signal frequency f_{SS}. The function of this block is to receive the beacon signal and provide an output to the ADF that will allow bearing to be resolved without ambiguities. The directional antenna usually is a simple ferrite rod, or a pair of fixed crossed loops (Bellini-Tossi). Loop and ferrite antennas exhibit sharp nulls, but contain a 180° ambiguity. Therefore the omnidirectional sense antenna is used, at least occasionally, to resolve the ambiguity by establishing a phase reference with the loop signal. Some ADFs, particularly avionics units, derive a sense signal from the loop outputs, thus avoiding the sense antenna. Various schemes are used to mix the sense and loop signals using the switching signal. Usually the loop signal is multiplied by the switching signal (although a few units switch the sense) before the signals are mixed and passed to the RF/IF stages. This multiplication creates sidebands which contain the actual bearing information.

An antenna configuration belongs to one of two classes, depending on whether the bearing information is stored in the magnitude or phase of the RF/IF signal. Figure 2.5 shows representative antenna configurations that contain bearing information in the phase. In the upper left is a continuously rotating ferrite rod or loop antenna. The motor speed

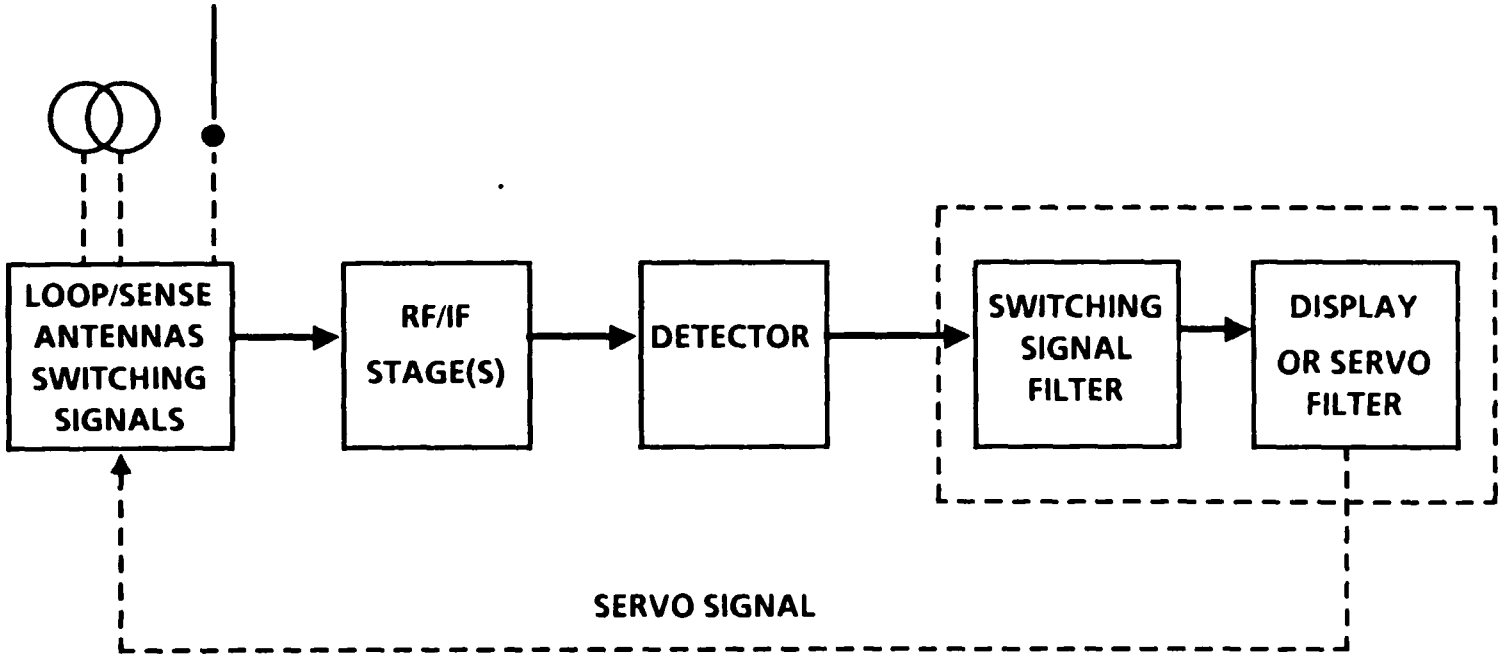

Figure 2.4: Interference Oriented Block Diagram for ADFs

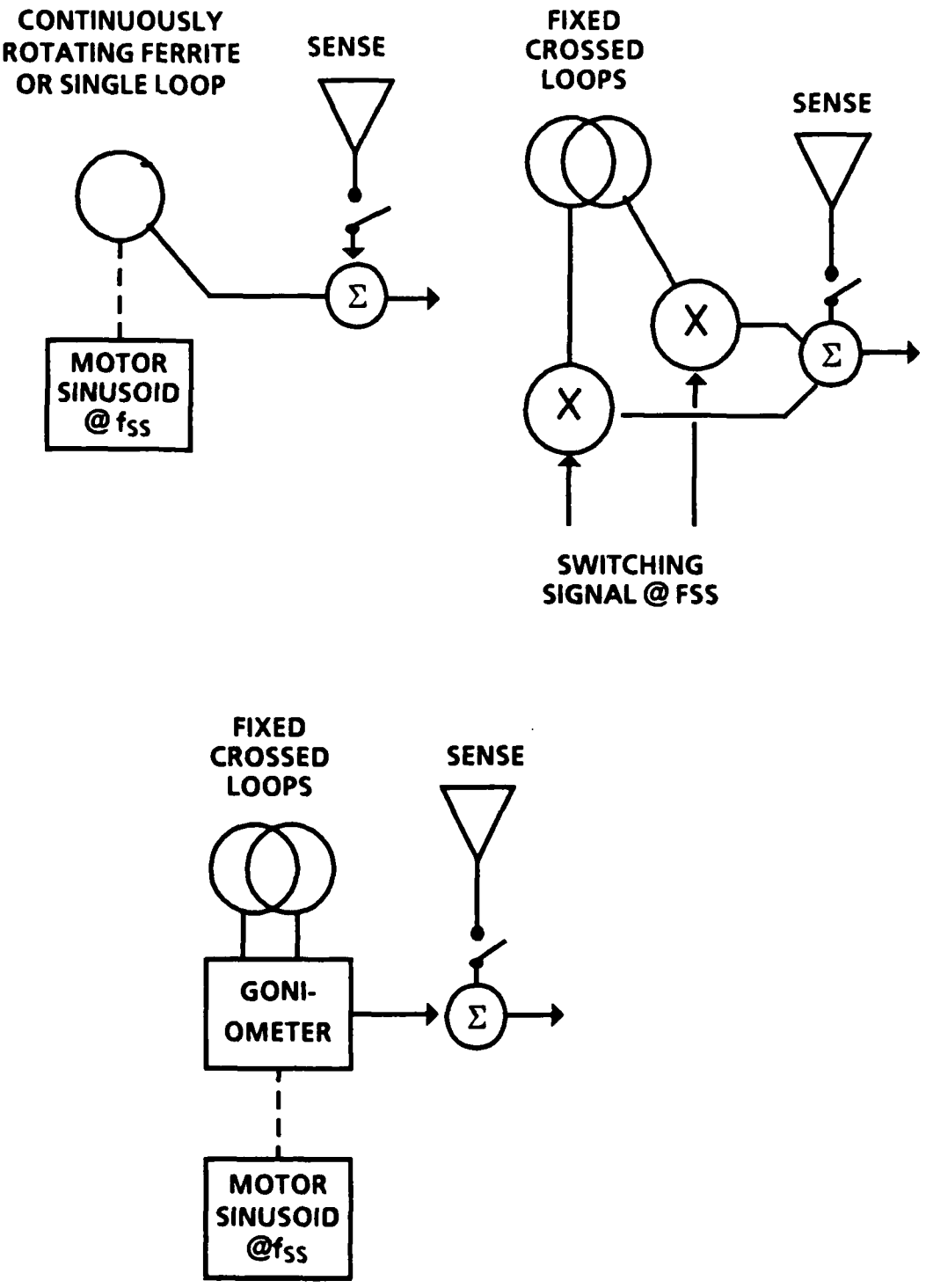

Figure 2.5: Antenna Configurations-Bearing in Phase

determines f_{SS} while the phase ϕ is the angle to the beacon compared to some fixed reference position of the rod, e.g. the ship's centerline. Here the switching signal is sinusoidal and the signal is of the form $\cos(2\pi f_{SS}t - \phi)$. The upper right design uses fixed crossed loops, with each loop output, $\cos\phi$ and $\sin\phi$, being multiplied by quadrature switching signals, $\cos(2\pi f_{SS}t)$ and $\sin(2\pi f_{SS}t)$. Once again the signal is of the form $\cos(2\pi f_{SS}t + \phi)$. In the lower example, the goniometer serves to recreate the field configuration at the antenna within the goniometer coils. A rotating search coil within the goniometer functions just like the rotating ferrite rod or loop, but has the advantage of allowing fixed antenna equipment. The signal f_{SS} is determined by the motor speed. In all these examples, the sense antenna is switched on when ambiguity must be resolved. Note that all these signals are modulating the carrier, and will appear as sidebands offset by f_{SS}.

Figure 2.6 shows antenna configurations where bearing information is carried by the magnitude. At the left a fixed crossed loop antenna and goniometer are used to recreate the beacon field in the search coil. Letting ϕ be the bearing angle error in this system, the search coil determines the magnitude of the received carrier according to $A\sin\phi$. The switching signal multiplies the carrier to create sidebands at $\pm f_{SS}$ whose magnitude reflects the bearing error. The sense is usually connected in such systems to resolve the ambiguity. Since loop signals and sense signals are generated by the H and E fields of the received beacon, respectively, the sense is sometimes shifted another 90° and added to the loop signal. The summed signal now varies between 0 (sense and maximum bearing error signal cancel due to 180° phase difference and same amplitude) and A (sense only since loop magnitude goes to 0 at true bearing). The right hand system is similar, except the sense is switched at f_{SS} in addition to phase shifting.

For interference analysis, the key characteristics of an antenna configuration are:

1. Is bearing information in phase or magnitude?
2. Is the sense always connected?
3. Is switching signal applied to loop or sense?
4. Is the switching signal sinusoidal or square?
5. What is f_{SS}?

2.5.3 RF/IF Stages

ADFs employ a variety of designs in their RF and IF stages. Bandlimiting may be done in a number of locations and more than one IF stage is used in some units. Many units are suited for reception of signals from several bands, including commercial broadcast stations,

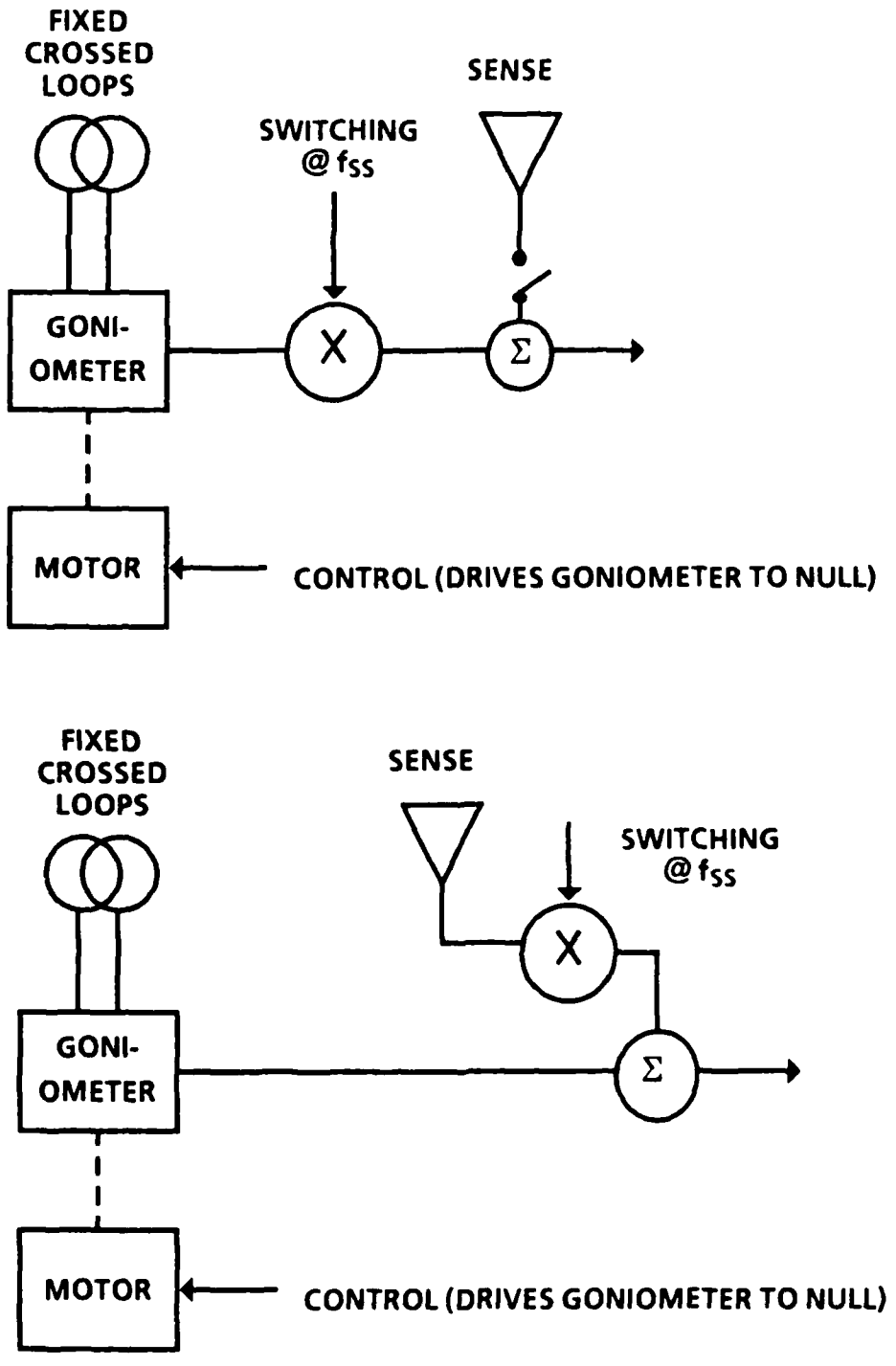

Figure 2.6: Antenna Configurations-Bearing in Amplitude

emergency beacons and aeronautical beacons, and utilize a switchable bandwidth. The most common intermediate frequency was 455kHz.

Our interference analysis only requires knowledge of the overall IF passband. While a few units claimed IF -6dB points of $\pm$1000Hz or less, most fell in the range of $\pm$2kHz to $\pm$4kHz for -6dB points. The -60dB points available were on the order of $\pm$10kHz. Our conclusion is that the RF IF stage will pass all the DGPS energy, and need not be considered in detail.

2.5.4 Detector

The detector block functions to bring the output of the RF/IF stages back to baseband. The detector could be determined in 14 of the ADFs studied; in 10 units a non-coherent AM detector was employed. Four units, all of which were avionics models, used coherent detection.

The non-coherent detectors can be thought of as simple low pass filters that extract the signal at f_{SS} and block higher frequencies. Some protection against DGPS interference would occur here if DGPS is well above the cutoff of the detector. However, most detectors appear to have been designed primarily to eliminate beacon tones or adjacent beacons, and have wide passbands compared to f_{SS}.

Coherent detectors in avionics ADFs relied on phase-locked loops to extract the reference phase from the carrier signal. While these designs provide improved performance at low signal-to-noise levels, they can be vulnerable to several DGPS-induced problems. See Figure 2.7.

The phase-locked loop consists of a mixer that multiplies the incoming signal and the signal of the voltage controlled oscillator. Normally the incoming signal is

$$s(t) = \cos(2\pi f_c t + \theta)$$

where f_c is the beacon carrier. The VCO operates at $\sin(2\pi f_c t + \hat{\theta})$ such that their product is

$$e(t) = \cos(2\pi f_c t + \theta)\sin(2\pi f_c t + \hat{\theta})$$

or

$$e(t) = \frac{1}{2}\sin 2(\hat{\theta} - \theta) + \frac{1}{2}\sin(4\pi f_c t + 2\hat{\theta} + 2\theta)$$

This signal then passes through the low pass filter, eliminating the $2f_c$ term and producing a signal proportional to the phase error, $\hat{\theta} - \theta$. When $\hat{\theta} - \theta$ is small, $\sin(\hat{\theta} - \theta)$ is approximated by $\hat{\theta} - \theta$ and the loop can be analyzed as a linear system. This corresponds to the 'locked' condition. When 'unlocked', the $\sin(\hat{\theta} - \theta)$ term must be considered and a nonlinear system results.

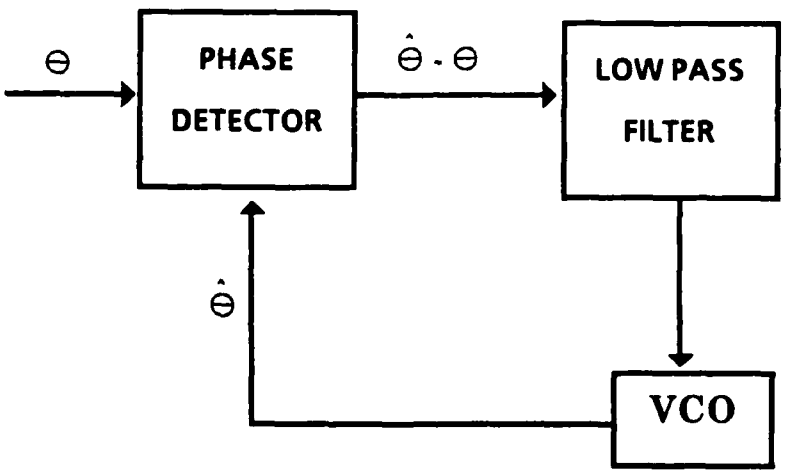

Figure 2.7: Phase Locked Loop Block Diagram

The modulation schemes under consideration use continuous phase changes to represent information, and have the potential to cause false lock or PLL unlock. Unfortunately the available information on ADF PLLs is insufficient to allow a detailed analysis of the nonlinear noise effects of DGPS on the phase estimate. In general, it is extremely difficult to analyze nonlinear PLL operation in the presence of noise, even with detailed knowledge of the PLL design [18]. PLL unlock can best be avoided by locating DGPS far enough from ADF filter passbands to ensure no PLL interference effects.

A false lock could occur if DGPS carrier were mistaken for the carrier of the PLL during pull-in. This would depend on the relative signal levels of DGPS and the beacon carrier and the acquisition characteristics of the PLL. PLLs are specified to have some 'lock-in range' over which they will locate and lock on a signal. For the ADFs we studied, this range was on the order of $\pm$250Hz to $\pm$300Hz. If DGPS were locked, the PLL output would no longer be coherent with the bearing signal and bearing error would result. Two units had 'lock detector' circuits that effectively shut off the ADF function whenever the frequency difference between the oscillator and the RF/IF input exceeded 10Hz. These same units had 100Hz cutoffs on their PLL low pass filter.

Unlock due to a 10Hz difference might occur when DGPS contributed a string of 1's or 0's, producing a progressive phase change. For example, at a bit rate of 100 bps, and 90° shift per bit, a string of similar bits appears as a 25Hz modulation. This 25Hz modulation might create jitter in the bearing estimate, or it might be interpreted as an unlock condition, causing the lock detector to operate. The loop would then try to resynchronize. This situation could cause noticeable jitter in the bearing estimates.

Another PLL unit warned of such jitter when locking on weak stations. That unit controlled the loop antenna from the lock detector. When unlocked, the loop is disabled and the signal is acquired from the sense antenna only. When locked, the loop is enabled so ADF can begin. If, for a weak station, the extra noise introduced by the loop causes unlock, the unit will audibly click on and off as the loop is enabled and disabled repeatedly. The manufacturer suggests tuning another frequency to resolve the problem. No data is available as to the relative signal-to-noise ratio required to prevent this problem.

Key characteristics for interference analysis are

1. Is the detector coherent or non-coherent?
2. What is the bandwidth of coherent loop filter?
3. What is the bandwidth of the non-coherent detector?
4. What is lock-in range for a PLL?

2.5.5 Switching Signal Filter

The next block of the generic ADF system processes the baseband signal from the detector to extract the bearing information contained at the switching signal frequency, f_{SS}. This is the single most important block of the system since it determines the selectivity of the ADF. Six realizations of this filter were observed:

1. LC filter
2. Synchronous filter
3. Microprocessor-based filter
4. Coherent detector at f_{SS}
5. Resolver (2nd goniometer search coil)
6. 2 phase AC induction motor (servomotor)

The first three function as bandpass filters to discriminate against other frequencies. The LC approach was used in the simpler units, although one device both passed f_{SS} and had a notch at its harmonics for servomotor control. Four units had synchronous filters, including one that had an adaptive synchronous filter that detected high noise and narrowed the bandwidth of the filter. The microprocessor system was not documented and has been considered as a high Q ($Q \geq 50$) bandpass filter.

The last three are coherent detectors and respond as if they were also high Q bandpass filters. The simplest coherent detector had a mixer driven by the original f_{SS} oscillator and multiplying the detected signal. After filtering the doubled frequency term, a DC signal proportional to the original phase information was obtained. The resolver unit applied the signal to be detected to the coils of a goniometer rotating at f_{SS}. Signals synchronized to the motor search coil. i.e. those at f_{SS}, are passed, while other frequencies move in and out of phase with the search coil. The largest number of units had some form of servomotor as the switching filter device. Much like the resolver, a servomotor develops torque only for one frequency of input signal, that which corresponds to the frequency of the reference coil. By driving the reference coil with the switching signal, the motor responds only to those frequencies at f_{SS}. The dynamic response of the overall servo system is analyzed in the next section.

The important parameters for the switching filter are:

1. What is the transfer function of switching signal filter?
2. What is the bandwidth?

2.5.6 Servo/Display Filter

The last generic block concerns the display of the bearing information. While conceptually important, this block was the least well described by technical materials on the ADFs, and will be considered part of the switching signal filter.

Generally the bearing is shown by electrical or mechanical displacement of an indicator. Most servos move an arrow or compass card against a reference circle to show bearing with respect to the ship or aircraft centerline. These devices must remove the ambiguity as part of the display. Units with CRT displays create a 'propeller' shape that is oriented in the true bearing direction and at 180° from true bearing. Enabling the sense blocks part of the display and removes ambiguity. Digital readouts gave bearing directly, while LED arrays gave readings to 5° steps around the compass. Claimed bearing accuracies were from $\pm 0.5°$ to over $\pm 5°$.

On most units, the servomotor is used for both switching signal filtering and display. The indicator would be directly attached to the shaft, and the last two blocks of the generic ADF are quite naturally combined. Virtually no data was obtained to allow separation of these functions for servomotors. Similarly, no information was available for characterizing the digital and LED displays. CRT's have no appreciable dynamics in representing the ADF switching filter outputs.

2.5.7 Taxonomy of ADF Approaches

From the perspective of interference analysis, ADFs we reviewed can be placed into 5 groups, described by their switching signal (f_{SS} and waveform), their detection method (coherent or non-coherent), and their switching filter/display methods (servo, CRT, or digital). Not all combinations were found. Though we were not able to determine the design of all 20 units, 14 were described in sufficient detail for classification, and the others have been assigned based on similar units. The categories include:

1. Sinusoidal, coherent detection, servomotor (4)
2. Sinusoidal, noncoherent, servomotor (7)
3. Sinusoidal, noncoherent, CRT (6)
4. Square wave, noncoherent, servo (2)
5. Square wave, noncoherent, digital (1)

One unit had both CRT and servomotor display, but was placed in a servo category since that determines the switching filter characteristics. Figure 2.8 shows the distribution of units in each category versus f_{SS}.

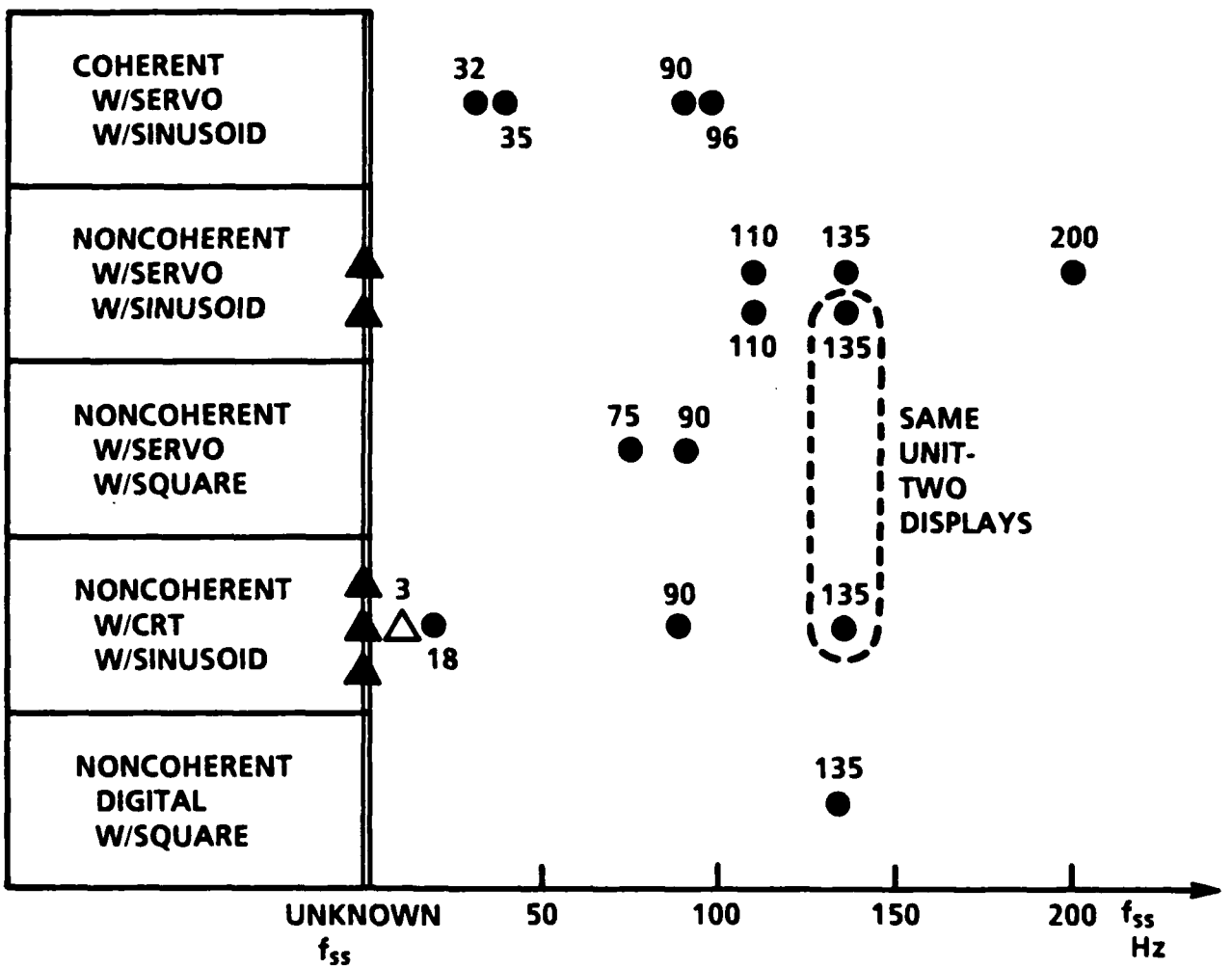

Figure 2.8: Distribution of ADF Unit Characteristics

2.6 Motor Analysis

Servomotor systems were the most common ADF design used both for detecting and displaying the bearing angle. Despite employing a variety of antenna and goniometer configurations, modulation and detection schemes, and display devices, servomotor ADFs all shared a common system structure. The received signal bearing is transformed to either magnitude or phase information at the switching signal frequency. Passing through RF and IF stages, this information is eventually detected and applied as a control voltage to the servomotor. In all units but one, a two phase AC induction motor was used. Two phase induction motor servos are widely used for position control, and here serve to alter the effective antenna position. On units with fixed crossed loop antennas and goniometers, the servo merely rotates the goniometer search coil; on units with ferrite rod antennas, the rod itself is rotated. Rotation of the goniometer search coil or ferrite rod changes the received signal and eventually the control voltage. As the antenna bearing approaches the true bearing of the received signal, the control voltage decreases. At the true bearing the control voltage goes to zero and the servo stops. Usually the bearing indicator is mounted on the same shaft as the goniometer search coil. For ferrite rod antennas, the display usually surrounds the antenna mount. The bearing readings therefore approach the true bearing with a time constant determined by the motor/shaft combination.

Two phase AC servomotors [20] typically have a reference phase voltage at sinusoidal frequency f_r that establishes a rotating flux field. The control phase sinusoidal voltage, also at f_r but usually phase shifted 90°, creates its own flux field that couples with the reference phase flux field to produce mechanical torque. When the voltages of the two phases are balanced, no torque is developed. Control voltages above or below the reference magnitude produce torque in one direction or the other. Servomotors have good stability characteristics, due to their very high rotor resistance which causes their torque-speed curve to be negative.

To understand the dynamic performance of AC servomotors we must consider three factors. First, the servomotor loses net torque when the control phase frequency differs from the reference phase frequency. Because developed torque depends on coupling two rotating fields, the coupled fields actually create a pulsating torque (always in the same direction) at the reference phase frequency. In many common servo applications, f_r = 400Hz. In ADFs, f_r ranged from 32Hz to 200Hz with most values about 100Hz to 135Hz. This pulsating torque encounters the motor mechanical damping which has a time constant on the order of τ_m = 0.5 sec, so that only the DC component of the pulsating torque is seen. Servomotors therefore can be considered as a mechanical form of coherent detector.

Second, there are two quite different time constants in servomotors. The first is the mechanical τ_m. Typically this ranges between 0.5 sec and 1 sec. Although no direct data

could be collected from manufacturers' information, several units gave the indicator slew rate, the time to respond to a 175° bearing reading change. These ranged from about 4 sec to 7 sec. Assuming 5τ as the response to a step input bearing signal would yield τ_m between 0.8 sec and 1.4 sec. The second time constant is τ_e, associated with the electrical behavior of the coils in the motor. This is typically 100 times faster than mechanical phenomena, and can be ignored.

Third, many of the servomotors have a servo amplifier that both filters and amplifies the detected bearing signal. These were found to be bandpass filters around f_r; a few had notches at the first harmonic of f_r, presumably to reduce jitter or bearing error from interaction with harmonics from the reference phase.

The overall block diagram of the servomotor/amplifier combination is given in Figure 2.9. The first block approximates the servoamplifier with a low Q second order filter with gain K. The second block contains the mechanical and electrical time constants, and an integrator, since the motor is used as a position servo. K_v is the motor voltage gain and typically is about 20 to 100 in servo applications.

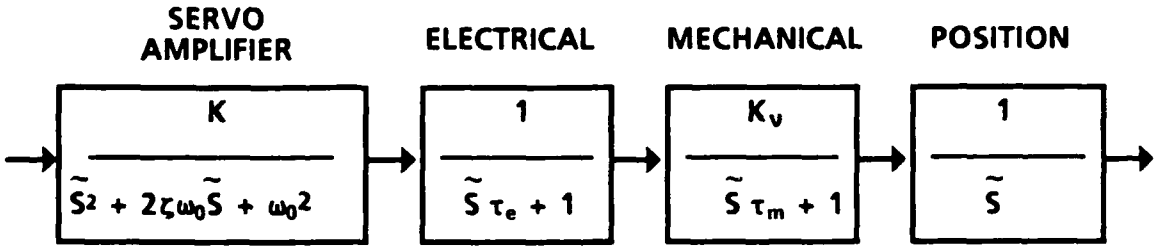

Figure 2.9: Motor Block Diagram

Figure 2.10 shows the ADF configuration for the servomotor. The initial bearing error, θ_e, is the difference between the antenna orientation and the true bearing of the received signal. θ_e arises from the antenna-goniometer-mixer circuitry and may be represented

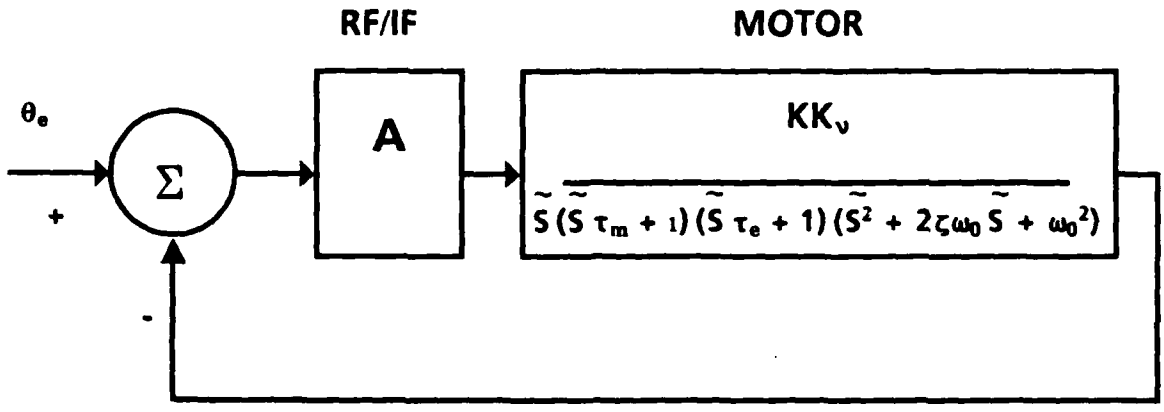

Figure 2.10: ADF Servo System Model

as a phase or magnitude, depending on the particular ADF. The error passes through the RF/IF stages and is detected in the first block. Since the RF/IF stages typically have passbands of several kHz, it is assumed that their total effect on the bearing error is a gain, A. The second block is the motor from Figure 2.9. The motor output is a displacement angle $\hat{\theta}$ that represents the rotation of the antenna. The objective of the servo system is to drive the bearing error, θ_e to zero. Due to the mechanical system associated with display of the bearing, the correct bearing is displayed when θ_e is zero,. The unity negative feedback represents the direct coupling seen in most units between motor position and antenna position.

The closed loop transfer function of Figure 2.10 can be written as:

$$H(s) = \frac{AKK_v}{\tilde{s}(\tilde{s}\tau_m + 1)(\tilde{s}\tau_e + 1)(s^2 + 2\zeta\omega_o s + \omega_o^2) + AKK_v}$$

where

$$\tilde{s} = j(\omega - \omega_r)$$

and

$$s = j\omega$$

The distinction of $\tilde{s}$ and s reflects the coherent behavior of the servomotor. Motor dynamics are determined by frequency variations about the reference f_r, or equivalently,

ω_r. For example, $\tilde{s} = 0$, the DC condition under which motor position increases steadily for constant input, corresponds to excitation by a control voltage at ω_r. The servo amplifier model is formulated in the usual manner.

Figure 2.11 shows the changes in $|H(s)|$ for a fixed value of f_r, the switching frequency of the ADF, for variations in τ_m, the mechanical time constant, and K_v, the voltage gain. Both smaller τ_m and higher K_v broaden the curve for $|H(s)|$. The slight peak at lower frequency is due to the servo amplifier. The effects of ζ and ω_o associated with the servo amplifier were insignificant compared to the effects of τ_m and K_v. These $||H(s)||$ curves are approximately like a bandpass circuit at the switching signal frequency with a Q of 10 to 50 or more.

2.7 Determining DGPS Interference for ADFs

We now develop a quantitative assessment of the potential interference of DGPS modulation for ADFs. The factors contributing to the interference will be considered by modeling the switching signal filter passbands and looking at the effects of switching signal modulation on the DGPS signal. Finally, we present a straightforward noise analysis based on the signal-to-interference ratio (SIR) at the output of the switching filter configuration. We show that in our linear analysis, the SIR determines the bearing error. Conservative assumptions are used throughout to compensate for the incomplete ADF data and the nonlinear and dynamic effects that are neglected.

2.7.1 Comparison of ADF Passbands

Using the taxonomy of ADF units given above, the extreme passbands for each class of ADF switching filter can be identified. These are given in Figures 2.12, 2.13, and 2.14. Each figure shows the passbands of the switching filter components centered on the highest and lowest switching filter frequency seen for that class of ADF. For example, Figure 2.12 shows the servo system passbands, centered at 200Hz and 35Hz, for $\tau_m = 0.5$ and 0.25. All other units had passbands falling between these extreme center frequencies, and it is unlikely that any other of the units differed greatly from the range of τ_m shown. These passbands then form the bounds of passband performance for ADFs relying on servo systems.

Similarly Figure 2.13 shows the extreme passbands for units that relied on bandpass filtering. Usually these units had CRT displays, and the center frequencies ranged from a low of about 3Hz to 135Hz. In the absence of detailed filter information, the filter characteristics are modeled by second order bandpass filters with Q of 10 or 100. The single non-coherent digital unit is put in this category and treated as a high Q filter.

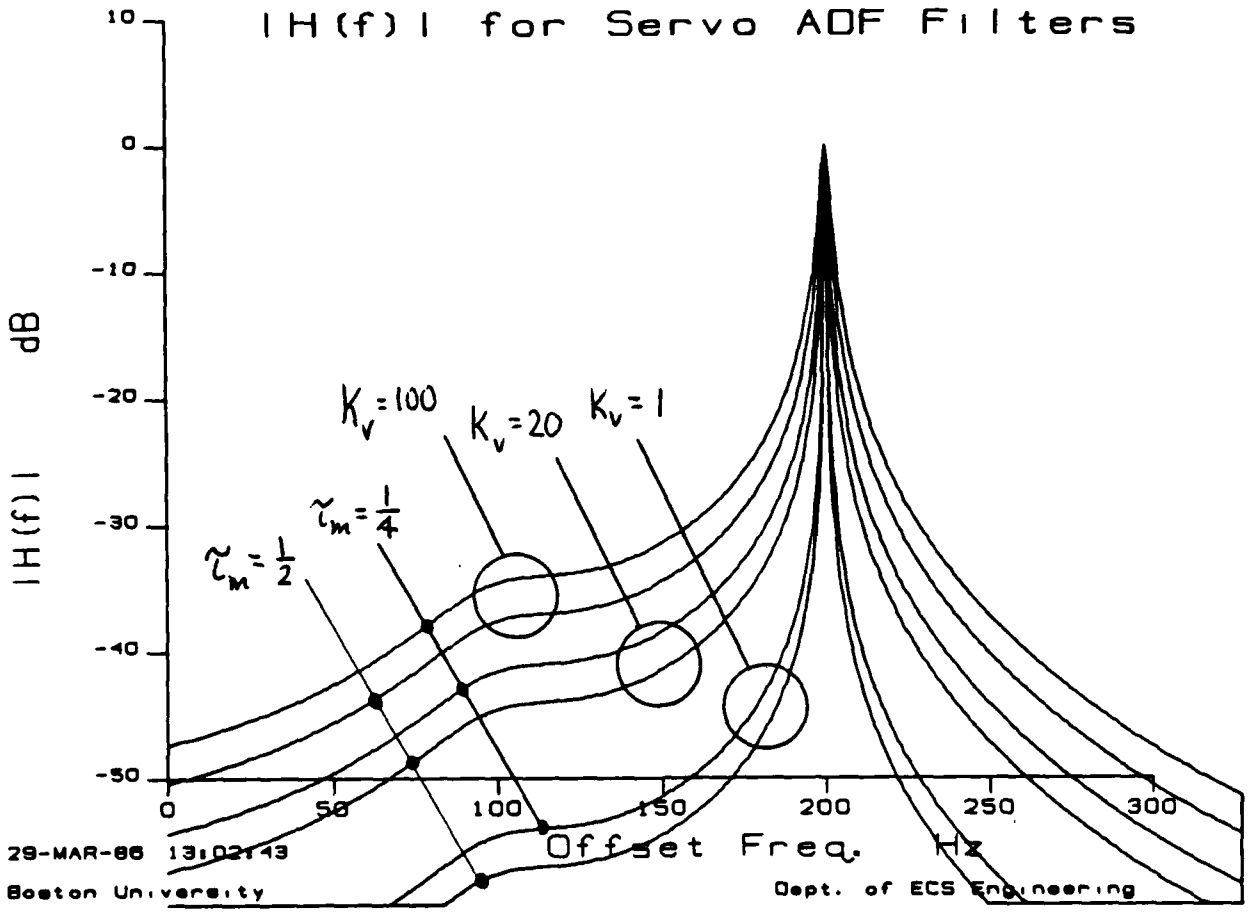

Figure 2.11: Frequency Response of Closed Loop Servo

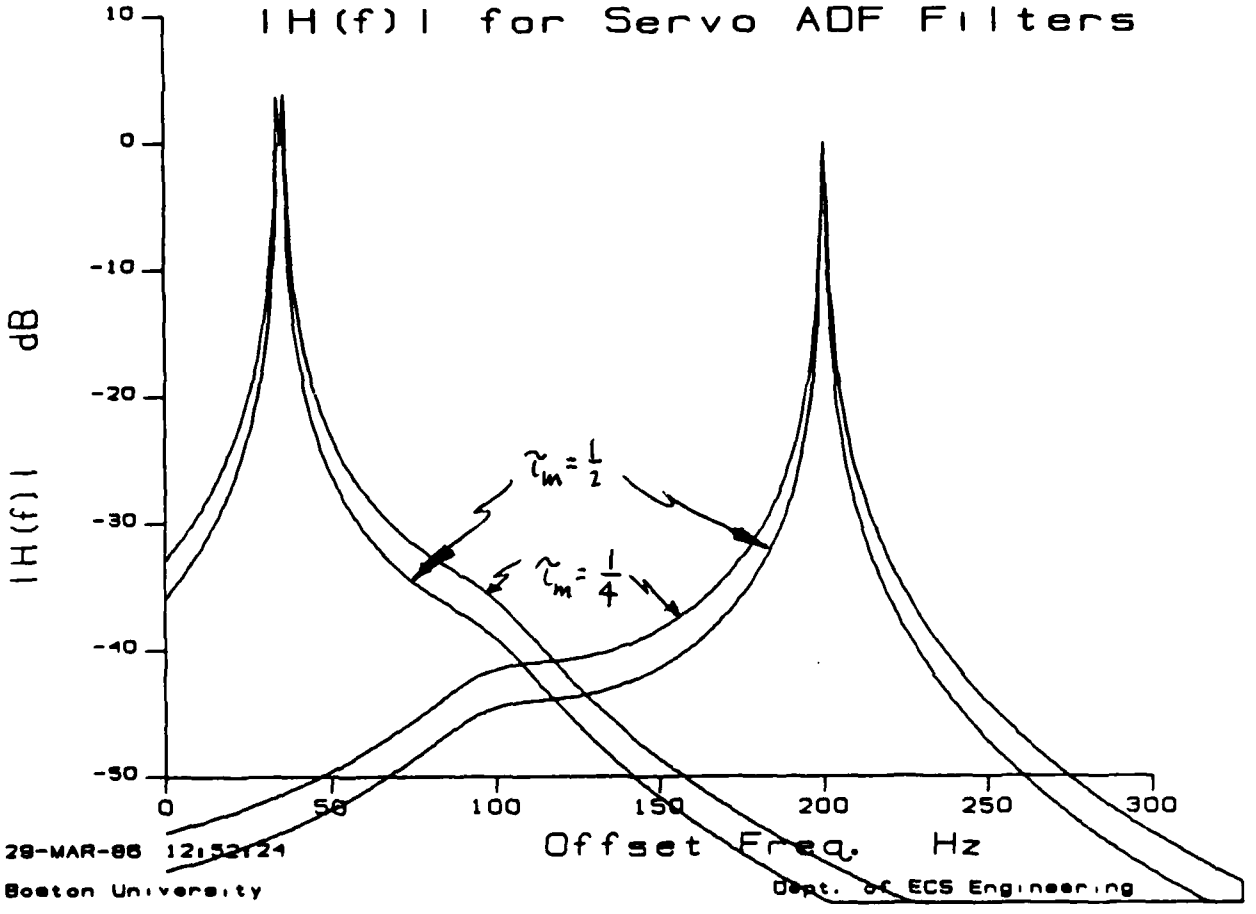

Figure 2.12: Passbands for Servo ADFs

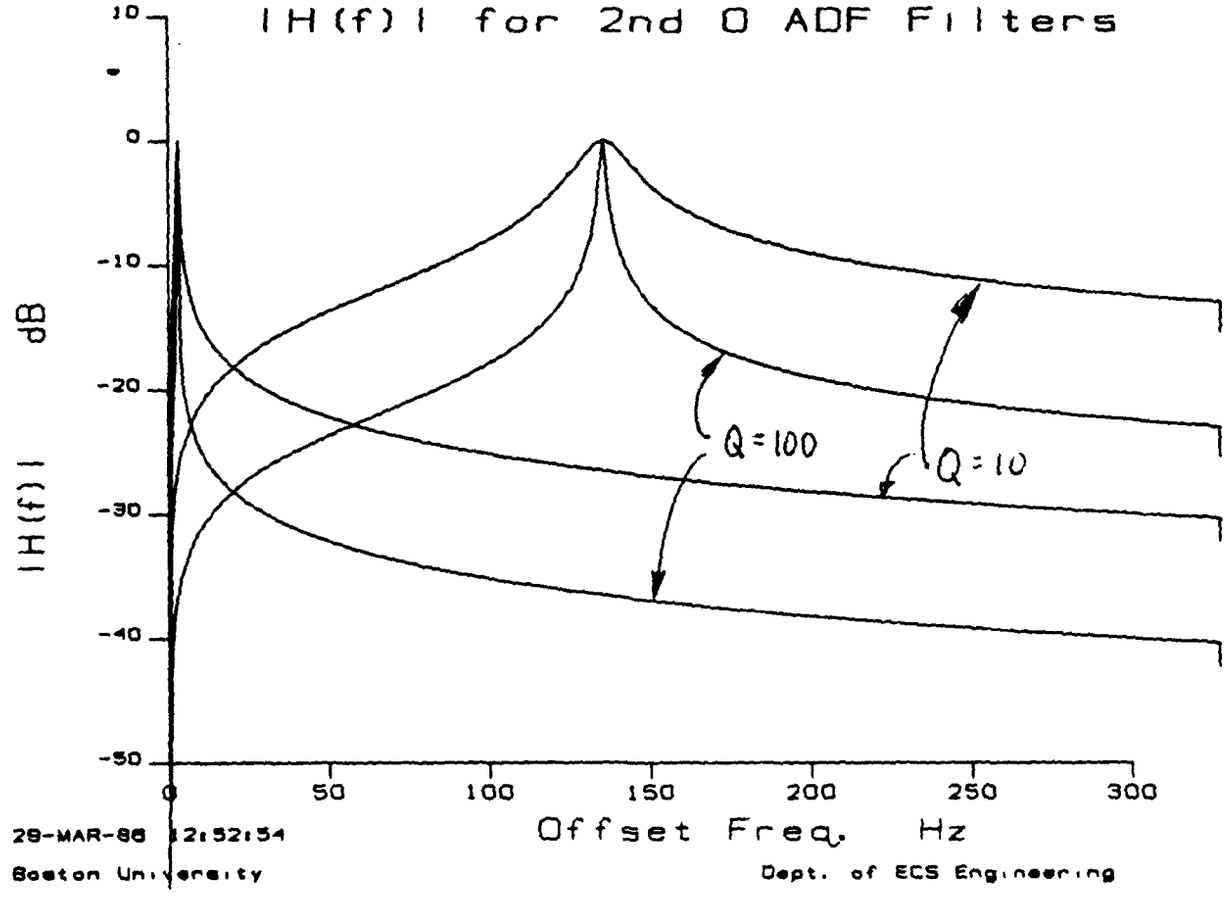

Figure 2.13: Passbands for Second Order ADFs

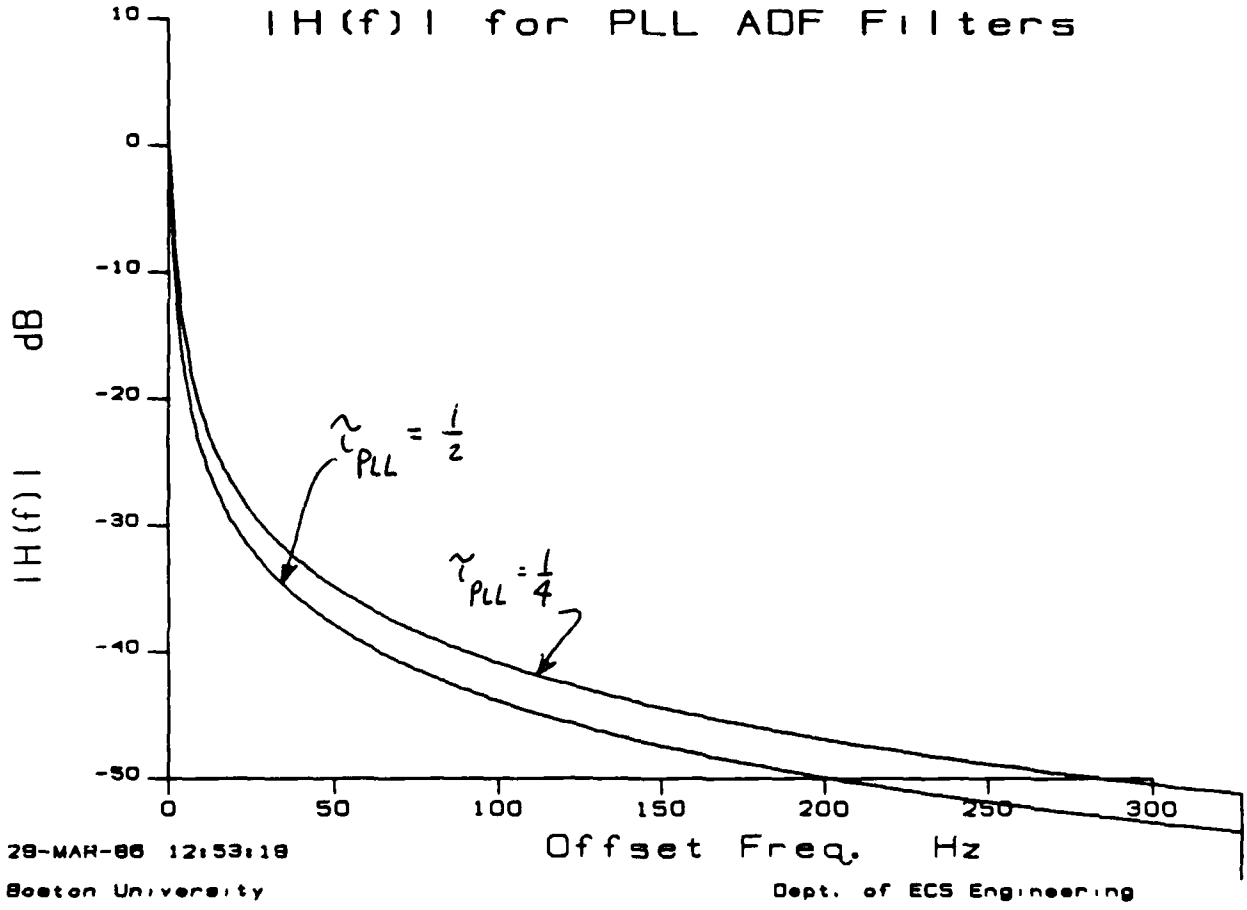

Figure 2.14: Passbands for Coherent PLL ADFs

Figure 2.14 represents the coherent detectors. The coherent units all had phase locked loops at the carrier frequency to detect either magnitude of phase information on bearing. As discussed earlier, the linear performance of these systems is like a very narrow filter about the carrier. We approximate this by a low pass filter with a cutoff of either 2Hz or 4Hz. In some coherent detection units using amplitude modulation, the PLL is cascaded with a synchronous filter. The one unit with sufficient detail to describe the synchronous filter had a cutoff of about 2Hz around the switching signal. We have cascaded our low pass PLL filter with a 2Hz synchronous filter in both curves. This representation cannot describe the unlock conditions of the PLL, but does approximate the normal operation of the coherent ADFs.

These passbands bound the performance of all the units we have studied. Modulation decisions that do not affect these extreme units should provide satisfactory performance for units at intervening frequencies and with filter parameters similar to those we have been able to examine in detail.

Qualitative assessment of competing modulation schemes can begin with these passbands and the previous diagrams of MSK and CPFSK spectra. For example, it is apparent that offsetting the DGPS signal in the 0 to 200Hz range could lead to interference by allowing DGPS energy to enter the passbands of some units. At the 0Hz end, the coherent detectors would be vulnerable to unlock, and non-coherent units with f_{SS} in the area of 35Hz to 90Hz could be affected. At offsets near 135Hz, several servo and CRT units would be vulnerable. Increasing offset above 200Hz increasingly removes the danger of interference, although it is desirable to keep offset low to avoid adjacent beacon effects. The single unit found at $f_{SS} = 200Hz$ does not seem to play any significant role in the ADF market. It is a ferrite rod marine unit, and is apparently no longer in production. Designed in Japan, there is a domestic company distributing literature on the unit, but they cannot provide engineering support or information. Below this unit, there are next a number of ADFs at f_{SS} =135Hz; therefore we will consider a passband at 135Hz to be the critical upper passband in our remaining analysis.

2.7.2 Interference Spectra

In this section we begin to quantify the significant mechanisms determining the exact nature of interference. This will allow us to replace the above qualitative arguments with quantitative measures of interference. The resulting recommendation about DGPS modulation will be based on this quantitative analysis and some inescapable qualitative concerns dictated by our conservative approach and the uncertainties around issues like PLL unlock in coherent detectors.

Because the switching signal of the ADF modulates DGPS as well as the beacon, inter-

ference can arise not only from the DGPS spectrum directly, but also through sidebands created by the switching. As DGPS offset is increased, the self-beacon central spectrum and its sidebands all move away from the carrier. At the same time, the adjacent beacon DGPS and its higher sidebands approach from lower frequencies. Fortunately the adjacent beacon spectra all have at least 15dB of protection, plus whatever DGPS protection ratio is present.

All DGPS interference spectra belong to categories with the following descriptions:

1. Self-beacon sinusoidal switching applied to loop
2. Self-beacon sinusoidal switching applied to sense
3. Self-beacon square wave switching applied to loop
4. Adjacent beacon sinusoidal switching applied to loop
5. Adjacent beacon sinusoidal switching applied to sense
6. Adjacent beacon square wave switching applied to loop

Only three ADFs were found to use square wave switching signals, and these all were applied to the loop antenna.

Figure 2.15 shows the first three cases with the sense signal connected. The center peak represents the DGPS spectrum, either MSK or CPFSK, as picked up by the sense antenna. It is centered at an offset f_{DGPS} above the beacon carrier. The sinusoidal modulation of the loop signal produces sidebands from the loop antenna, located at $f_{DGPS} \pm f_{SS}$. Each has 1/2 the power of the original PSD.

The second part of Figure 2.15 also has sinusoidal modulation, but now the sense is modulated. The composite spectrum looks similar to the first case, with the DGPS spectrum centered at f_{DGPS} and half-power sidebands at $f_{DGPS} \pm f_{SS}$. These spectra change differently as the ADF finds a bearing. As the loop antenna rotates, the loop signal decreases either in amplitude or phase, depending on the ADF.

In an amplitude-based ADF, the loop components of the spectrum decrease, and the sense spectrum remains unchanged. Switched sense and switched loop naturally cause their respective parts of the spectra to decrease. In a phase-based system, bearing is in the phase, so spectral amplitudes will remain even when phase error decreases. Magnitude-based systems therefore experience some reduction in DGPS energy entering the ADF as true bearing is reached. Phase based systems see no such reduction.

The third part of Figure 2.15, shows the effect of square wave modulation on the loop antenna. As before, the sense appears at f_{DGPS}. Now the loop appears as multiple sidebands, located at odd multiples of $\pm f_{SS}$.

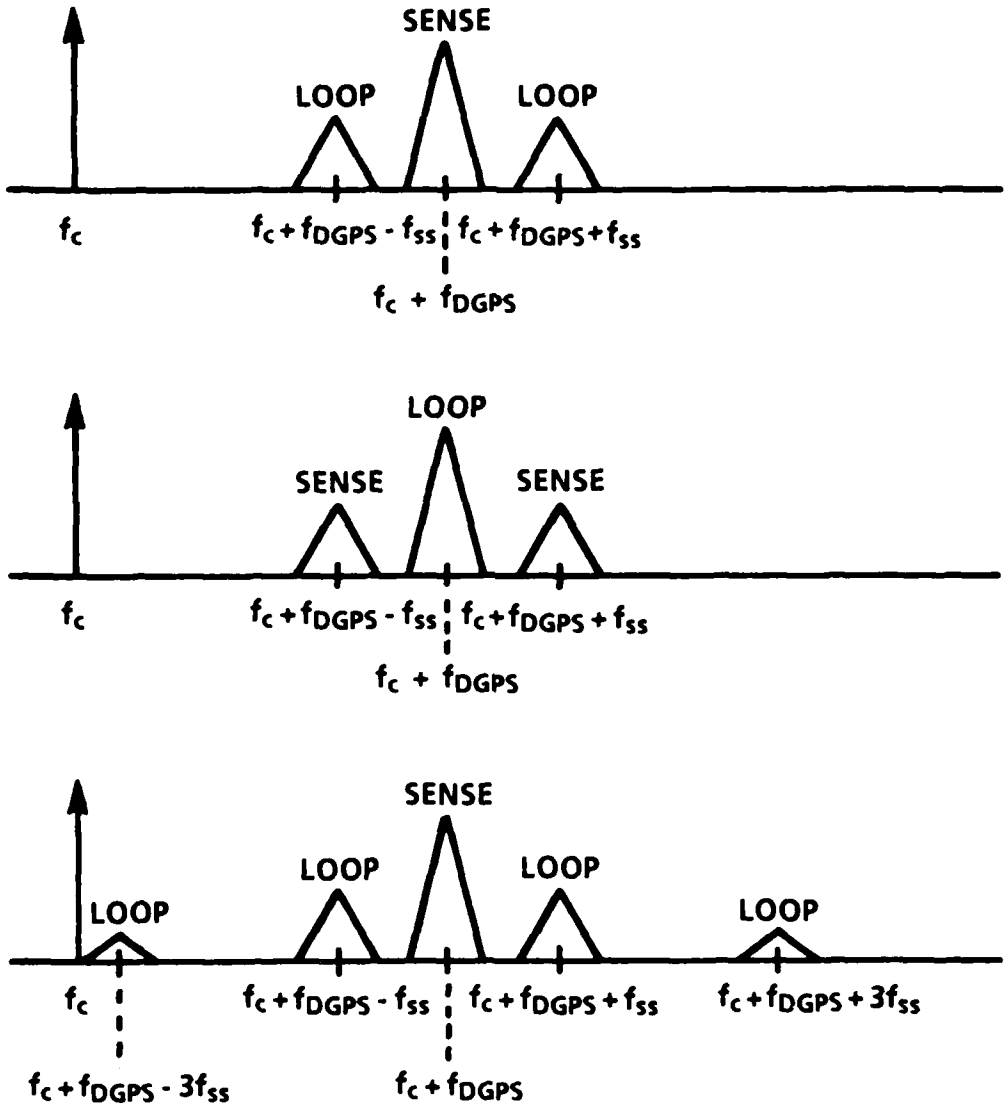

Figure 2.15: Host Beacon Switching Signal Effects

The dynamics of bearing acquisition are too complicated to be addressed in this linear analysis. Qualitatively, if the user starts the unit and large bearing errors are present, the loop sidebands will be high and interference large. This could make the unit wander if the noise effects are on the order of the signal magnitude. Alternatively, with sufficent signal-to-noise, the unit should start to turn to the true bearing, in which case the loop interference signals should decrease. To be conservative, we assume that the unit is experiencing maximum loop signal in all the sidebands.

Figure 2.16 repeats the effects of switching signal modulation for the loop and sense of the adjacent beacon. Now the noise spectra will appear below the host beacon of interest. For example, let the beacon spacing be f_Δ. With respect to the host beacon carrier, an adjacent beacon with sinusoidal switching of the loop will have its DGPS sense spectrum at $-f_\Delta + f_{DGPS}$. At $-f_\Delta + f_{DGPS} \pm f_{SS}$ there will be the half-power sidebands from the modulation of the loop. The magnitude of these spectra will be down by the 15dB adjacent beacon protection ratio, plus the DGPS protection ratio. Similar descriptions apply to the remaining two parts of Figure 2.16.

2.7.3 Quantitative Interference Analysis

Denote $P_I(f)$ and $P_{S(f)}$ as the power spectral densities of the interference, DGPS, and the desired signal at the input of the switching signal filter configuration. The various passbands shown in Figures 2.12, 2.13 and 2.14. above describe the switching signal filter configuration and are represented here by $SSF(f)$. The total DGPS power at the output of the switching signal filter is

$$P_I = \int_{\infty}^{\infty} SSF(f)|^2 P_I(f) df$$

Further the total output signal power is assumed to be given by

$$P_S = \int_{\infty}^{\infty} SSF(f)|^2 P_S(f) df$$

$$= \int_{\infty}^{\infty} P_S(f) df$$

This equality follows because we assume that SSF(f) is flat across the power spectral density of the desired signal.

The time domain signal at the output of the switching signal is

$$y(t) \quad A\cos(\omega_{SS}t + \phi) + n_c(t)\cos\omega_{SS}t \quad n_s(t)\sin\omega_{SS}t$$

where A is signal amplitude, ω_{SS} is the switching signal angular frequency, and ϕ is the actual bearing. $n_c(t)$ and $n_s(t)$ are the inphase and quadrature components of the DGPS

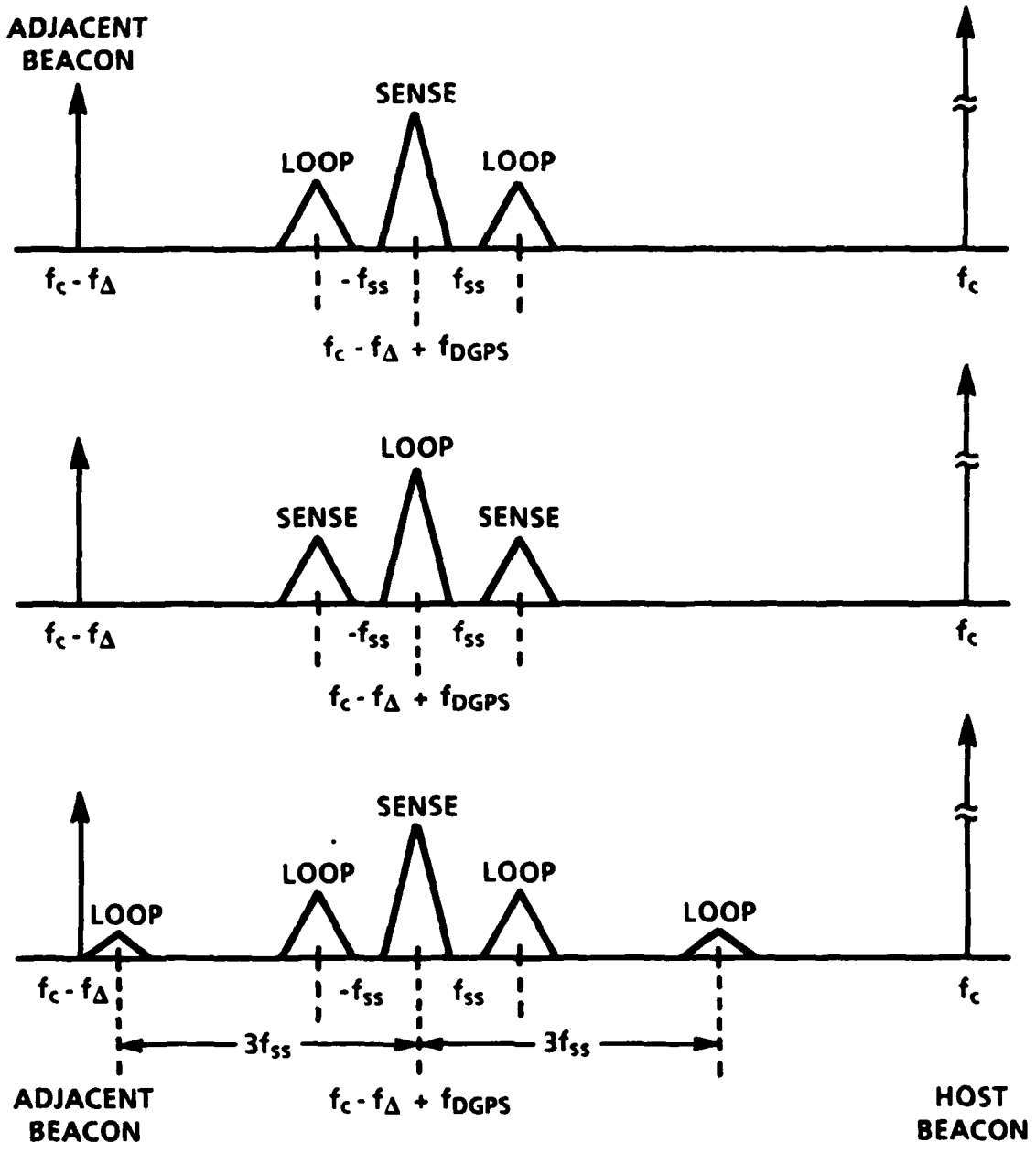

Figure 2.16: Adjacent Beacon Switching Effects on DGPS

interference. In an amplitude modulated system. A. not ϕ, would carry the bearing information.

Consider first the phase modulated system. and let $\phi = 0^o$ without loss of generality. Then the ADFs bearing estimate will be

$$\hat{\phi} = \arctan\{\frac{n_s(t)}{A + n_c(t)}\}$$

Assume that the signal-to-interference ratio is better than 0 dB, and the arctan function may be approximated by its linear term. This allows the following approximation for the variance of the bearing estimates

$$\sigma^2(\hat{\phi}) = \frac{\overline{n_s^2}}{A^2} = \frac{1}{2SNR}$$

where

$$SNR \triangleq \frac{P_S}{P_I}$$

If θ were bearing an amplitude modulated system, the ADF bearing estimate would be

$$\hat{\theta} = \frac{n_s(t)}{A + n_c(t)}$$

No approximation is needed for the variance

$$\sigma^2(\hat{\theta}) = \frac{\overline{n_s^2}}{A^2} = \frac{1}{2SNR}$$

In words, the standard deviation or jitter of bearing estimates, for both phase and amplitude modulation systems, is inversely proportional to the square root of the signal-to-interference ratio at the output of the switching signal filter. This relationship is plotted in Figure 2.17.

The display devices after the switching signal filter may further smooth this estimate. In the case of servo systems, we have already considered this smoothing through the mechanical time constant. CRT displays introduce little smoothing, while the digital unit is likely to incorporate smoothing beyond its filter. Using the passbands of Figures 2.12 to 2.14 again ensures a more conservative assessment.

We now decompose the bearing error as follows

$$\sigma^2(\hat{\phi}) = \frac{1}{2}\frac{P_I}{P_S}$$

$$\sigma^2(\hat{\phi}) = \frac{1}{2}P_{subcarrier}P_{filter}P_{adjacent}P_{harmononic}P_{sideband}$$

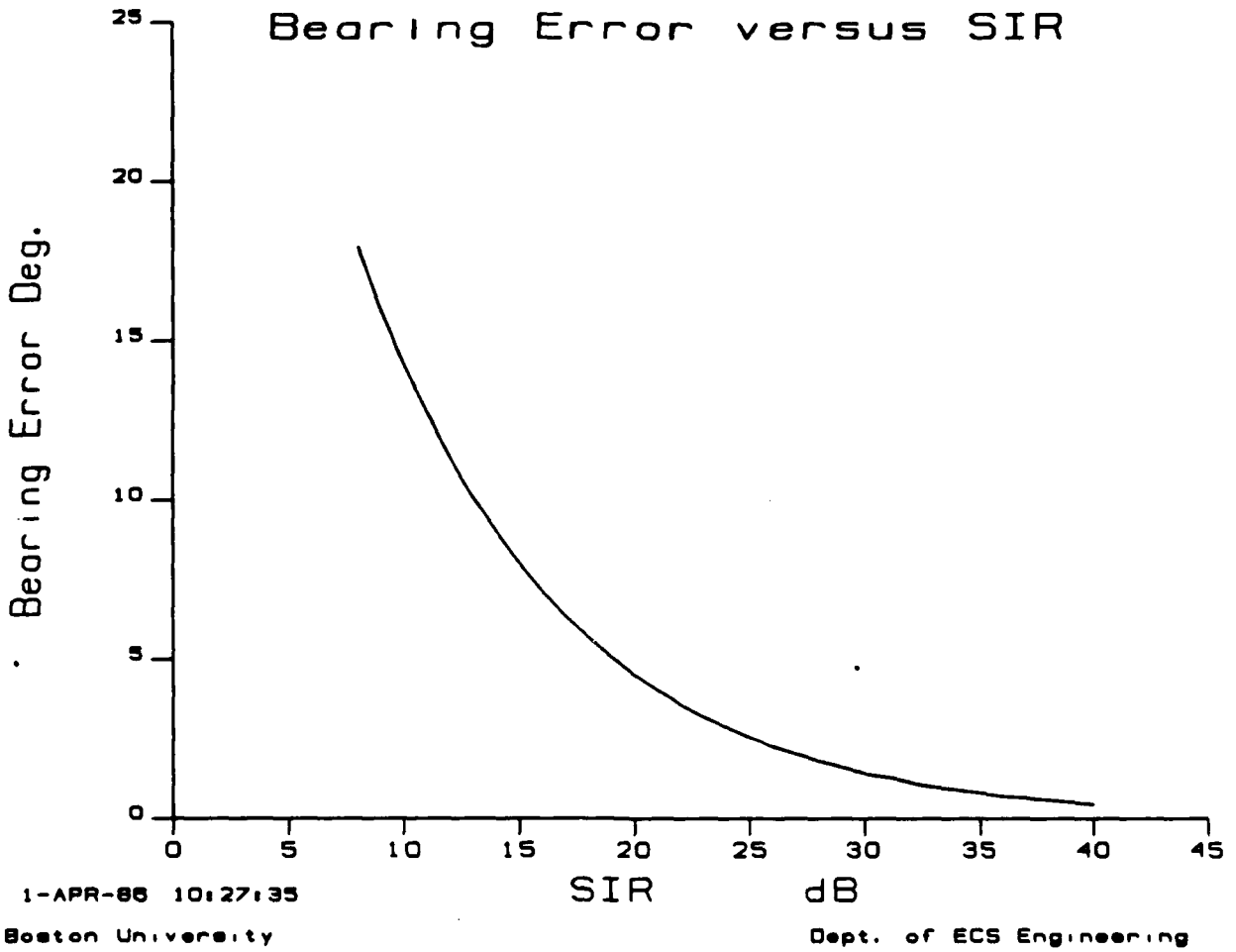

Figure 2.17: Bearing Error vs. SIR

where

$$P_{subcarrier} \in \{\frac{1}{2}(-3dB), \frac{1}{4}(-6dB)\}$$

$$P_{filter} \leq 1 \approx \frac{BW_{filter}}{BW_{interference}}(determined\ below)$$

$$P_{adjacent} \in \{0.0316(-15dB), 1\}$$

$$P_{harmonic} \in \{1(sinusoid), \{0, 0.81, 0, 0.09, 0, 0.03, 0, \ldots\}(square\ wave)\}$$

$$P_{sideband} \in \{\frac{1}{2}\}$$

Table 2.2 shows the values of these factors when the various ADF switching configurations are considered. The value of P_{filter} is left undefined because we seek to find the critical P_{filter} values.

Table 2.2: P-factors for Interference

ADF Spectra	1/2	P_{sub}	P_{filter}	P_{adj}	P_{harm}	P_{side}	Product
Self-carrier	1/2	1/2	x	1	1	1	$0.250x$
Self-sinusoid	1/2	1/2	x	1	1	1/2	$0.125x$
Self-square 1	1/2	1/2	x	1	0.81	1/2	$0.101x$
Self-square 3	1/2	1/2	x	1	0.09	1/2	$0.011x$
Adj-carrier	1/2	1/2	x	0.0316	1	1/2	$0.079x$
Adj-sinusoid	1/2	1/2	x	0.0316	1	1/2	$0.040x$
Adj-square 1	1/2	1/2	x	0.0316	0.81	1/2	$0.0032x$
Adj-square 3	1/2	1/2	x	0.0316	0.09	1/2	$0.00035x$

Table 2.3 shows the values of P_{filter} that are upper limits of the acceptable range. For example, to guarantee that $\sigma(\hat{\phi}) \leq 2^o$, when considering the sinusoidal sideband resulting from switching, $P_{filter} \leq 0.0097$. For such a P_{filter}, $\sigma(\hat{\phi}) \leq 2^o$ for a sideband from a squarewave, ($P_{filter} \leq 0.0121$) but not for the carrier DGPS spectrum ($P_{filter} \leq 0.0049$).

P_{filter} can be determined by passing a DGPS spectrum through one of the passbands. Depending on the offset of the DGPS with respect to the center frequency of the passband, different P_{filter} values will result.

Figures 2.18, 2.19, and 2.20 show the results of numerical integration of

Table 2.3: P_{filter} Values for Bearing Error

ADF Spectra	3^o	2^o	1^o
Self-carrier	0.0110	0.0049	0.0012
Self-sinusoid	0.0219	0.0097	0.0024
Self-square 1	0.0271	0.0121	0.0030
Self-square 3	0.2492	0.1108	0.0277
Adj-carrier	0.3481	0.1551	0.03797
Adj-sinusoid	0.6931	0.3070	0.0760
Adj-square 1	0.8576	0.3829	0.0949
Adj-square 3	7.8861	3.5063	0.8765

$$SIR = \frac{P_I}{P_S} = \frac{\int_{-\infty}^{\infty} |SSF(f)|^2 P_I(f) df}{\int_{-\infty}^{\infty} P_S(F) dF}$$

where P_I is MSK. Figure 2.21 shows the results for a second order filter when P_I is CPFSK(m=1). Note that the CPFSK discrete frequencies cause a peak in the energy entering a passband when the DGPS offset corresponds to $B/2$. The peak should be on the order of 1/3, since that is the energy in the discrete components. This is reduced somewhat since the passband value must be considered. The clipped shape of the Q=100 curves is an artifact of the integration and plotting step sizes. It is also clear how the higher symbol rate spreads the MSK spectrum and produces a smaller P_{filter} at low offsets. However, at larger separations, the higher symbol rate modulation has more energy in its sidelobes, and P_{filter} is greater. Comparing the motor curves with the PLL curves indicates servo and PLL ADFs are similar in their interference behavior. In fact, since most PLL units also have a servomotor display and/or a digital filter, the PLL performance will generally be better than the simple motor switching filter configurations. The PLL- servomotor combination is not reflected in these figures. High Q second order ADFs are similar to motor and PLL systems as well. Only low Q units show dramatically higher vulnerability to noise effects.

As DGPS offset increases, the train of spectra consisting of the DGPS spectrum at the DGPS carrier and its sinusoidal or squarewave sidebands, slide across the various passbands we have shown. We seek a value of f_{DGPS} that will prevent unacceptably large bearing errors in any ADFs. For any particular ADF, as f_{DGPS} increases, there will be a series of peaks in $\sigma(\dot{\phi})$ as successive self beacon sidebands pass through the ADF passband. At very large f_{DGPS}, the adjacent beacon sideband and DGPS carrier spectra cause another series of peaks in $\sigma(\dot{\phi})$, but with considerably lower magnitude due to the adjacent beacon

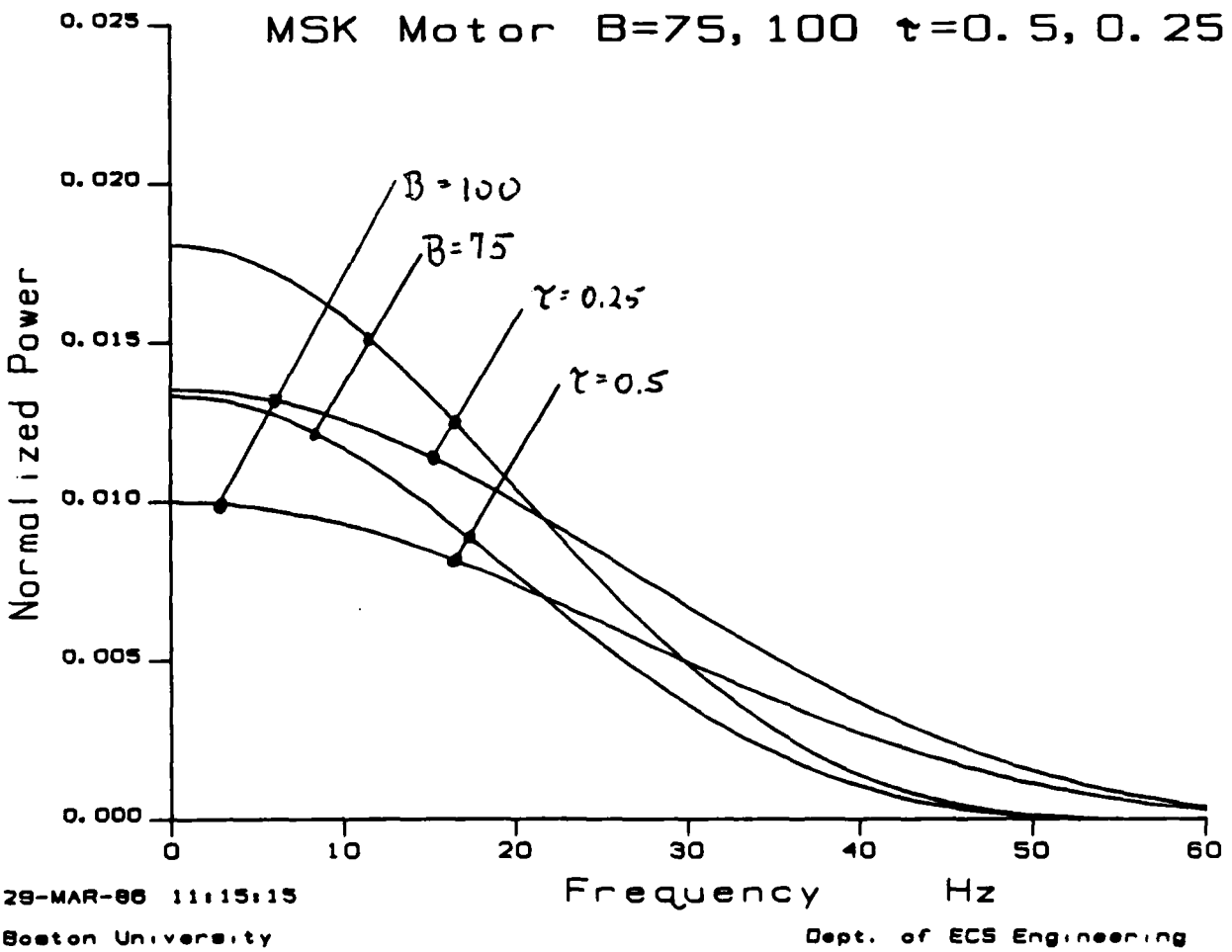

Figure 2.18: P_{filter} for Motor

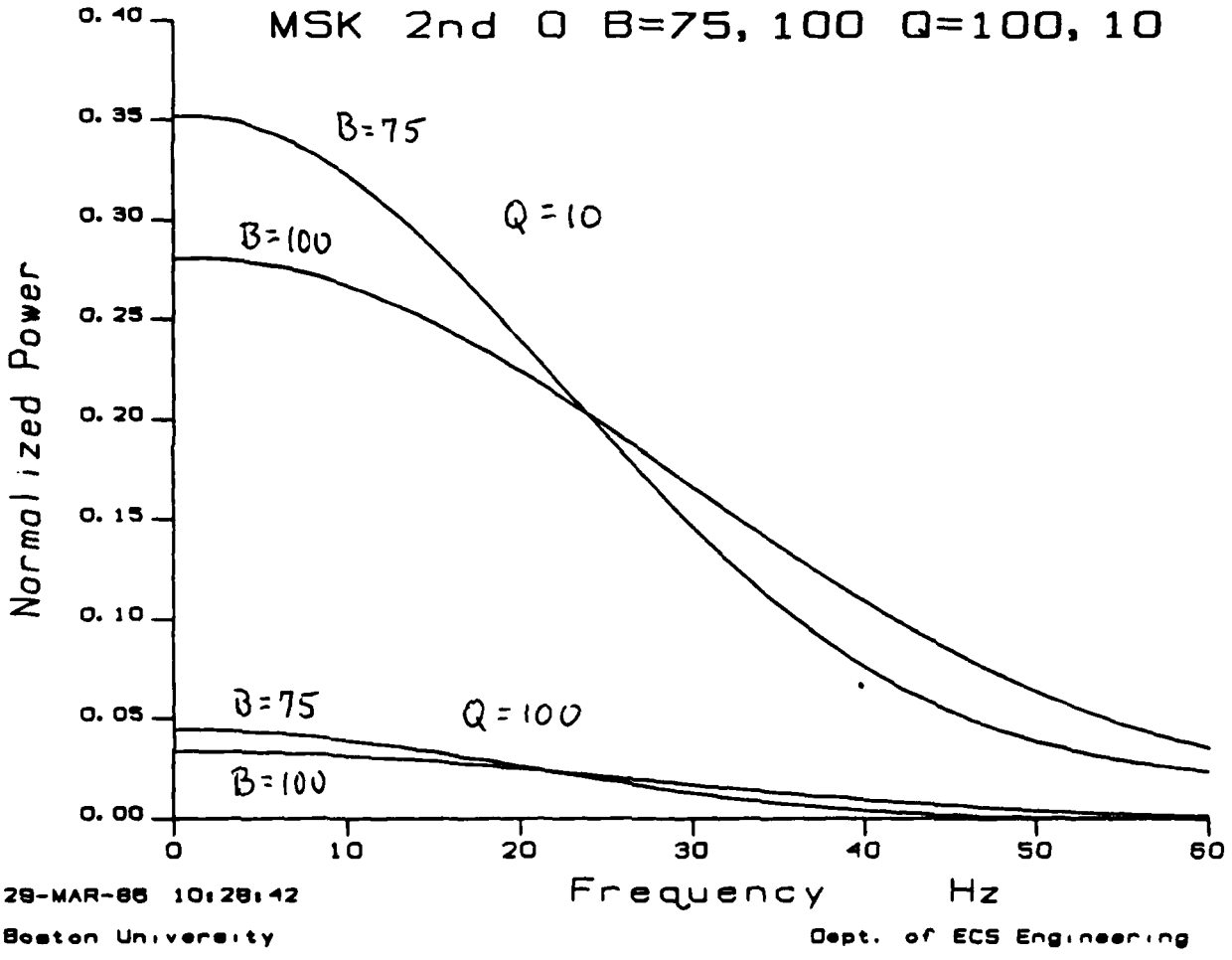

Figure 2.19: P_{filter} for 2nd Order ADF

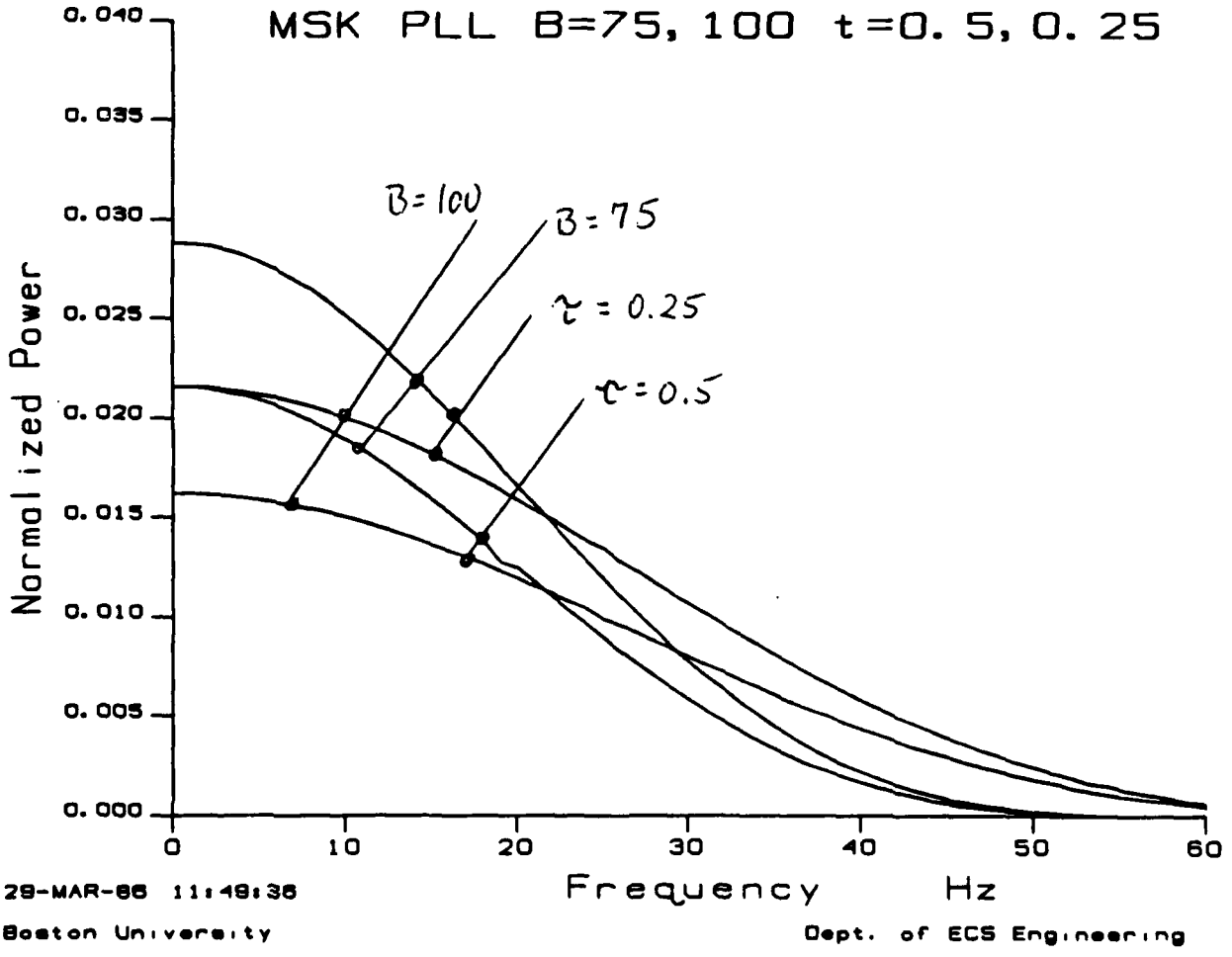

Figure 2.20: P_{filter} for PLL ADF

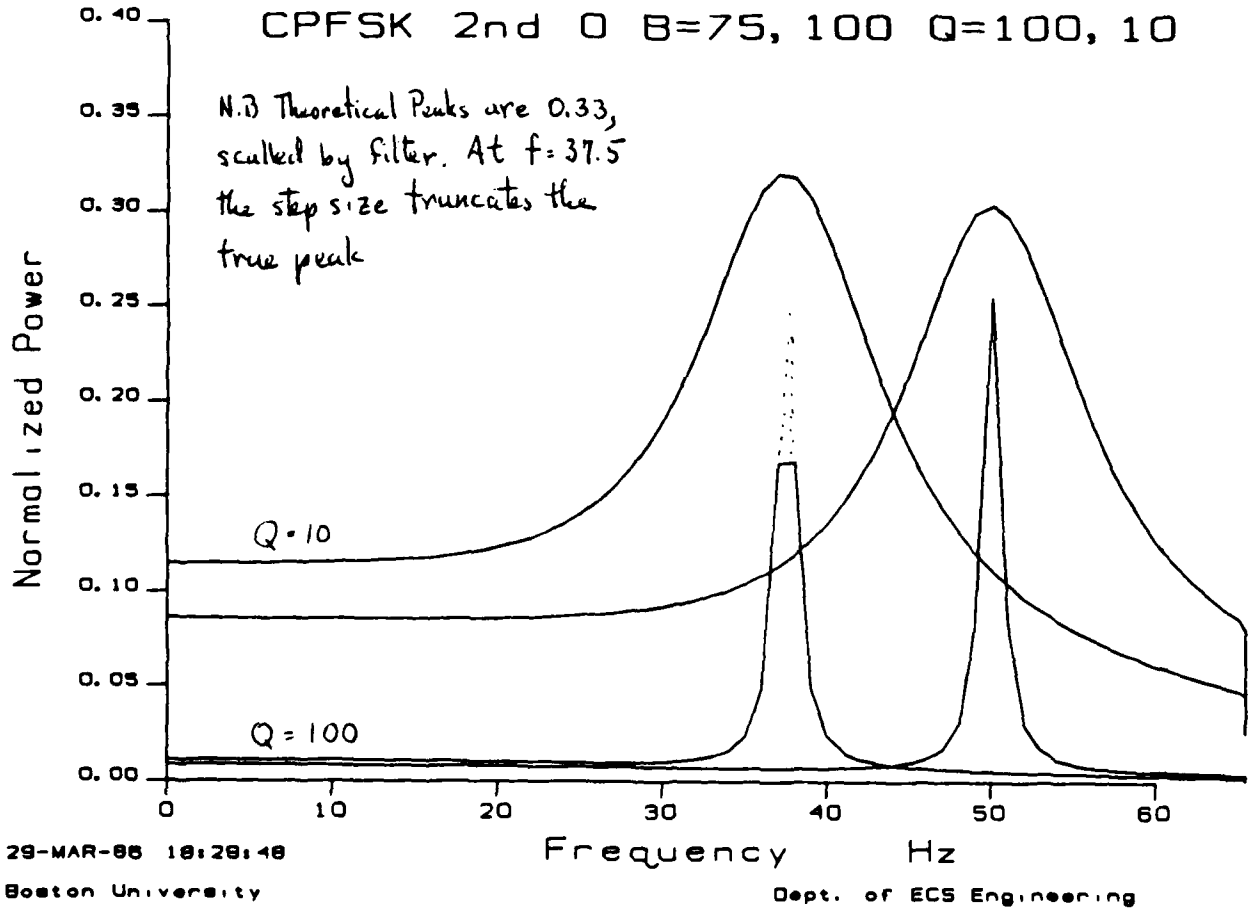

Figure 2.21: P_{filter} for CPFSK in 2nd Order ADF

protection ratio of 15dB.

DGPS offset f_{DGPS} must be within the valleys of $\sigma(\hat{\phi})$. Because of overlapping passbands, and the possiblity that ADFs we did not examine have passbands within desirable valleys, the safest course of action is to put f_{DGPS} into the extended valley above the highest passbands. Discounting the one unit with a 200Hz passband center frequency, we are looking at f_{DGPS} above 135Hz.

Could DGPS reside at an offset on top of the last passbands near 135Hz? Table 2.3 shows that the critical P_{filter} is 0.01 for $\sigma(\hat{\phi}) = 3^o$ when the DGPS passband separation is zero. A 2^o value is 0.0049. Clearly all the ADFs cannot meet these criteria, so we must consider the next possible $\sigma(\hat{\phi})$ peak. This would occur when the choice of f_{DGPS} causes the sinusoidal sideband to overlay the ADF passband. The 3^o value of P_{filter} would be 0.02 and the 2^o value would be 0.01. All units but the second order, Q=10 units would satisfy a 2^o criterion, providing an additional 40 to 50Hz of separation were provided. The extra 40 to 50Hz separation causes the sinusoidal sideband to fall 40 to 50Hz beyond the ADF passband, and reduces the sideband's contribution to $\sigma(\hat{\phi})$.

This argument would result in a total $f_{DGPS} = 135Hz + 135Hz + 50Hz$ or 320Hz. The first 135Hz offsets the DGPS main signal to the center of the ADF passband. The second 135Hz represents further offset that brings the main DGPS signal well past the ADF passband, but allows the sinusoidal sideband to fall in the center of the ADF passband. The last 50Hz represent the offset of the sinusoidal sideband above the center of the passband.

Since the critical P_{filter} for the squarewave sidebands are always higher than the sinusoidal value, we need not consider the squarewave harmonics unless we decide a larger f_{DGPS} is required. The third harmonic squarewave peak in $\sigma(\hat{\phi})$ has 2^o and 3^o P_{filter} values of 0.25 and 0.11. These are readily met by all units, so we need not increase f_{DGPS} to accommodate units with squarewave sidebands. An offset of 0Hz has been suggested as an attractive solution from the standpoint of frequency management. Three problems should be noted. First, the nonlinear PLL behavior in such a situation is difficult to predict, and could have severe consequences, including unlock or even temporary ADF shutdown by lock detector circuits. Second, any DGPS signal located at 0Hz would be broad enough to enter the passbands of the units with lower f_{SS} values. Finally, with zero offset, the DGPS signal will be modulated by f_{SS} to lie directly on the passbands of all ADFs. We saw above that additional offset can sometimes reduce these effects, but the presence of units with f_{SS} between 3 and 35Hz leaves no room for such separation.

These discussions have focussed on MSK. CPFSK, having one-third of its energy in its discrete frequency components, will always experience unacceptably high $\sigma(\hat{\phi})$ when the discrete component falls in the ADF narrow passband. Peak P_{filter} will be on the order of 0.3 regardless of the ADF unit when this happens. This means that even the third

squarewave harmonic would create 3° or more bearing error.

2.8 Conclusions

Based on the above analysis, we make the following recommendations:

1. Modulation should be MSK. CPFSK, with its discrete frequency components, is subject to P_{filter} values near 0.3, and could produce unacceptably large $\sigma(\hat{\phi})$ even at large offsets due to its DGPS sidebands having discrete components.

2. Offset should be greater than 325Hz. One unit with $f_{SS} = 200Hz$ and second order units with low Q might experience errors greater than 3° for this offset. However, such units are apparently out of production or of comparatively low quality. An offset to include these units would have to be between 450 and 600Hz.

3. DGPS protection ratio should be -3dB. A -6dB ratio would still require an offset sufficient to reach the sinusoidal sideband. Going to -6dB would only reduce the need to slide somewhat beyond the sinusoidal sideband, changing the total offset from say 325 to 275Hz.

4. Symbol rate should be 100 symbols per second (rate 1/2 coding). This serves to spread the energy in the spectra, and reduces $\sigma(\hat{\phi})$. For a given ADF, this reduction occurs because the DGPS interference spectrum is widened compared to the ADF passband. It also improves the range of the DGPS transmission, as discussed in section 3.

Two major concerns should be mentioned. First, there may be further ADFs that we did not encounter in our survey. If their characteristics differed greatly, the conclusions might need revision. The conservative worst case approach employed here makes it unlikely that any ADFs will have significantly different interference characteristics from those seen here. Second, a linear analysis is only approximate for ADFs. It is suggested that bench testing be performed on at least a subset of ADFs to ensure that nonlinearities do not degrade ADF performance in the presence of DGPS.

Chapter 3

Atmospheric Noise and Multipath Effects

3.1 Introduction

Atmospheric noise is generated by lightning strokes and dominates other noise sources in the very low, low and medium frequency bands. (VLF,LF, and MF designate the bands from 3-30 kHz, 30-300 kHz and 300-3000 kHz, respectively.) This noise process appears as a low power Gaussian background with bursts of high power impulses. The impulsive nature of the noise motivates the use of some form of limiting in the receiver and the use of error detecting and correcting (EDAC) codes in the system. Additionally, atmospheric noise power varies widely with location and time, and this variation is statistically described in [4] and [13]. Finally, atmospheric noise bursts can last a substantial fraction of a second and so interleavers must be used.

At LF frequencies, signals propagate either along the earth's surface in a "groundwave" mode or reflect off the ionosphere in a "skywave" mode. The groundwave amplitude is fairly stable and well described by data given in CCIR, 1966. In contrast, skywave amplitude and phase vary widely and must be statistically described. (See references [5] and [6].) At short ranges ($\leq 200km$), the groundwave field is much stronger than the skywave field and no interference or fading will appear. However, at intermediate ranges (200 to 600 km)the groundwave and skywave fields can be nearly equal and fading is possible.

The organization of Chapter 3 is now described. In section 3.2, we provide a brief overview of error detecting and correcting codes. This material is designed to introduce the terminology of codes, which we will use in this report.

Section 3.3 computes the probability of bit error for the DGPS link. This analysis incorporates receiver limiting, the non-Gaussian nature of atmospheric noise and EDAC codes. It does not incorporate the bursty nature of atmospheric noise, which we consider

in section 3.6. It assumes that the noise power, skywave amplitude and skywave phase are fixed, and it results in a family of curves, which give probability of bit error versus signal to noise ratio.

Section 3.4 computes the probability of link availability, which is defined as the probability that the SNR required for $Pr(\epsilon) \leq 10^{-5}$ is achieved. As such, $Pr(link\ available) = 1 - Pr(outage)$. This portion of our overall analysis incorporates the variation of the noise power, skywave amplitude and phase as described in [4], [5], [6], and [13].

Section 3.5 presents and discusses the combined results of sections 3.3 and 3.4. It gives the range to which the link will be available with probability 0.90 under "worst case" conditions in Boston, Massachusetts.

Finally, section 3.6 considers the burst nature of atmospheric noise and the techniques which must be used to overcome these bursts.

3.2 Error Detecting and Correcting Codes

In the sections that follow, we will show that error detecting and correcting (EDAC) codes greatly enhance the performance of the radiobeacon-DGPS link. In this section, we briefly introduce coding and its associated terminology. Error correction coding is essentially a signal processing technique used to improve the reliability of communication on digital channels. Even though specific coding techniques differ widely in their details, they all share the fundamental features depicted in Figure 3.1.

As shown, the data sequence is broken into vectors of length k. There are 2^k such data vectors and the code maps each of these into a unique n-tuple (a vector of length n) and these n-tuples are known as codewords. For each codeword, there are 2^{n-k} n-tuples with no corresponding data vector. A good code is designed such that these extra n-tuples form buffer zones around the codewords. Consequently, many channel errors must occur before a given codeword is confused with an n-tuple from another codeword's buffer zone. Good codes have a large distance between all codewords in the code. The most common measure of distance is Hamming distance, which is the number of places in which the two codewords differ.

There are two classes of codes:

- block codes
- convolutional codes

In this report, we consider convolutional codes only and a convolutional encoder is shown in Figure 3.2. As shown, two new information bits are input to the encoder in each cycle and three channel symbols are output from the encoder in each cycle. Consequently,

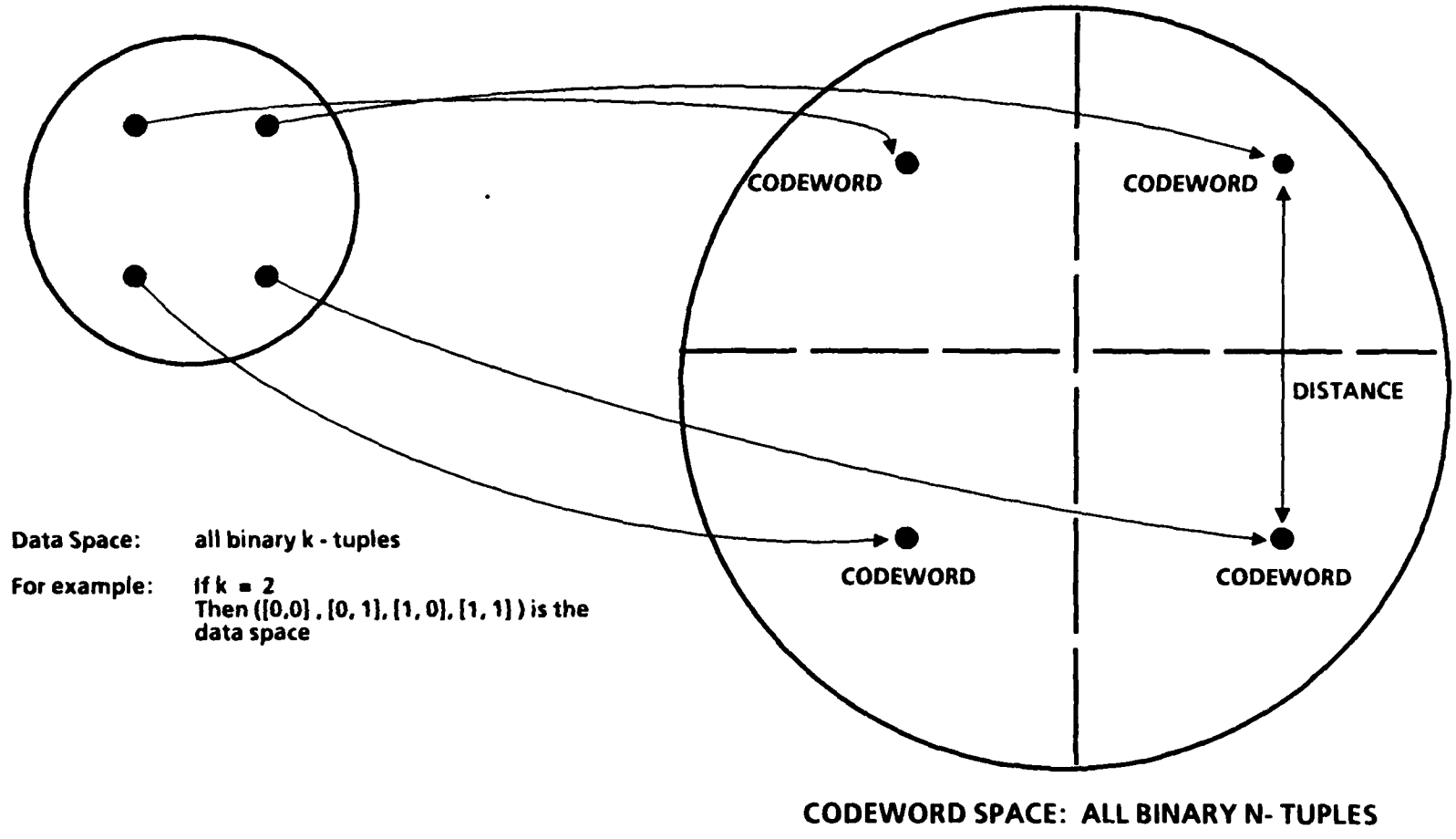

Figure 3.1: Mapping Data into Codeword Space

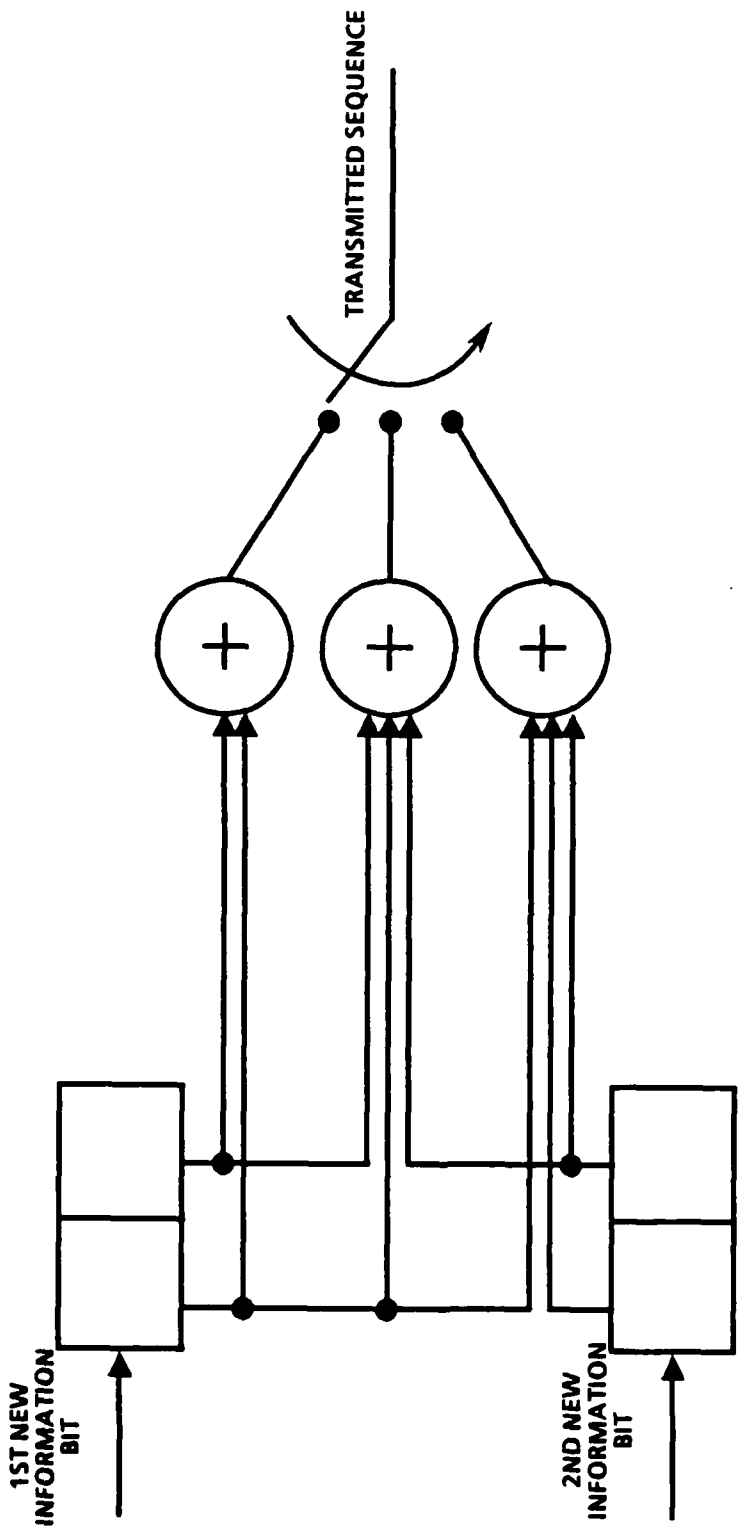

Figure 3.2: Convolutional Encoder for Code with R = 2/3 and v = 2, k = 4

this is an encoder for a rate (R) 2/3 convolutional code. Rate gives the ratio of the transmitted bandwidth without coding to the bandwidth with coding. Generally, improved performance (greater minimum distance) is achieved with codes which have lower rates.

In addition to the two new information bits, the encoder of Figure 3.2 uses two old information bits when it creates the symbols to be transmitted. The number of old bits used is the "constraint length" (v) of the code. Increasing the constraint length usually increases the minimum distance of the code, but also increases the data latency of the coded system.

In this report, convolutional codes with rates 1/2 and 2/3 are considered. In sections 3.2 and 3.3, the rate 1/2 code has a constraint length of 6 and a minimum distance of 10. The rate 2/3 code has $v = 6$ and $d_{min} = 6$. However in section 3.5, we consider smaller constraint lengths, because of data latency concerns.

3.3 Probability of Bit Error

In this section, we bound and approximate the probability of bit error for a digital data link, which employs coding and receivers with either hard limiting or clipping. Our receiver models are shown in Figure 3.3, which also shows a linear receiver. As shown, the limiter and clipper are placed at the output of a filter, which is matched to the channel symbol. Consider one of the codewords in our code

$$x = (x_1, x_2, \ldots x_N)$$

If a $x_n = 0$ has been sent, then the input to the nonlinearity is $V_s + \eta_n$, where V_s is the voltage due to signal and η_n is a sample of filtered atmospheric noise. If a $x_n = 1$ has been sent, then the input to the nonlinearity is $-V_s + \eta_n$. If we normalize the energy in the impulse response of the channel symbol matched filter to unity, then we have the following identities.

$$V_s = \sqrt{E_c}$$

$$\sigma^2 = \frac{N_0}{2}$$

where E_c is the energy in the received symbol and σ^2 is the variance of η.

The output of the nonlinearity is denoted

$$y = (y_1, y_2, \ldots y_N)$$

and is used to form a set of decision statistics for the receiver. The receiver decides the codeword x was sent if and only if

$$\sum_{n=1}^{N} m(y_n, x_n) \geq \sum_{n=1}^{N} m(y_n, \hat{x}_n)$$

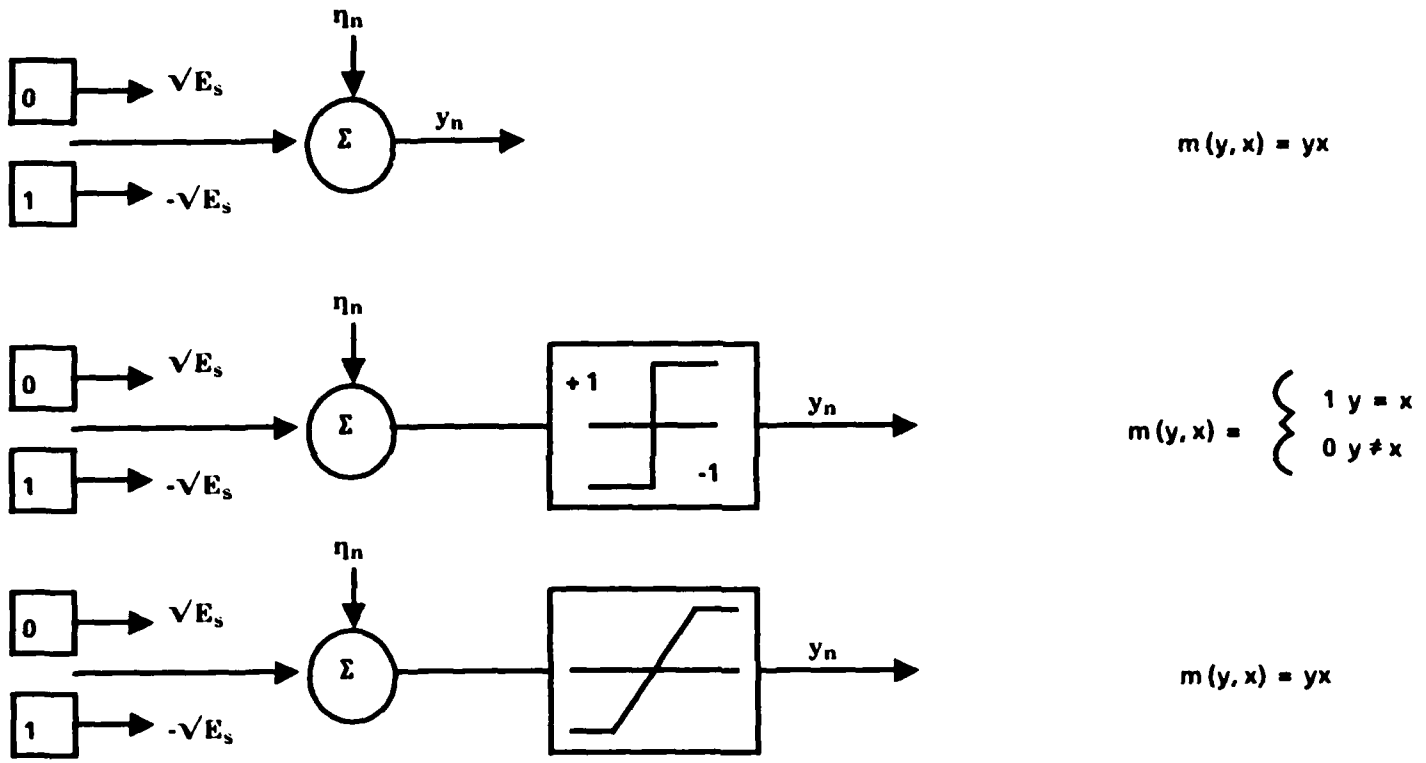

Figure 3.3: Channel/Receiver Models

where $m(y,x)$ is the receiver "metric". The metric for the linear and clipping receiver is

$$m(y,x) = yx$$

and for the hard limiting (or hard decision) receiver is

$$m(y,x) = 1 \quad if\ y = x$$

$$= 0 \quad if\ y \neq x$$

In this paper, we restrict attention to probability of bit error as approximated by the union bound (equ. (6-11) of [7], or equ. (4.4.8) of [14].)

$$P_e \leq \frac{1}{b} \sum_{d=d_f}^{\infty} w_d P_d \tag{3.1}$$

This bound is for a rate $\frac{b}{n}$ code, which has a minimum free distance of d_f. The incorrect paths of weight d have a total information weight of w_d. In this paper, we consider a rate 2/3 convolutional code (constraint length (v) equal to 6), which has $d_f = 6$, $w_6 = 1$, $w_7 = 81$, $w_8 = 402$ ([7]). We also consider a rate 1/2 code (v=6), which has $d_f = 10$, $w_{10} = 36$, $w_{11} = 0$, $w_{12} = 211$, $w_{13} = 0$, and $w_{14} = 1404$.

P_d is the pairwise error probability for 2 sequences separated by Hamming distance d. Consequently, if x and $\hat{x}$ differ in d locations, then

$$P_d = Pr(\sum_{n=1}^{N} m(y_n, x_n) \leq \sum_{n=1}^{N} m(y_n, x_n) \mid x\ sent) \tag{3.2}$$

We now compute P_d under the following assumptions:

- The noise samples η_n and η_m are independent for $n \neq m$. For atmospheric noise, which does occur in bursts, this assumption is equivalent to assuming ideal interleaving.

- The distribution of the instantaneous noise envelope is well modelled by the curves in Figure 83 from Report 322 [4] of the International Radio Consultative Committee (CCIR). These curves give the cumulative exceedance distribution (unity minus the distribution function) of the noise envelope relative to the rms value of the envelope. They are parameterized by the models single variable: voltage deviation (V_d)

$$V_d = 20log_{10} \frac{r}{\bar{r}}$$

where r is the noise envelope. The CCIR model is empirically derived and difficult to express with simple mathematical expressions. However, its "tails" are "power

Rayleigh" ([12]) and a computer program (APDAN) exists ([1]), which returns values of the exceedance distribution for a given value of envelope and voltage deviation. We have modified APDAN so it also returns the envelope density function ($f_R(r)$) and we use this feature extensively in what follows.

- Finally we assume that the skywave/groundwave interference is such that the fade depth is constant. This assumption is reasonable, because the skywave phase and amplitude have a long correlation time (tens of minutes) at LF and lower MF frequencies.

With independent noise samples (η_n) we may apply the Chernoff bound to equation (2)

$$P_d \leq \min_{\lambda \geq 0} \prod_{n=1}^{N} E(exp\lambda(m(y_n, \hat{x}_n) - m(y_n, x_n)) \mid x_n)$$

If we define

$$D = \min_{\lambda \geq 0} E(exp\lambda(m(y_n, \hat{x}_n) - m(y_n, x_n)) \mid x_n)$$

$$= \min_{\lambda \geq 0} D(\lambda)$$

then, we have

$$P_d \leq D^{w_H(x,\hat{x})} \tag{3.3}$$

where $w_H(x, \hat{x})$ is the Hamming distance between x and $\hat{x}$.

For a hard limiter,

$$D = \sqrt{4\epsilon(1-\epsilon)} \tag{3.4}$$

where

$$\epsilon = Pr(\eta \geq \sqrt{E_s})$$

We can compute ϵ as a function of the envelope density provided by APDAN by using a result from [12]

$$\epsilon = \frac{1}{\pi} \int_{\sqrt{E_s}}^{\infty} p_R(r) cos^{-1}\left(\frac{\sqrt{E_s}}{r}\right) dr \tag{3.5}$$

For a clipper, we have

$$D(\lambda) = E(exp\lambda(\hat{x}_n y_n - x_n y_n) \mid x_n)$$

$$= E(exp\lambda y_n(-2\sqrt{E_s}))$$

For simplicity, we consider a piecewise constant clipper with $2I + 1$ pieces and which clips at $y = clip\sigma_\eta$. In this case

$$D(\lambda) = \sum_{i=-I}^{I} exp(\lambda(-2\sqrt{E_s})\frac{iclip\sigma_\eta}{I})Pr(\eta + \sqrt{E_s} \text{ is in the } i-th \text{ region}) \qquad (3.6)$$

Note that the piecewise constant clipper is particularly convenient, because minimization over λ may be performed after computation of the probabilities. We have used inequalities (1) and (3) and equation (7) to compute the probability of error bounds shown in Figures 3.4 and 3.5 for the rate 1/2 code and the rate 2/3 code, respectively. These results can be compared to Figure 3.6, which gives $Pr(\epsilon)$ for a very "weak" repetition code. The performance of the repetition code is nearly the same as the performance of a link without coding.

For hard decisions, the Chernoff bound on P_d computed above can be compared to exact results by using the binomial distribution. For d odd, we have

$$P_d = \sum_{k=0}^{\frac{d-1}{2}} (1-\epsilon)^k \epsilon^{d-k} \begin{pmatrix} d \\ k \end{pmatrix}$$

For d even

$$P_d = \sum_{k=0}^{\frac{d}{2}-1} (1-\epsilon)^k \epsilon^{d-k} \begin{pmatrix} d \\ k \end{pmatrix} + \frac{1}{2}(1-\epsilon)^{d/2}\epsilon^{d/2} \begin{pmatrix} d \\ d/2 \end{pmatrix}$$

These results are shown in Figures 3.7 and 3.8. The results in these Figures were compared to the Chernoff bound results for hard decisions and found to be in close agreement. The performance of the weak repetition code using hard decisions is shown in Figure 3.9 for comparison.

3.4 Probability of Link Availability

In this section, we compute the probability of link availability as a function of range from the transmitter. In other words, we compute the probability that the signal to noise ratio will be large enough to achieve a specified $Pr(bit\ error)$. For this component of our analysis, we make the following assumptions:

- Noise power is accurately modelled by Report 85-173 of the National Telecommunications and Information Administration (NTIA). This report uses a sequence of 24 world maps to plot the average noise measured by a worldwide network of noise monitors over the past 9 years. Each map gives contours of equal noise level and corresponds to one of 24 season-time blocks. The four seasons are, of course, winter, spring, summer, and fall and the six time blocks are 0000-0400, 0400-0800, etc. Each map has a curve which allows translation of the plotted value of noise power to any

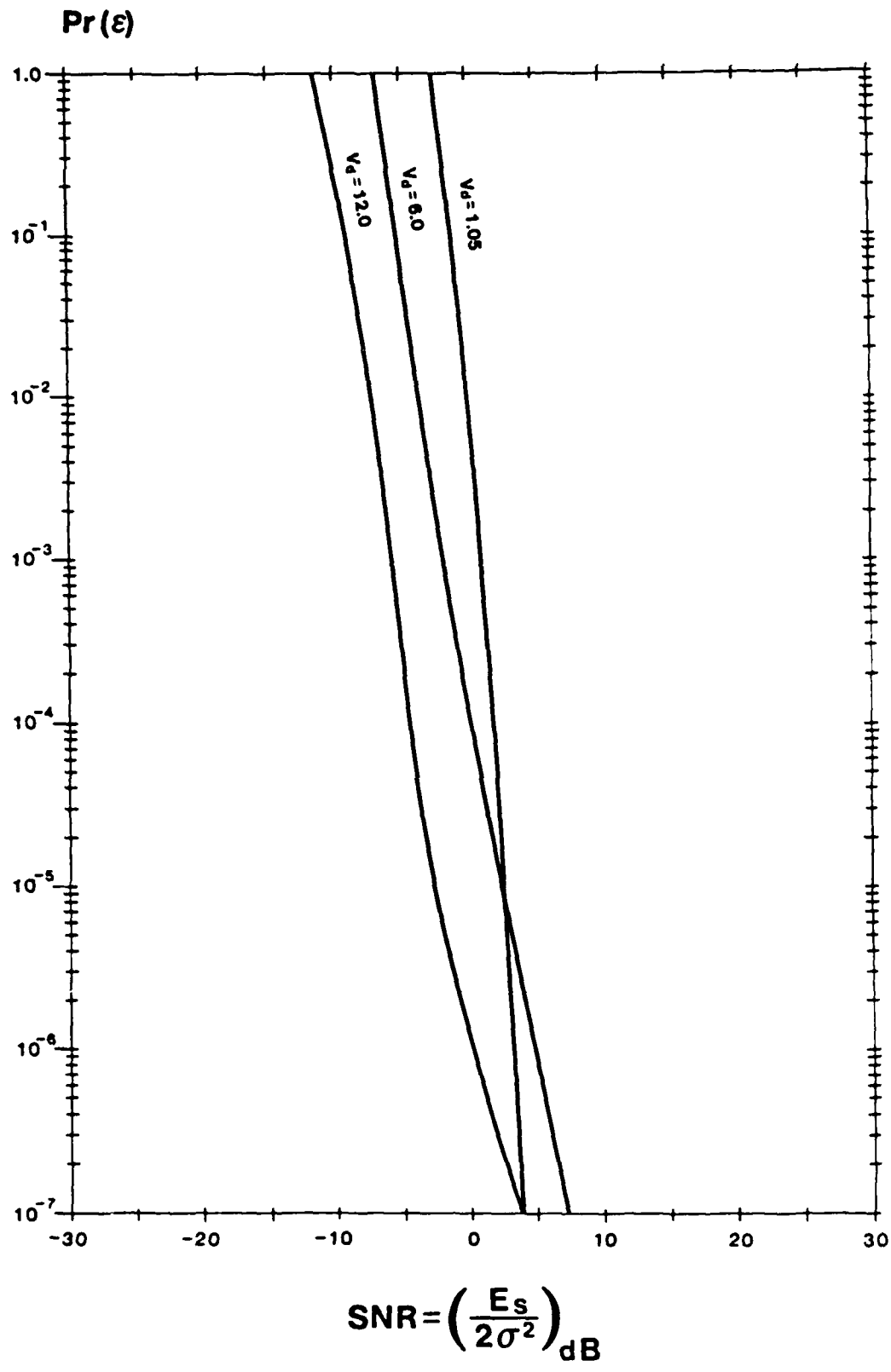

Figure 3.4: Chernoff Bound, Rate 1/2 Convolutional Code, Clipping Receiver (Clip = 1σ)

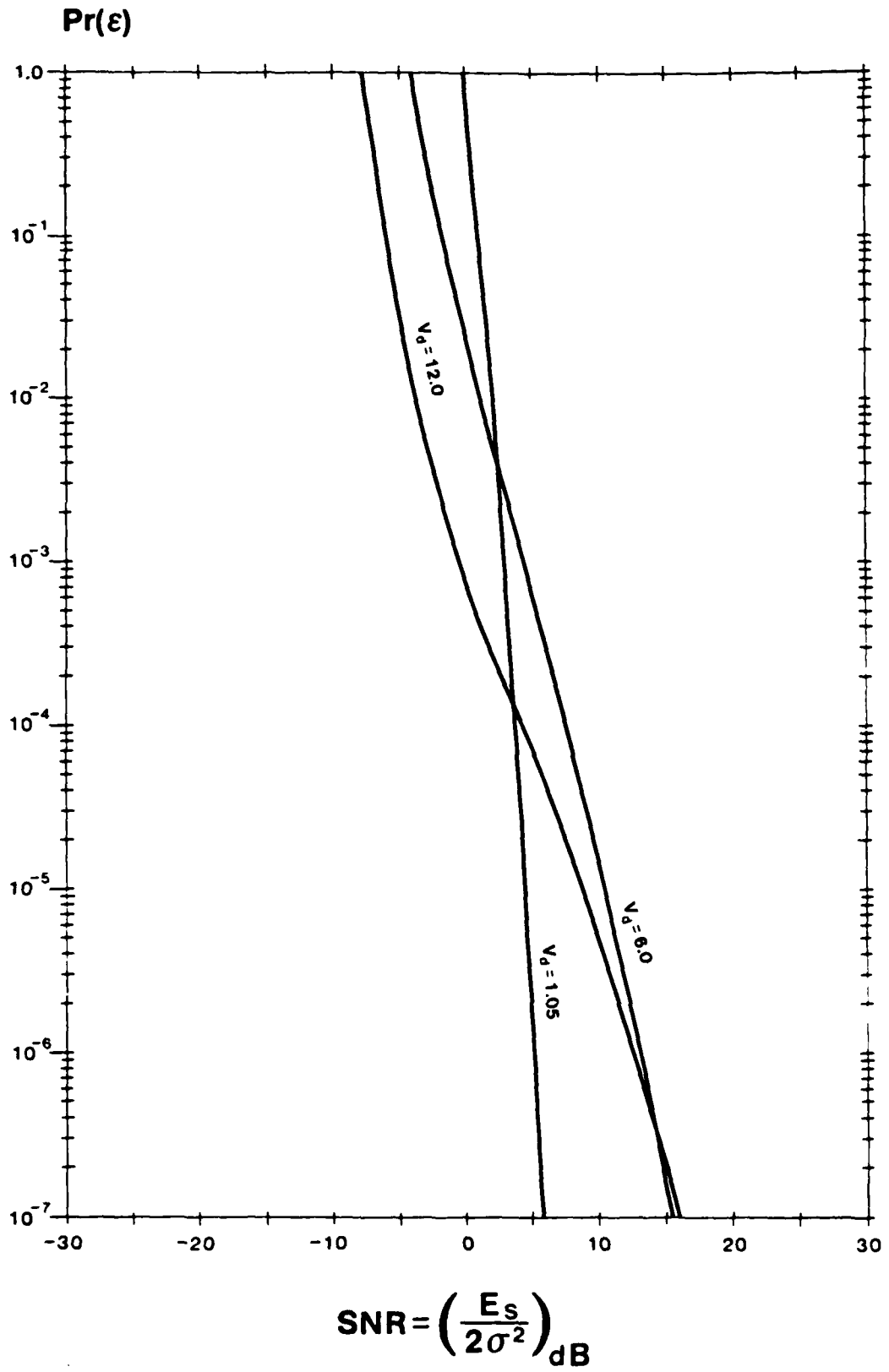

Figure 3.5: Chernoff Bound, Rate 2/3 Convolutional Code, Clipping Receiver (Clip = 1σ)

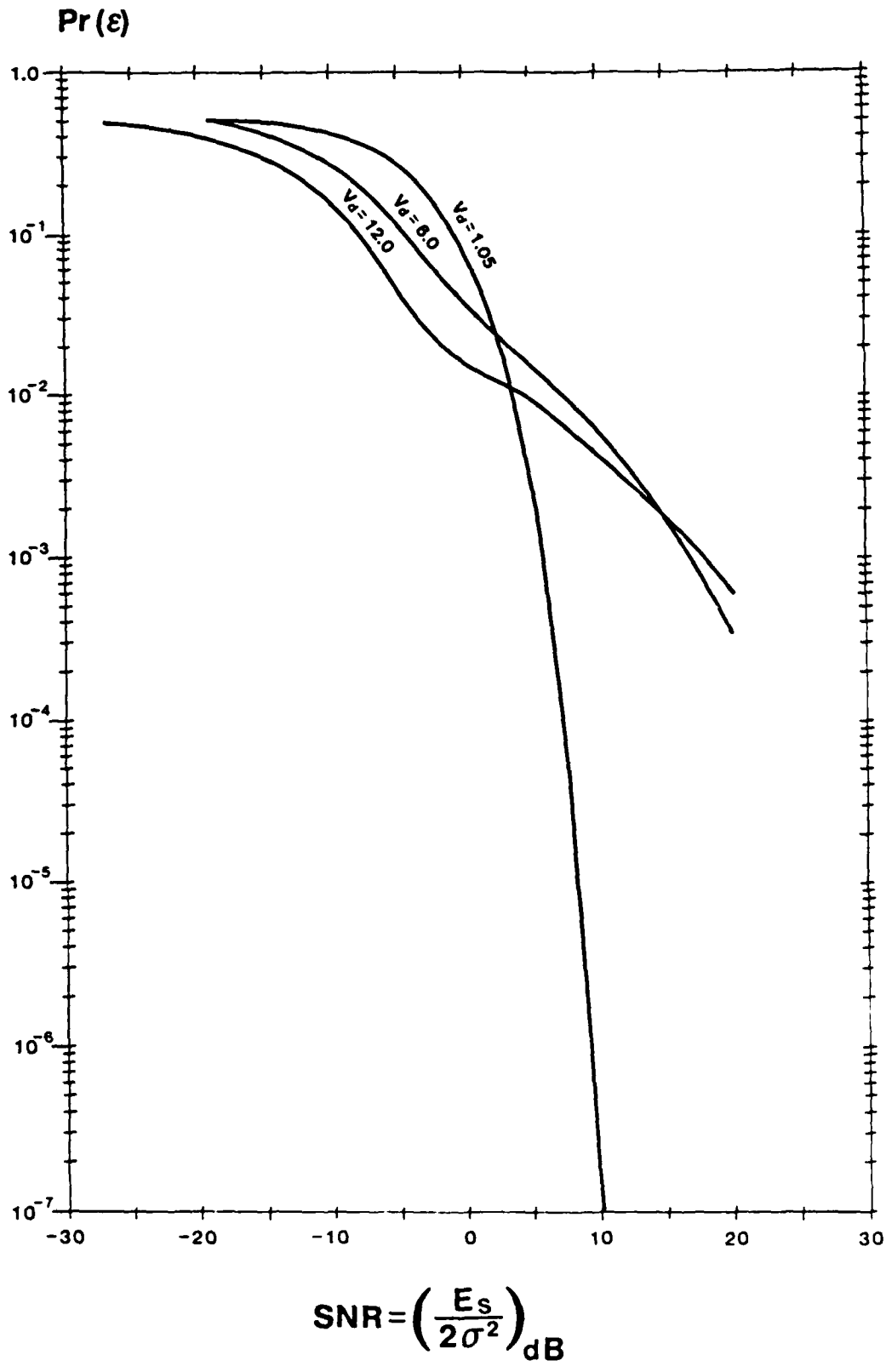

Figure 3.6: Chernoff Bound, Rate 1 2 Repetition Code, Clipping Receiver (Clip = 1σ)

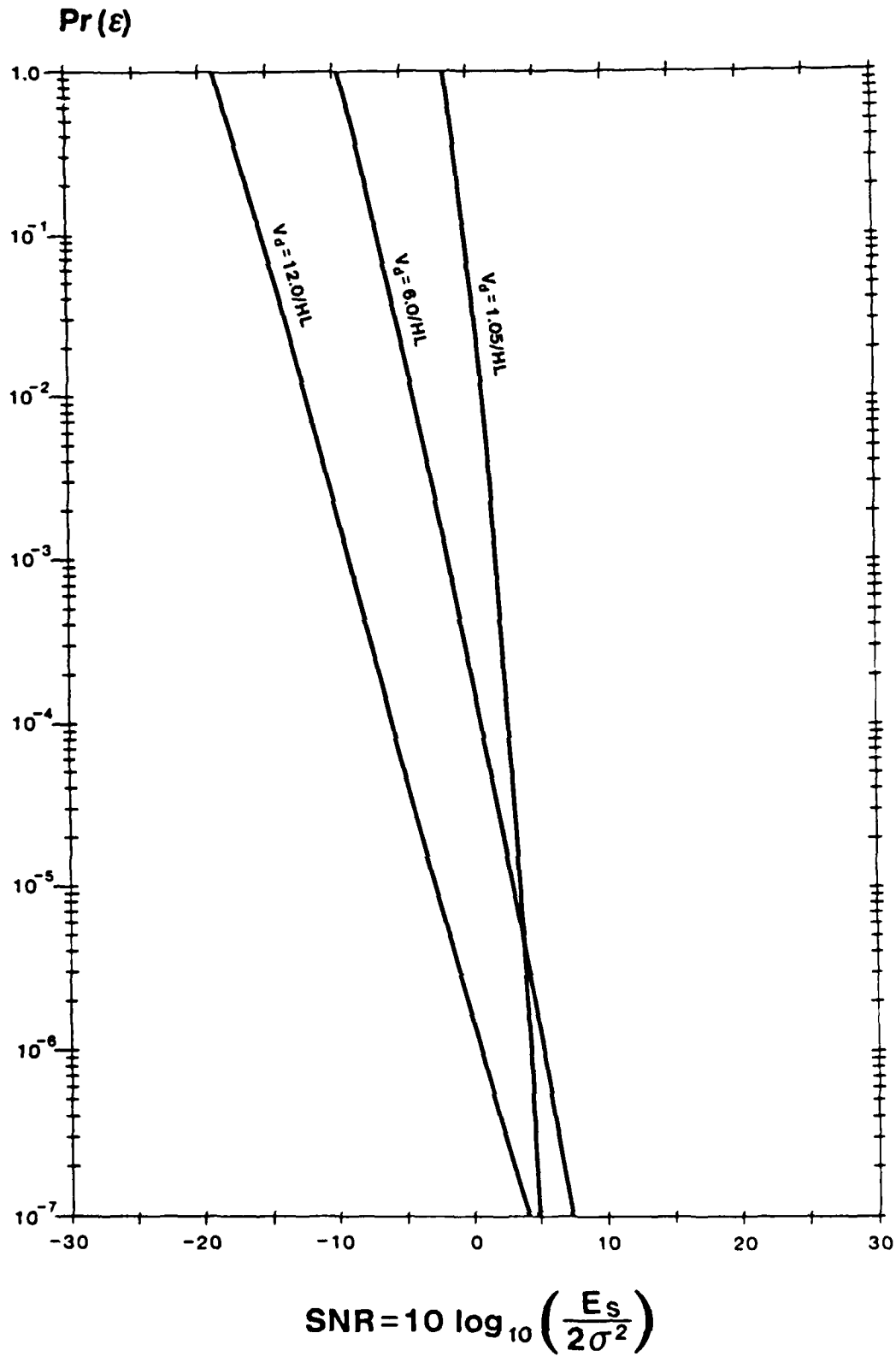

Figure 3.7: Binomial Distribution, Rate 1 2 Convolutional Code. Hard Limiting Receiver

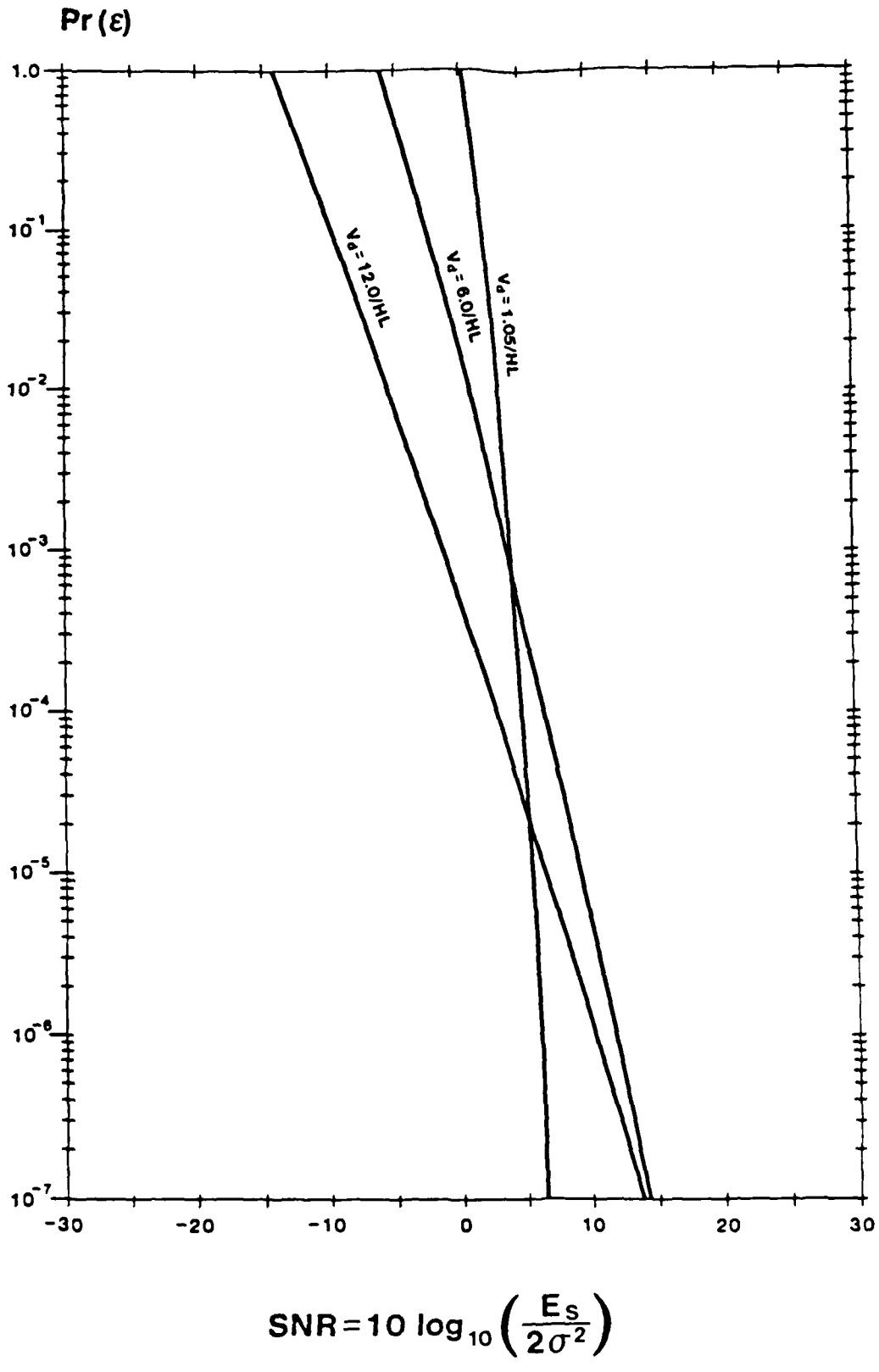

Figure 3.8: Binomial Distribution, Rate 2 3 Convolutional Code, Hard Limiting Receiver

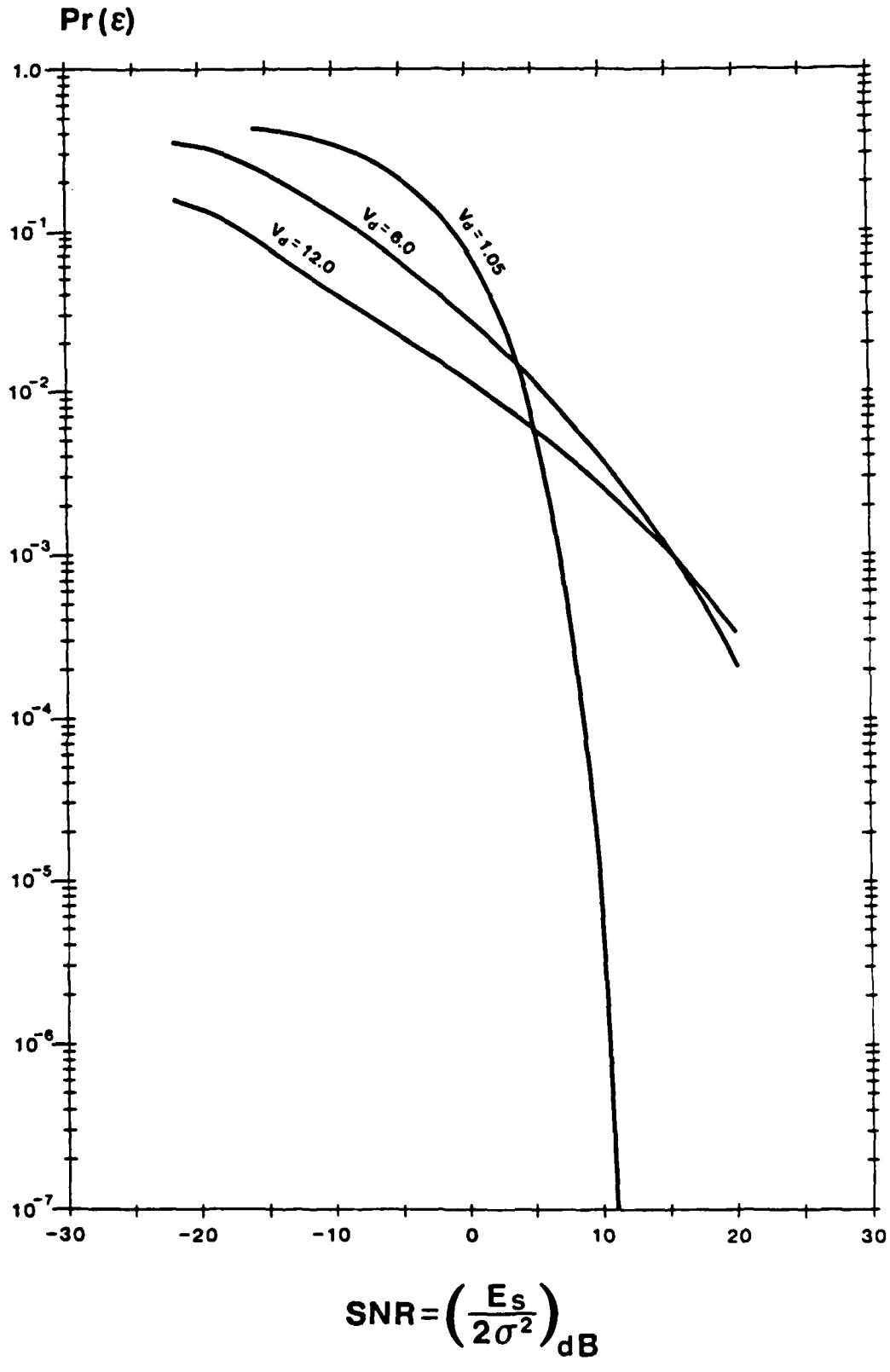

Figure 3.9: Binomial Distribution, Rate 1/2 Repetition Code, Hard Limiting Receiver

frequency. For a given season-time block, the variation of measured noise power (in decibels) away from the average noise power is adequately represented by a two-sided Gaussian distribution. For values of noise power below the average noise power, one standard deviation ($\sigma_{\eta,l}$) applies and for values of noise power above the average another standard deviation ($\sigma_{\eta,u}$) applies. Both $\sigma_{\eta,l}$ and $\sigma_{\eta,u}$ can be computed using the NTIA Report.

- Groundwave field strength is accurately predicted using the curves in [3]. These curves give field strength versus distance with center frequency and ground conductivity as parameters. The example curves we present later assume a center frequency of 300 kHz and propagation over seawater.

- Skywave field strength is accurately modelled by the techniques summarized in CCIR Report 575-1. These methods use the following form for the median skywave field strength

$$\overline{S}(dB\ above\ 1\mu V/m) = C - s(d) + P + \triangle_A - \triangle_t$$

where C is a constant which depends on the prediction method used and $s(d)$ gives distance dependence. P is a correction for transmitters which radiate other than 1kW and the $\triangle_k$ belong to set of correction factors. In our case, we use the correction factors for the vertical directivity of the transmitting antenna ($\triangle_A$) and time of day ($\triangle_t$). The distribution of skywave field strength away from its median may be estimated by using a set of curves in [5]. For the times when the median skywave is strong, we find that the distribution of skywave strength (in decibels) is well approximated by another 2-sided Gaussian distribution. In other words, 2 standard deviations ($\sigma_{S,u}$ *and* $\sigma_{S,l}$) will approximately characterize the random variations of skywave at a given time.

- Finally, we assume that the relative phase of the received groundwave and skywave is uniform on $[0, 2\pi)$. This assumption seems reasonable at 300 kHz where the wavelength (1000 *meters*) is reasonably small compared to the irregularites in ionospheric height.

In the case of groundwave only propagation, we can write

$$Pr(linkavailable) = Pr(SNR \geq k) = Pr(\frac{E_s}{N_o} \geq k)$$

$$= Pr(E_{n,dB} \leq -k_{dB} + G_{dB} + P) \tag{3.7}$$

where $E_{n,dB}$ is the noise power in decibels above $1\mu V/m$. k_{dB} is the required signal to noise ratio from Figures 3.4 through 3.9. G_{dB} is the groundwave power for a radiated power of

$1kW$ and P accounts for radiated power other than $1kW$. Since decibel values of noise strength have a 2 sided normal distribution,

$$Pr(link\ available)$$

$$= 1 - Q\left(\frac{-k_{dB} + G_{dB} + P_{dB} - \overline{E}_{n,dB}}{\sigma_{\eta,l}}\right) \quad if \ -k_{dB} + G_{dB} + P_{dB} \leq \overline{E}_{dB}$$

$$= 1 - Q\left(\frac{-k_{dB} + G_{dB} + P_{dB} - \overline{E}_{n,dB}}{\sigma_{\eta,u}}\right) \quad if \ -k_{dB} + G_{dB} + P_{dB} > \overline{E}_{dB} \qquad (3.8)$$

In the case of groundwave and skywave propagation, our analysis is more complicated. At short ranges ($\leq$ 200 km.), groundwave will certainly dominate skywave and $Pr(link\ available)$ will be unaltered. At intermediate ranges (200 to 700 kilometers), the possibility of groundwave skywave interference should reduce the $Pr(link\ available)$. At long ranges (greater than 700 kilometers), skywave will certainly dominate groundwave and $Pr(link\ available)$ should increase.

Our analysis begins with the following definition

$$R_{dB} = G_{dB} + F_{dB}$$

where R_{dB} is the received signal strength. G_{dB} is the received groundwave strength and therefore the effect of skywave is contained in F_{dB}. ($-F_{dB}$ can be interpreted as fade depth.) Using linear quantities, we get

$$R = FG = | G + S\cos\theta |$$

or

$$F = | 1 + \frac{S}{G}\cos\theta |$$

where S is the skywave strength in microvolts per meter and θ is the phase of the received skywave relative to groundwave. It is convenient to define the skywave strength normalized by the groundwave strength as

$$\hat{S} = \frac{S}{G}$$

$$\hat{S}_{dB} = S_{dB} - G_{dB}$$

Clearly, $\hat{S}_{dB}$ has a "two-sided" Gaussian distribution with mean $\overline{S}_{dB} - G_{dB}$ and "standard deviations" $\sigma_{S,u}$ and $\sigma_{S,l}$.

We can now write

$$Pr(link\ available) \approx \sum_{i} Pr(SNR > k \mid f_{i,dB} - \Delta < F_{dB} \leq f_{i,dB} + \Delta) \qquad (3.9)$$

$$Pr(f_{i,dB} - \Delta < F_{dB} \leq f_{i,dB} + \Delta)$$

where we have approximated an integral by a sum. The first term in the above sum can be written as

$$Pr(SNR > k \mid f_{i,dB} - \triangle < F_{dB} \leq f_{i,dB} + \triangle)$$
$$\approx Pr(E_{n,dB} \leq -k_{dB} + G_{dB} + P + f_{i,dB}) \tag{3.10}$$

Unfortunately, the second term in the above sum requires more work.

$$Pr(f_{i,dB} - \triangle < F_{dB} \leq f_{i,dB} + \triangle)$$
$$= P_F(10^{(f_{i,dB}+\triangle)/20}) - P_F(10^{(f_{i,dB}-\triangle)/20}) \tag{3.11}$$

where $P_F(f) = Pr(F < f)$ is the distribution function of F. With $F = \mid 1 + \hat{S}cos\theta \mid$, we find

$$P_F(f) = \int_D \int p_{\hat{S},\theta}(\hat{S},\theta) d\hat{S} d\theta$$

where D is the region where $\mid 1 + \hat{S}cos\theta \mid \leq f$. After some algebra, we find that if f is less than one, then

$$P_F(f) = \frac{1}{\pi} \int_{\pi/2}^{\pi} P_{\hat{S},dB}(20log_{10}(\frac{1+f}{-cos\theta})) - P_{\hat{S},dB}(20log_{10}(\frac{1-f}{-cos\theta}))d\theta \tag{3.12}$$

where $P_{\hat{S},dB}$ is a two sided Gaussian distribution.

$$P_{\hat{S},dB}(x) =$$

$$1 - Q\left(\frac{x - \overline{S}_{dB} + G_{dB}}{\sigma_{s,l}}\right) \quad if\ x \leq \overline{S}_{dB} - G_{dB}$$

$$1 - Q\left(\frac{x - \overline{S}_{dB} + G_{dB}}{\sigma_{s,u}}\right) \quad if\ x > \overline{S}_{dB} - G_{dB}$$

If f is greater than 1, then

$$P_F(f) = \frac{1}{\pi} \int_0^{\pi/2} P_{\hat{S},dB}(\frac{f-1}{cos\theta})d\theta + \frac{1}{\pi} \int_{\pi/2}^{\pi} P_{\hat{S},dB}(\frac{f+1}{-cos\theta})d\theta \tag{3.13}$$

Equations (3.8) through (3.13) have been used to generate Figures 3.10 through 3.20, and these Figures are parameterized by the quantity $k_{dB} - P$.

As shown, as $k_{dB} - P$ increases the range of reliable communication decreases. This is reasonable, because increasing k_{dB} means the required signal to noise ratio is increasing. Decreasing P means that less power is being radiated relative to 1 kW. The Figures show separate curves for groundwave only propagation and combined groundwave/skywave propagation. As shown, groundwave only propagation would give more reliable service at short and medium ranges, but would give less reliable service for longer ranges. The combined propagation modes do result in possible fading effects at medium ranges. Figures 3.10 through 3.20 are further discussed in the next section.

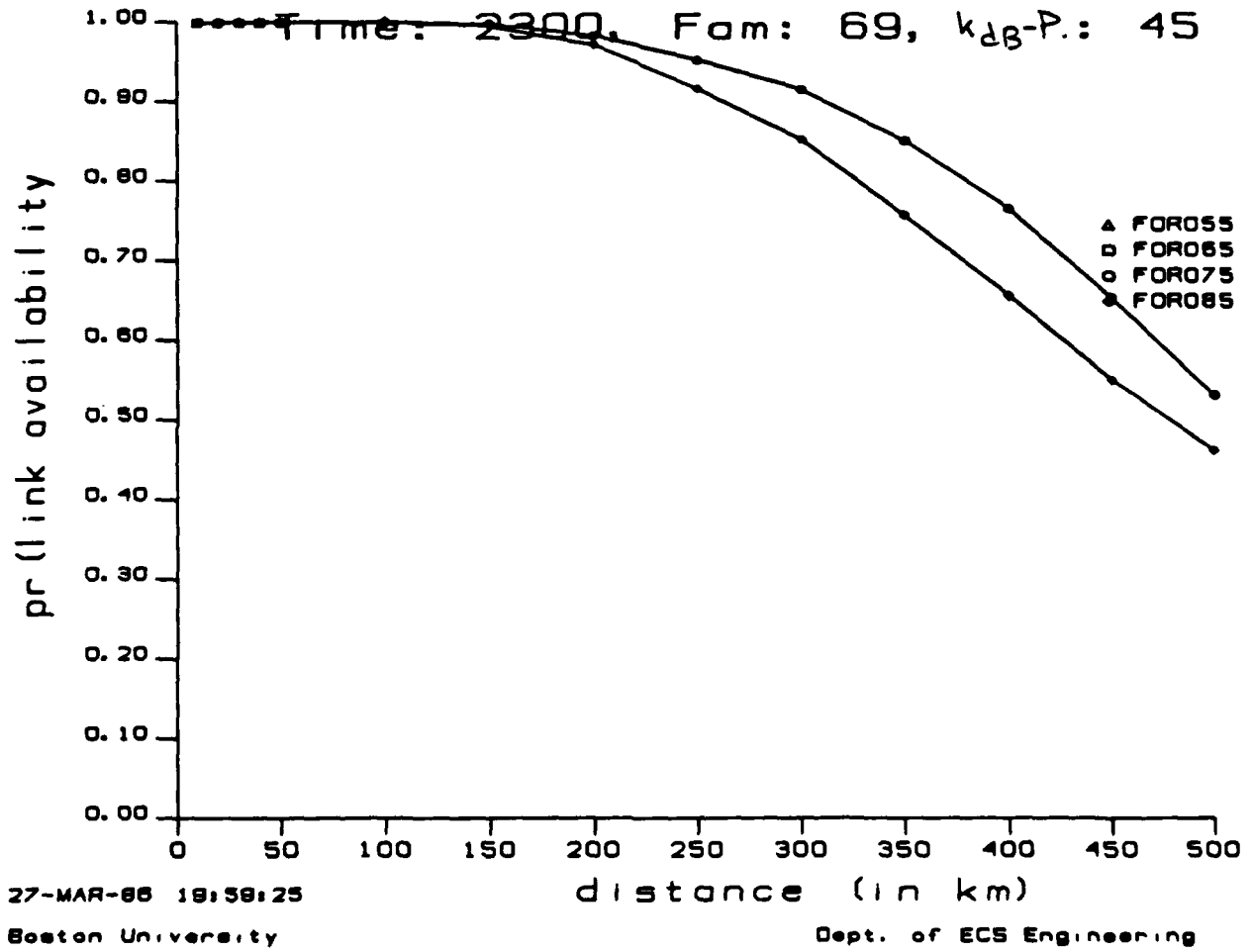

Figure 3.10: Pr(Link Availability) for 2300 hr, $F_{am} = 69$, and $k_{dB} - P = 45$

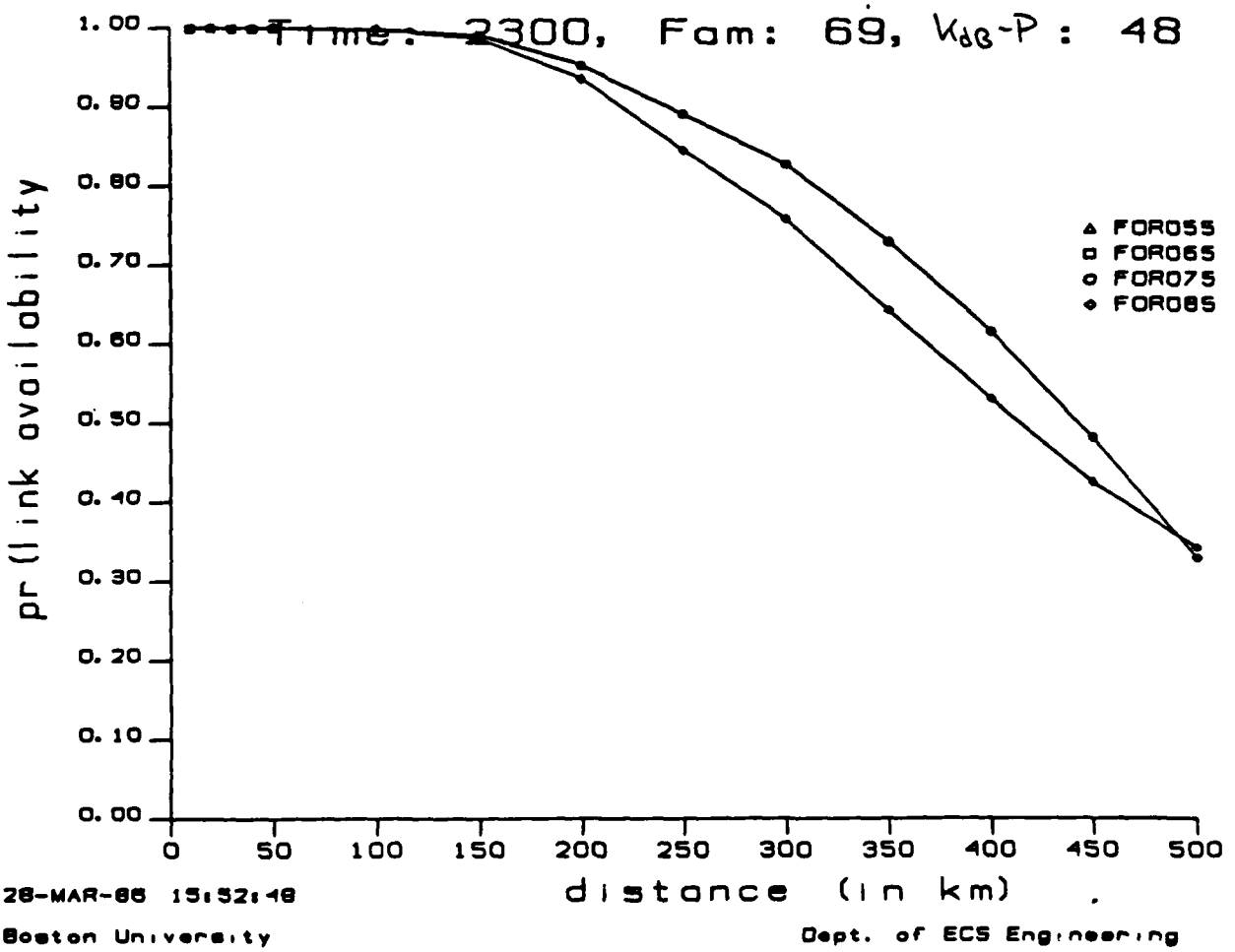

Figure 3.11: Pr(Link Availability) for 2300 hr, $F_{am} = 69$, and $k_{dB} - P = 48$

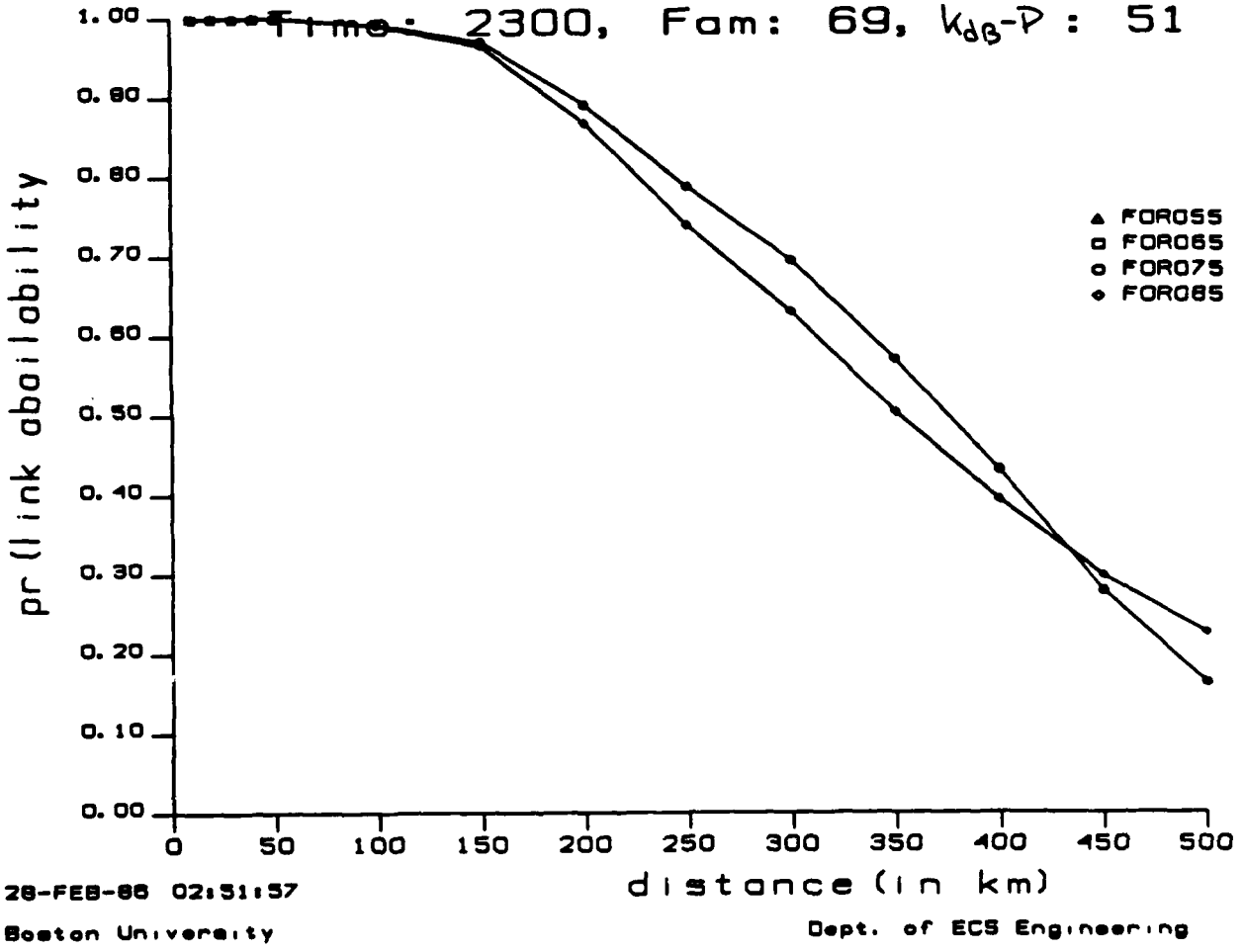

Figure 3.12: Pr(Link Availability) for 2300 hr, F_{am} = 69, and $k_{dB} - P$ = 51

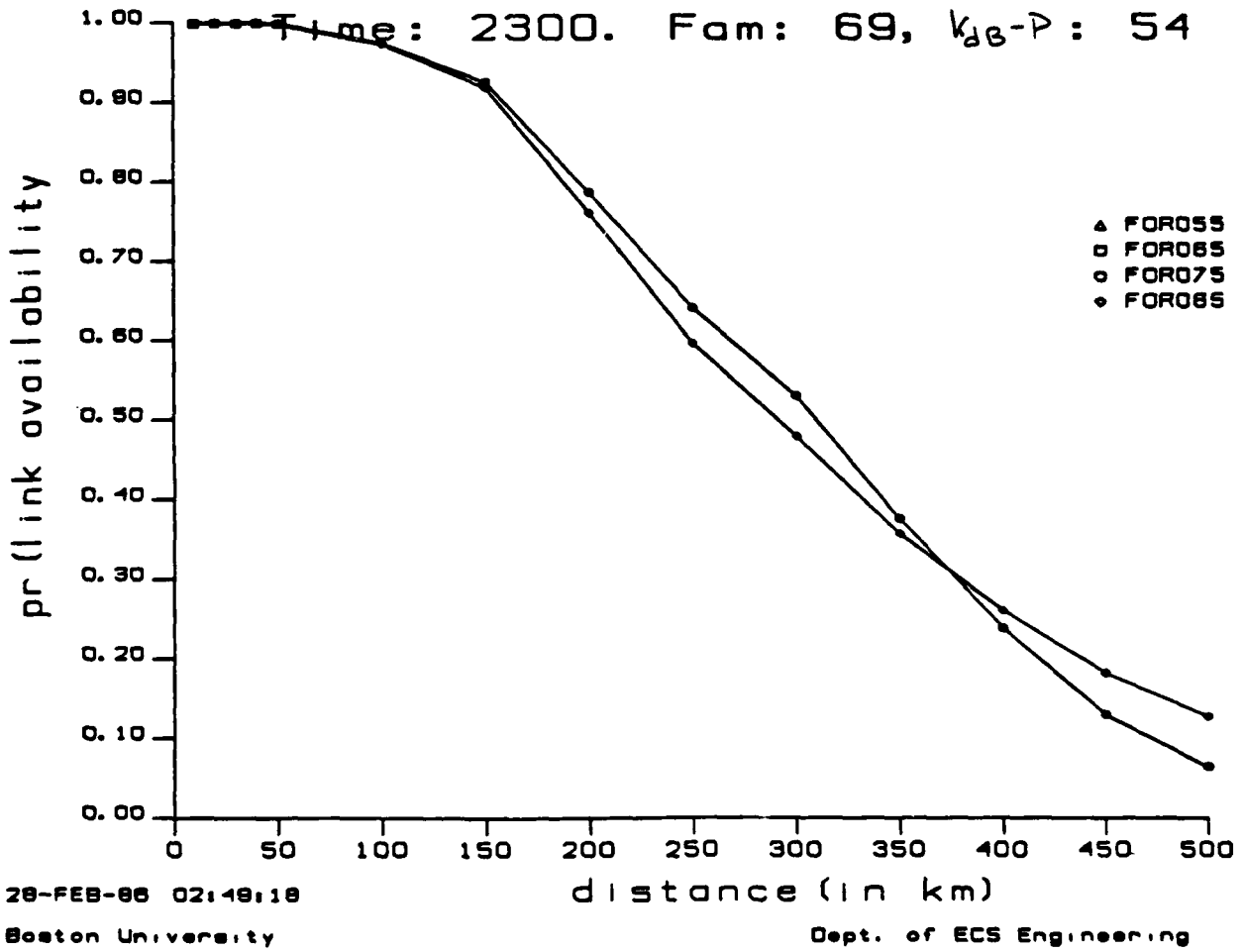

Figure 3.13: Pr(Link Availability) for 2300 hr, $F_{am} = 69$, and $k_{dB} - P = 54$

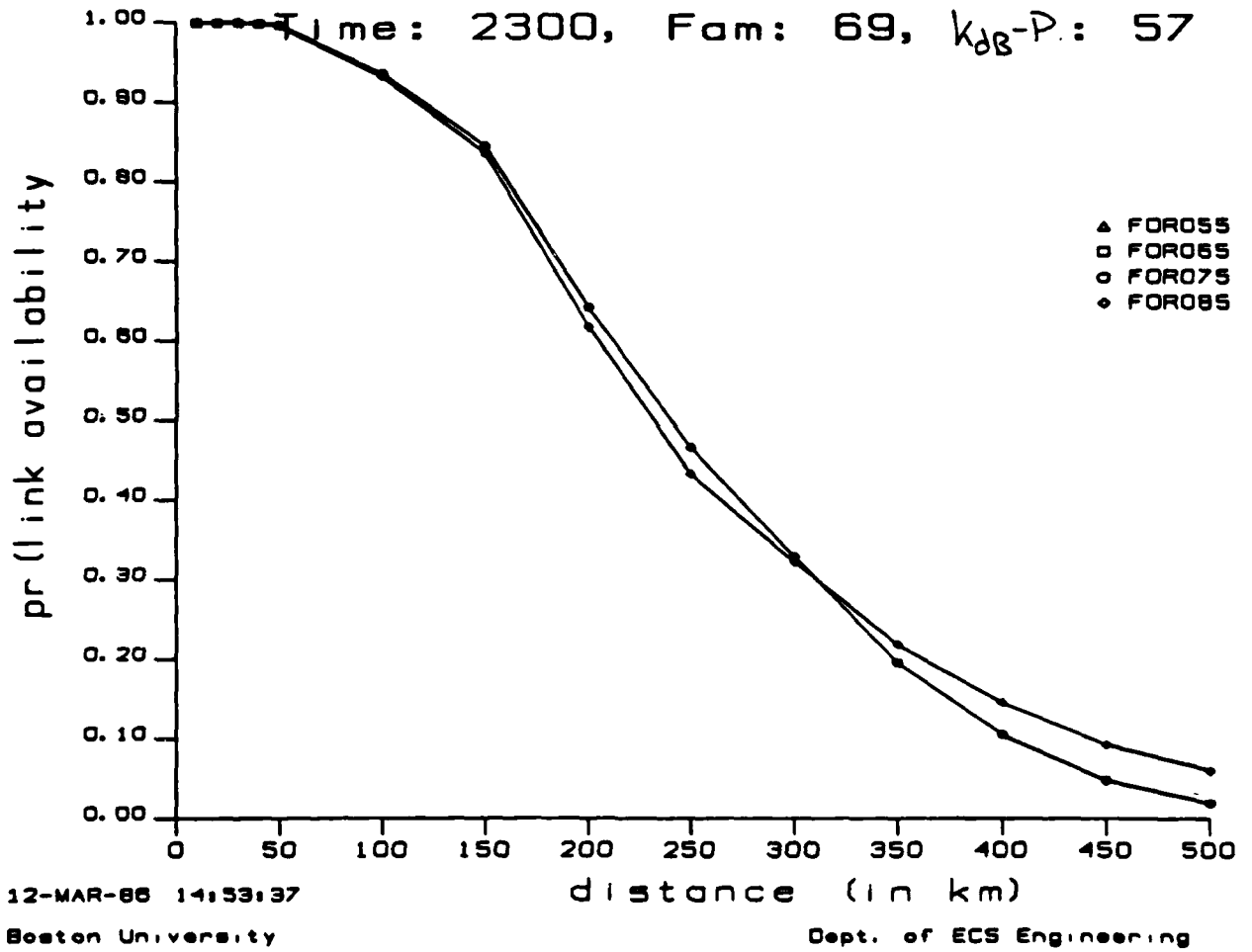

Figure 3.14: Pr(Link Availability) for 2300 hr, $F_{am} = 69$, and $k_{dB} - P = 57$

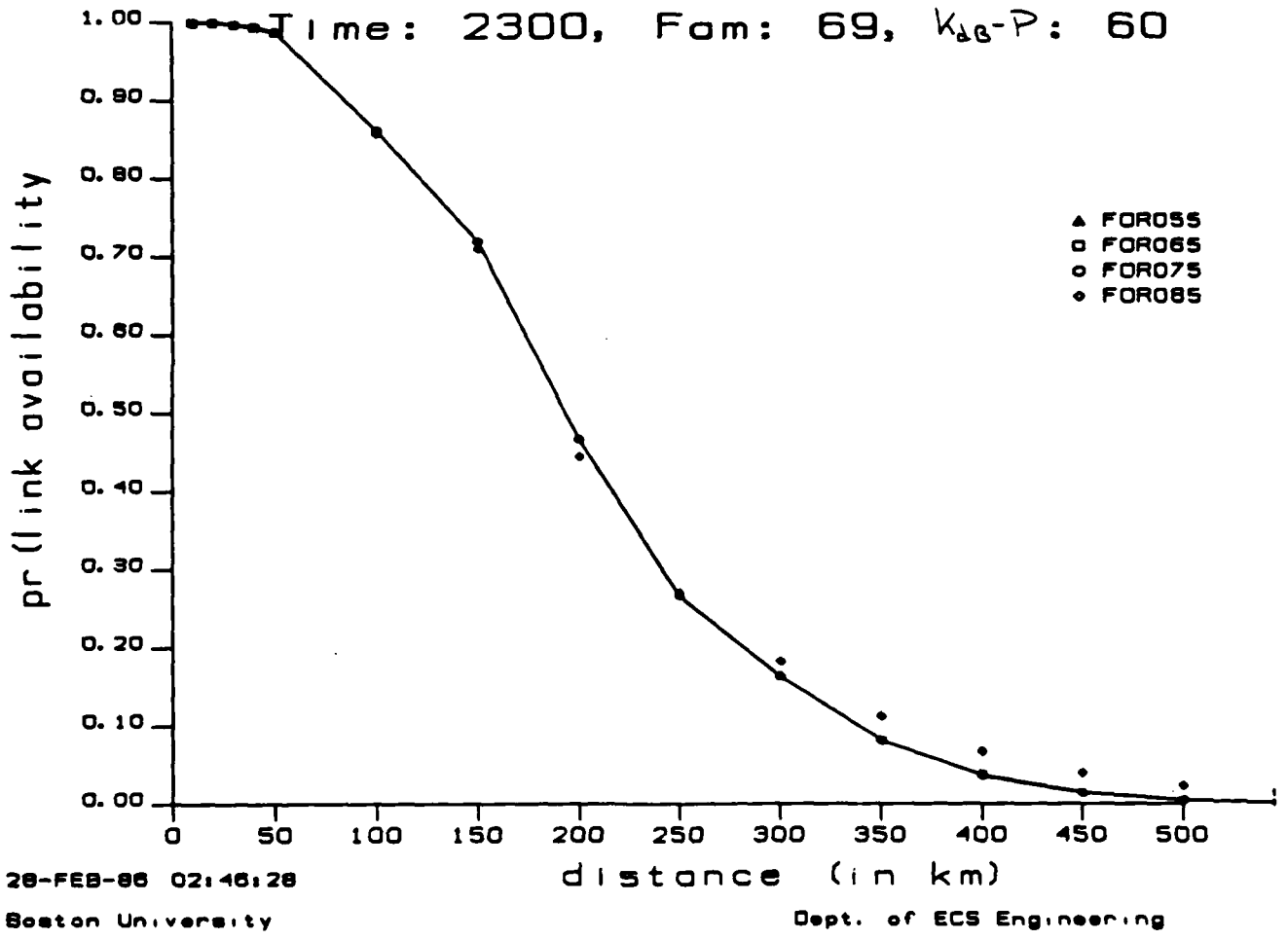

Figure 3.15: Pr(Link Availability) for 2300 hr, $F_{am} = 69$, and $k_{dB} - P = 60$

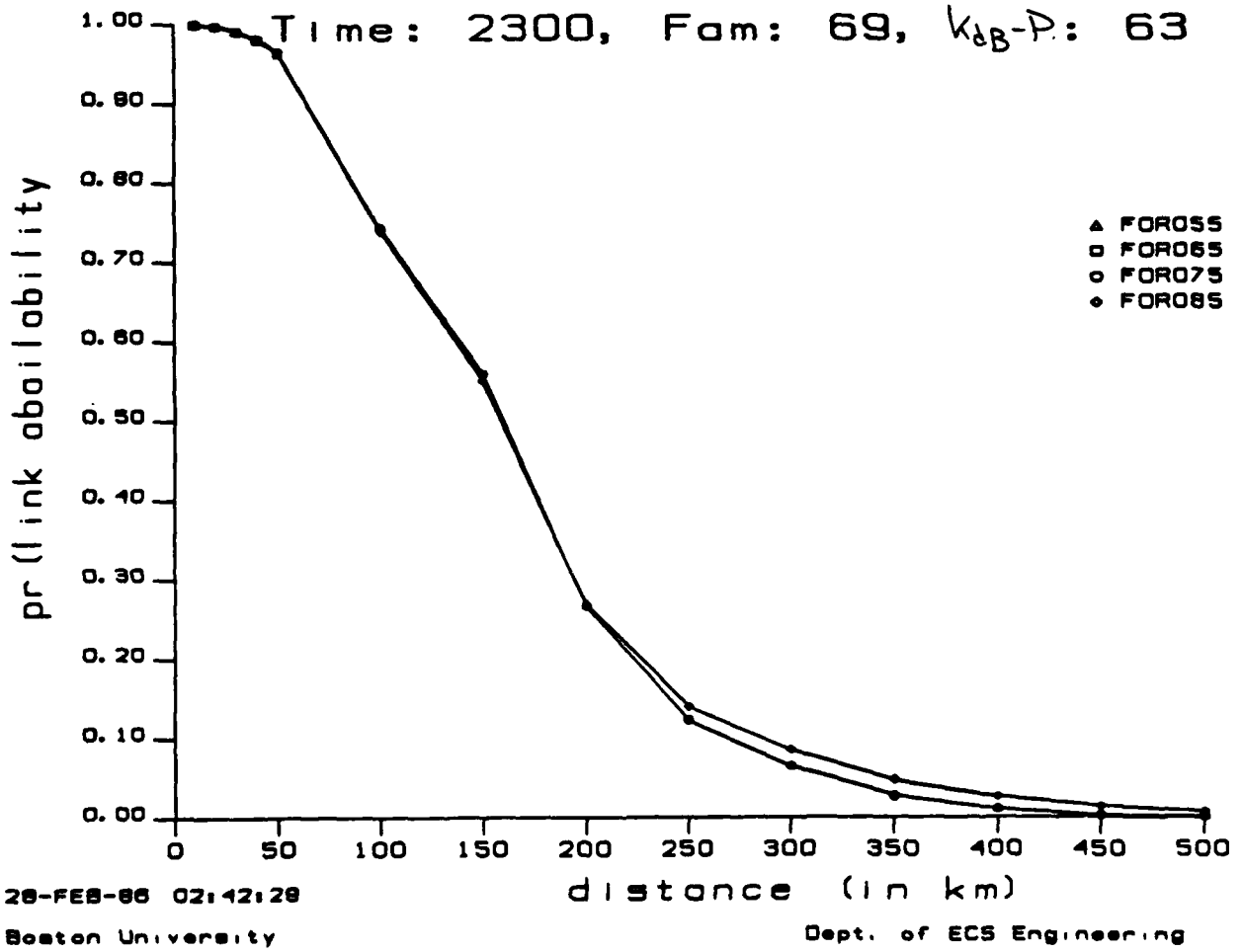

Figure 3.16: Pr(Link Availability) for 2300 hr, F_{am} = 69, and $k_{dB} - P$ = 63

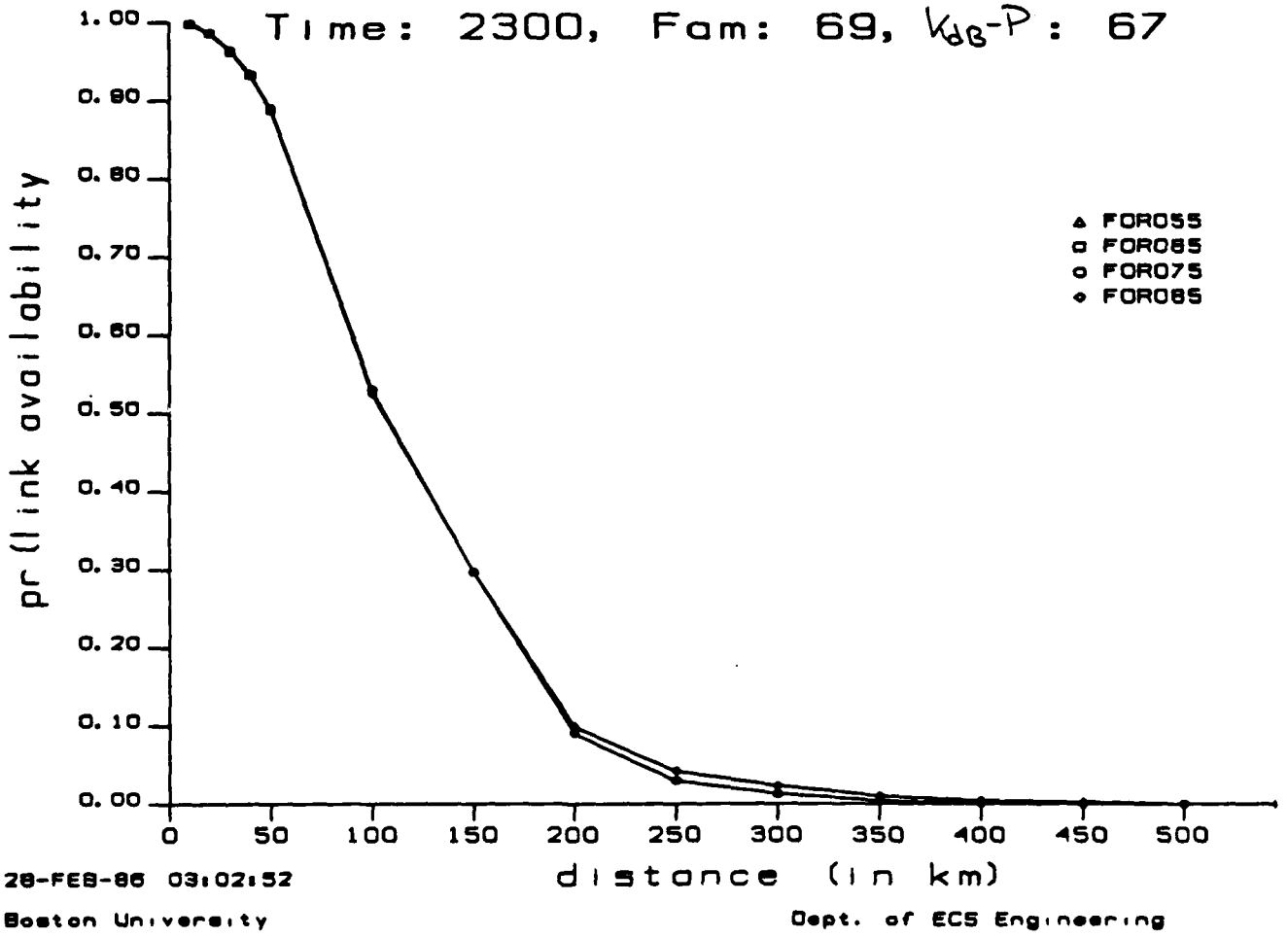

Figure 3.17: Pr(Link Availability) for 2300 hr, $F_{am} = 69$, and $k_{dB} - P = 67$

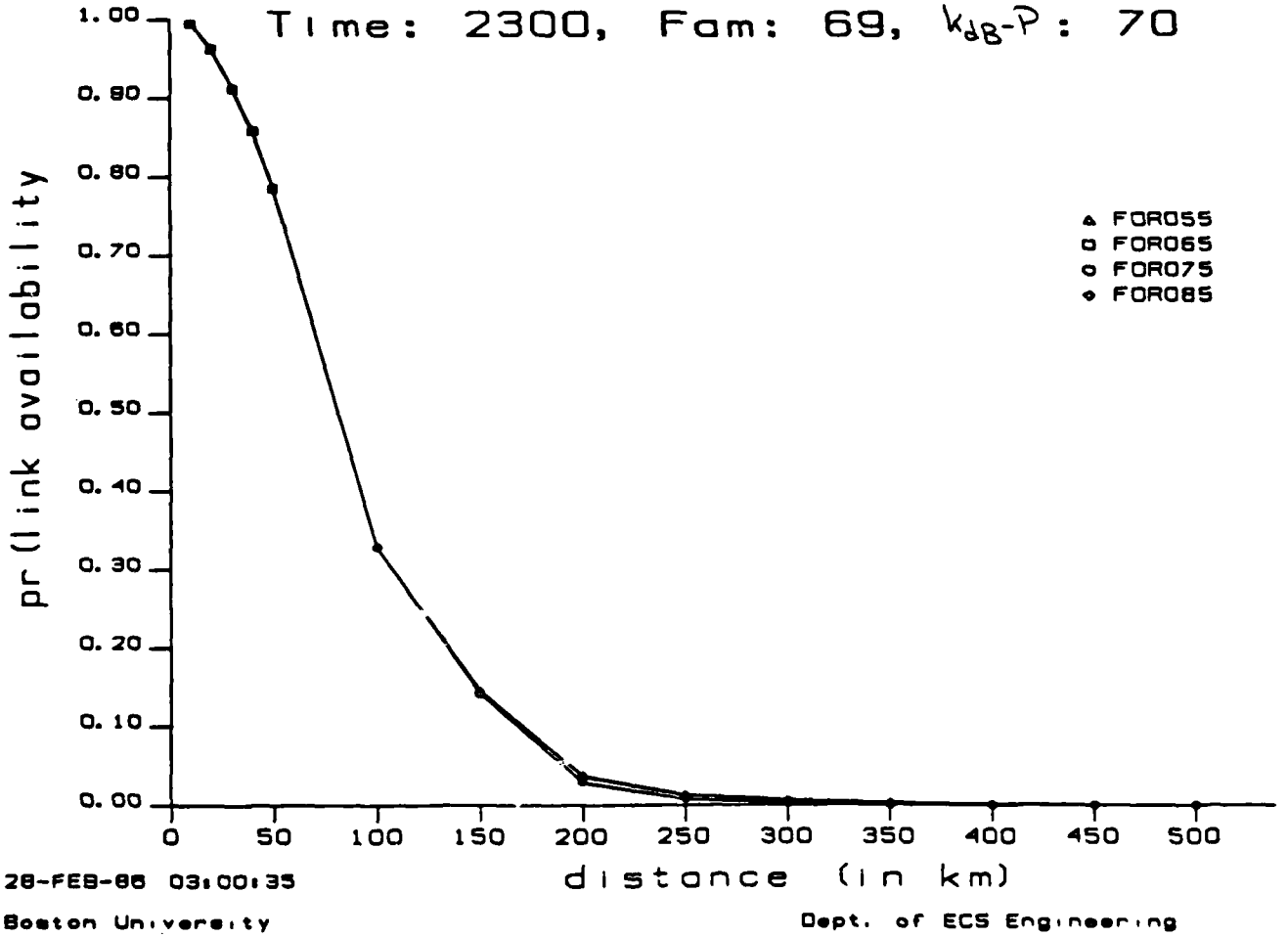

Figure 3.18: Pr(Link Availability) for 2300 hr, F_{am} = 69, and $k_{dB} - P = 70$

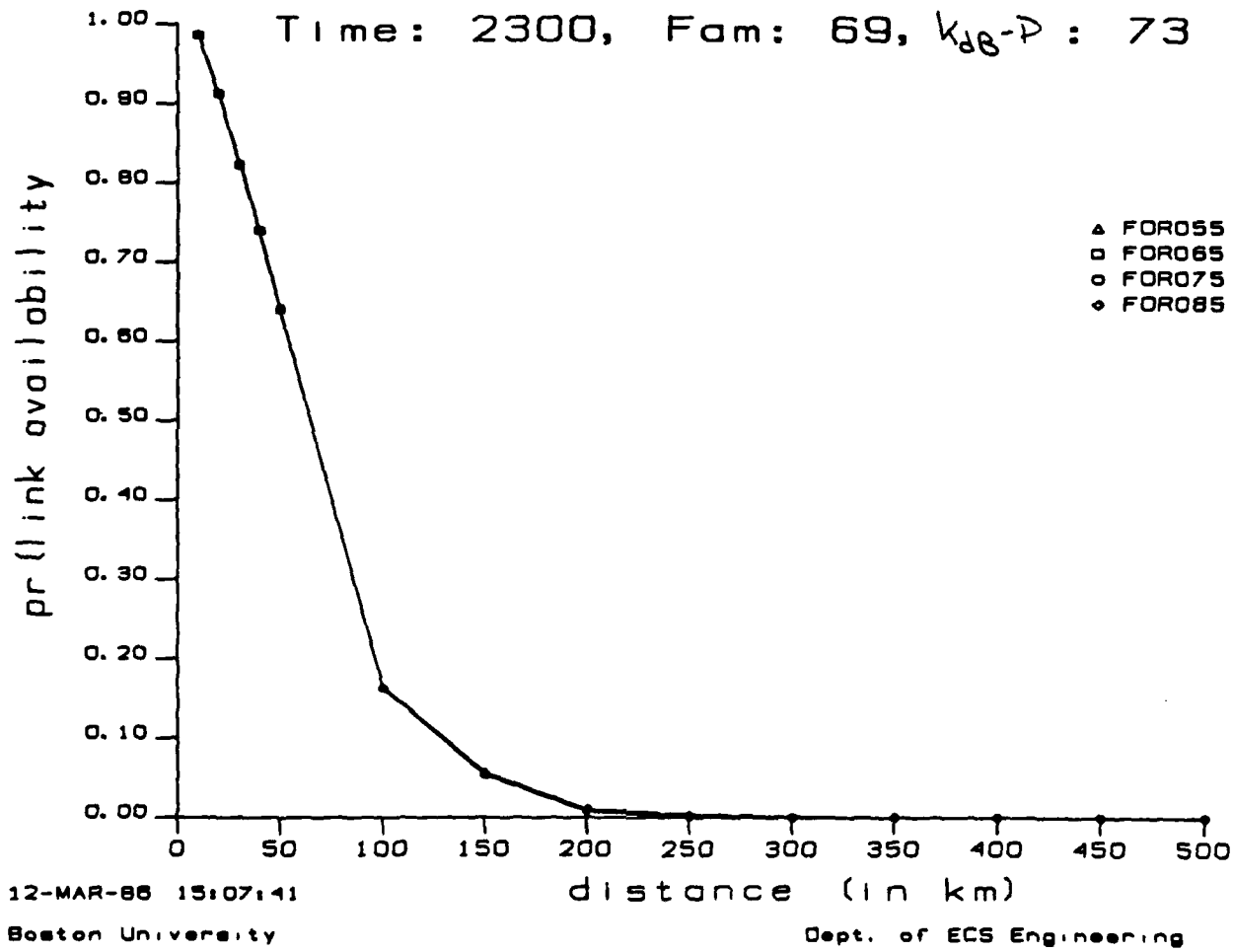

Figure 3.19: Pr(Link Availability) for 2300 hr, $F_{am} = 69$, and $k_{dB} - P = 73$

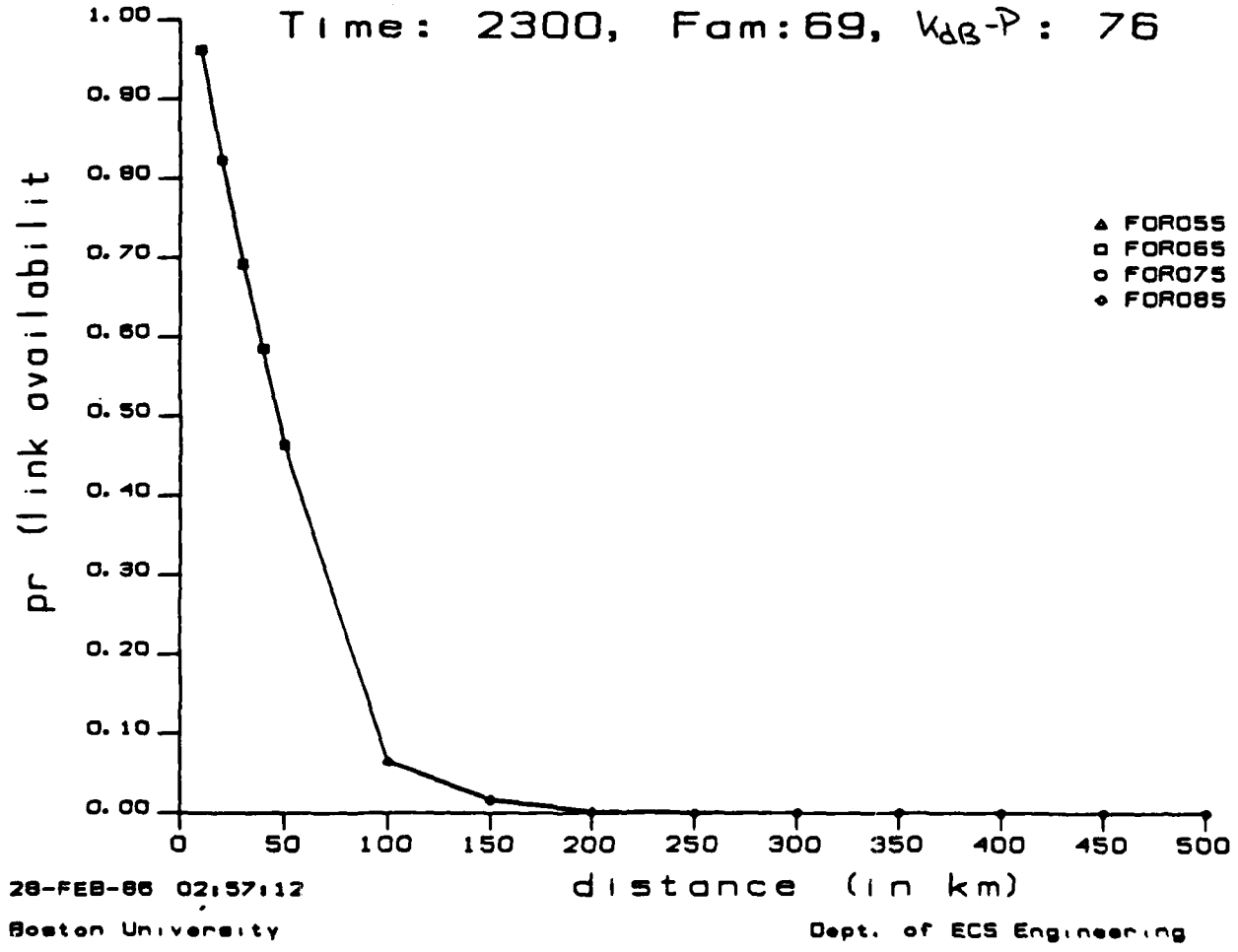

Figure 3.20: Pr(Link Availability) for 2300 hr. F_{am} = 69, and k_{dB} - P = 76

3.5 Numerical Results and Discussion

The main results of Chapter 3 are given in Table 3.1, which shows the range to which a link will be available with probability 0.90 under "worst case" conditions in Boston, Massachusetts. In Boston, worst case conditions occur summer nights near midnight, because the mean atmospheric noise power is greatest and skywaves are strongest. Table 3.1 gives the 90 percent range for no coding, the rate 1/2 (v=6) and rate 2/3 (v=6) codes. As shown, the uncoded system performs very poorly when the noise power is high. However, the coded systems have much greater operating ranges. Remember, atmospheric noise power is very variable and most of the time any of the systems will have much greater ranges.

Table 3.1: Beacon Ranges with and without Coding

	10 nautical mile beacon		30 nautical mile beacon	
	$k_{dB} - P$	Range	$k_{dB} - P$	Range
No Coding				
Limiter	84 (dB)	$\leq 10km$	75 (dB)	15 (km)
Clipper	84	$\leq 10km$	75	15
Rate 1/2, v=6				
Limiter	59	100	50	195
Clipper	58	110	49	210
Rate 2/3, v=6				
Limiter	65	55	56	130
Clipper	66	50	57	120

The table was derived using the following procedure.

1. The required signal to noise ratio for $Pr(\epsilon) \leq 10^{-5}$ is determined for hard limiters and clippers from Figures 3.4 through 3.9. For hard limiters, these SNRs are 28, 9, and 3 dB for no coding, rate 2/3 coding and rate 1/2 coding. For clippers these SNRs are 28, 10, and 2 dB. To these values we add a 3 dB "pad" to account for departures from the ideal conditions used in the analysis. These required SNRs are represented as k_{dB} in equations (7) and (10).

2. The term P in equations (7) and (10) is the radiated power of the beacon relative to 1kW. The radiated power of a beacon is indirectly specified. A "30 nautical mile" beacon produces a field of $50\mu V/m$ at a range of 30 nm over seawater. A "10 nautical

mile" beacon produces $50\mu V/m$ at 10 nm. In general,

$$P_R(Watts) = \frac{E(mV/m)d(nm)}{9.5 \times 10^3}$$

Using this relation, we find that a 30 nm beacon radiates -41dB relative to 1kW, and a 10 nm beacon radiates -50dB relative to 1kW. From these values, we subtract 3 dB, because the DGPS subcarrier contains 3dB less power than the main carrier. Hence, we have $P = -53$ and -44 for the two beacons.

3. At this point, values for $k_{dB} - P$ can be computed for all combinations of coding, hard limiting versus clipping, and beacon power. These values are given in the above table. The ranges shown are derived from Figures 3.10 through 3.20 where we have used the Figure for the closest possible value of $k_{dB} - P$

3.6 Channel Memory

3.6.1 General

In this subsection, we address the memory associated with any atmospheric noise channel and its effect on the DGPS link. Some wideband atmospheric noise traces are shown in Figure 3.21 ([8]). As shown, a single spike arises from the fields generated by a single lightning stroke. Several additional strokes occurring approximately 50 milliseconds apart may accompany a main stroke and generate a sequence of spikes. Repeated strokes are called multiple discharges and have been observed to consist of 20-30 strokes lasting for fractions of a second. These multiple discharges give rise to channel memory, because the channel "remembers" that a stroke has just occurred and is more likely to provide another stroke. This situation contrasts with a random error channel, where the probability of a stroke in a given interval does not depend on whether or not a stroke has occurred recently.

Most importantly, a code which performs well on a random error channel may perform very poorly on a burst error channel. To illustrate this point, consider an example, based on a simple random error process and a simple burst error process. Both processes are discrete state and discrete time processes. More specifically, they are either "on" or "off" and they change state only at the beginning of a channel symbol. Both processes cause symbol errors with probability one if they are on. However, the random error process can change state every symbol interval and its state is independent from symbol to symbol. The probability of the random error process being on is b_r. The burst error process turns on at the beginning of a symbol interval with probability b_b and if it turns on, then it stays on for 3 symbols.

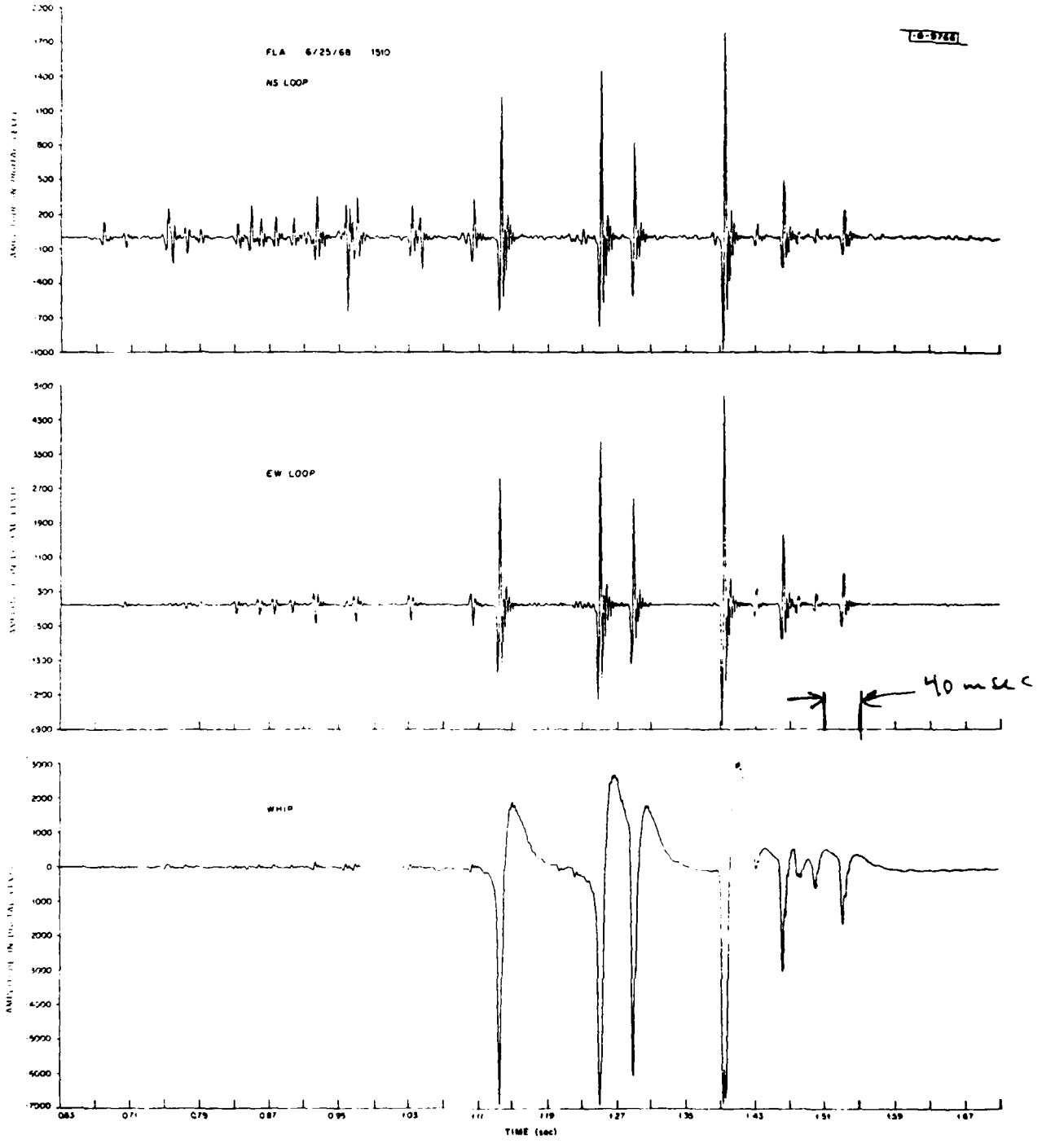

Figure 3.21: ELF Waveforms Recorded in Florida (June 1968)

These 2 processes have very different effects on the performance of a rate 1/5 repetition code. The random error process will cause a data bit error if 3 or more symbols are in error.

$$Pr(\epsilon) = 10b_r^3 a_r^2 + 5b_r^4 a_r + b_r^5$$

where $a_r = 1 - b_r$. However, for the burst error process

$$Pr(\epsilon) = \frac{a_b}{3b_b + a_b}[1 - a_b^2] + \frac{b_b}{3b_b + a_b}[1 + 2(1 - a_b^3)]$$

where $a_b = 1 - b_b$. These 2 expressions are compared in Figure 3.22 where we have normalized the proceses such that they have equal duty cycle. As shown, the burst error process causes bit error with probability approximately equal to b_r. In contrast, if b_r is reasonably small, then the random error process causes many fewer errors. The burst error process is much more destructive, because it prevents the code from "averaging" the effect of the noise. If a single burst occurs, then it overwhelms the correcting capability of the code.

The following two techniques are available to combat burst error processes

- burst error correcting codes
- interleaving

Burst error correcting codes have been designed and shown to be effective in [2] and [10]. However these codes are not robust, which means that they perform poorly if the burst statistics are not accurately known. Interleaving is a much more robust technique and we now describe it.

3.6.2 Interleaving

Interleavers separate symbols, which are decoded together, by an amount of time equal to the maximum burst duration. In other words, they separate the N codeword symbols in a given decoding span by at least B seconds, where B is the maximum burst duration. The intervening spaces are filled by symbols from other decoding spans, which are similarly spaced. A minimum delay/minimum storage interleaver is shown in Figure 3.23, which also shows the DGPS channel and the corresponding deinterleaver ([14]). If the interleaver input sequence is

$$v_i, v_{i+1}, v_{i+2} \cdots$$

then the transmitted sequence will be

$$v_i, v_{i-J}, v_{i-2J}, \ldots v_{i-(I-1)J}, v_{i-I}, v_{i+1-J} \cdots$$

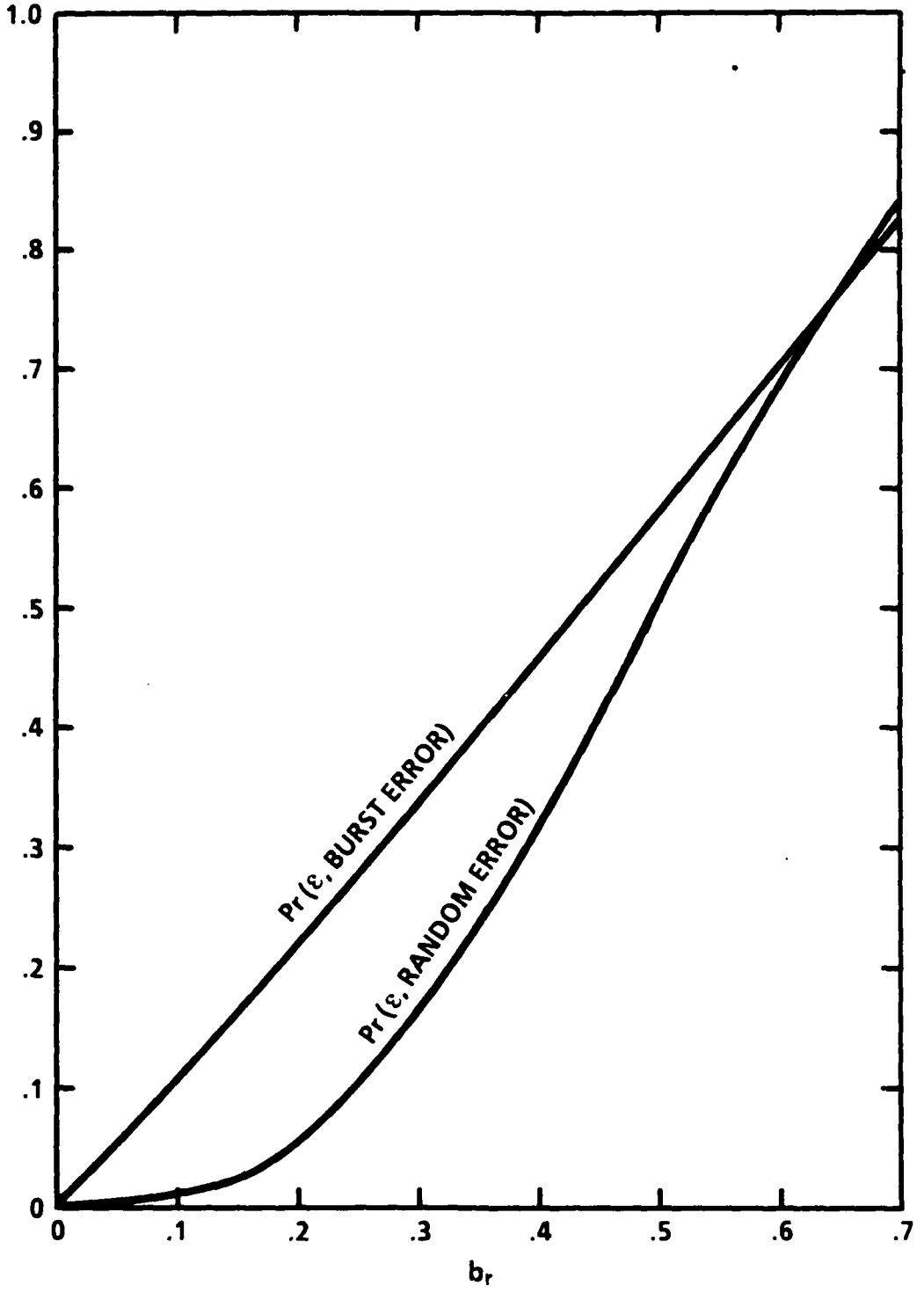

Figure 3.22: Pr(Bit Error) vs. Burst Error and Random Error Processes

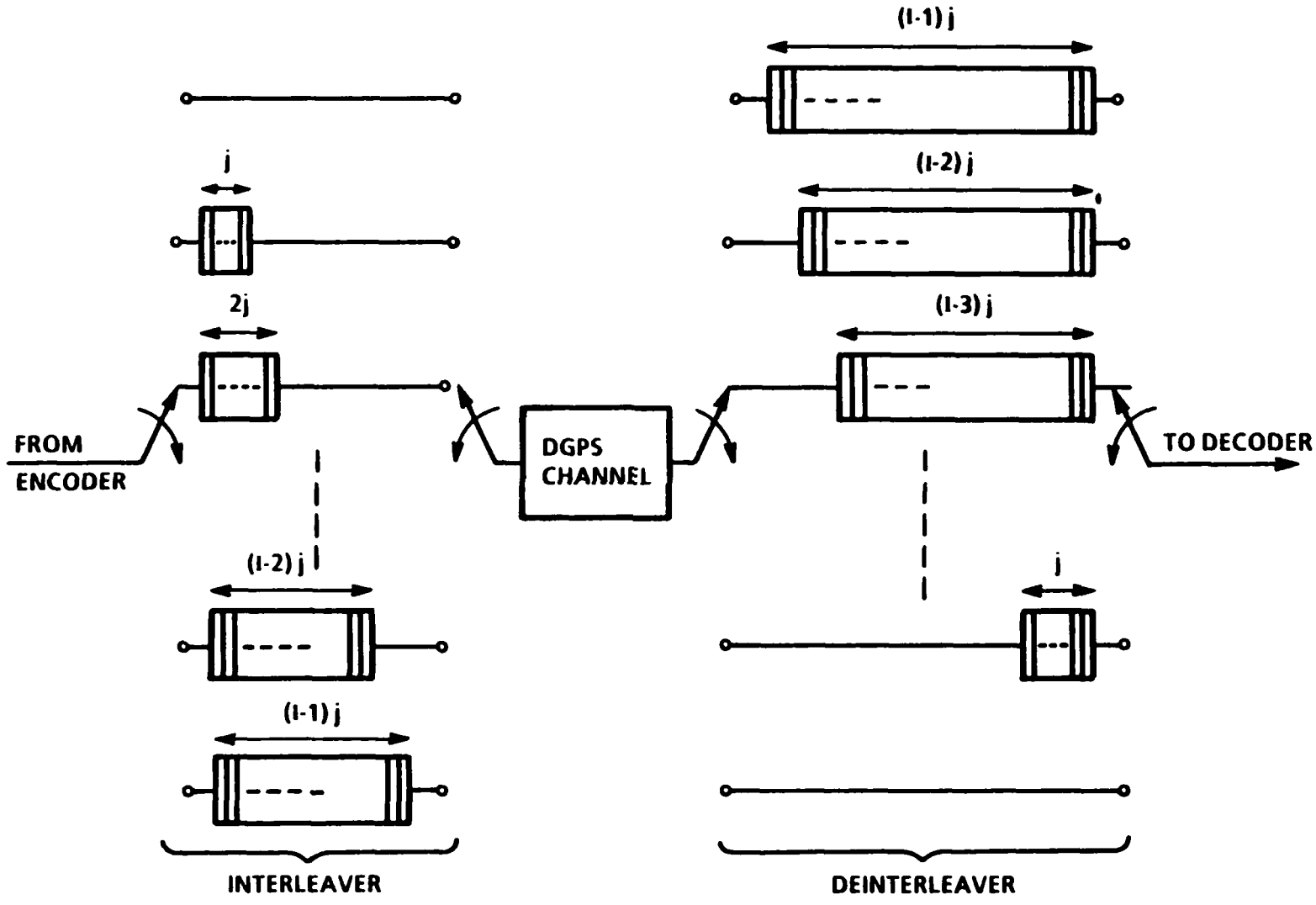

Figure 3.23: Interleaving Technique for Memory Elimination

If input symbols have separation less than $J = jI$, then they will have minimum channel transmission separation of I. Consequently, the interleaver of Figure 3.23 is known as a (I, J) interleaver. We should select J and I such that all symbols which are decoded together will be separated by B seconds. Consequently, J should be at least equal to the codeword length if block codes are used or the "decoding span" if convolutional codes are used. I should be equal to the maximum burst length in channel symbols (B/T_c).

The delay introduced by this (I, J) interleaver is $J(I-1)T_c$ or approximately NB, where N is either codeword length or decoding span. To determine delay, we need values for N and B and we now consider those topics in turn.

3.6.3 Decoding Span (N)

The decoding span of a convolutional code depends on the constraint length of the code and the type of decoder used. There are 3 classes of convolutional decoders.

- Viterbi decoding
- syndrome decoding
- sequential decoding

The decoding span for Viterbi decoders may be estimated using the following rules of thumb. If the code has $R = 1/2$ and constraint length equal to v, then $N = 5v/R$ channel symbols. If the code has $R = 2/3$, then $N = 8v/R$ channel symbols and if $R = 3/4$, then $N = 10v/R$.

Syndrome decoders can have much shorter decoding spans, but achieve this reduction by sacrificing some of their error correcting capability. This tradeoff will be investigated in Technical Task No. 2.

Sequential decoders are generally used with codes which have much greater constraint lengths ($v \geq 20$) than the codes considered in this Report. Nonetheless, they will be studied in Technical Task No. 2.

3.6.4 Atmospheric Burst Duration (B)

Atmospheric burst duration has been measured by [8], [9], and [11], and in this subsection we summarize the observations made by J. Evans ([8]). Evans defined x as the length of the interval between bursts and used noise data from Florida to compute

- the sample probability density function of x $(p_X(x))$
- the sample "survivor function" of x $(R(x))$. $R(x)$ is the fraction of burst intervals greater than x. So $R(x) = \int_x^\infty p_X(u)du$

- the sample hazard function $H(x) = p_X(x) / R(x)$

The hazard function is also known as failure rate, age-specific failure rate, or force of mortality. It is useful, because $H(x)dx$ is the probability of a spike in the next dx seconds given that the last spike was x seconds ago. Alternatively, $H(x)dx$ is the probability of a burst interval between x and $x + dx$, given that the interval is at least x. For a Poisson process, which has independent increments $H(x) = \lambda$, where λ is the average arrival rate of the process. In other words, if the atmospheric noise channel had no memory, then its hazard function would be constant. In reality, its hazard function will decrease to some constant only after its memory lapses.

Figures 3.24 and 3.25 show atmospheric noise hazard functions measured by Evans. As shown, all measurements decrease to nearly constant behavior after 0.2 seconds. Consequently, we take $B = 0.2$ seconds for the remainder of this Report. However, more data on atmospheric noise burst duration will be sought under Technical Task No. 2.

3.6.5 Data Delay

Using the relation $delay = NB$ seconds and the results of the previous two subsections, we can compute the delay of a DGPS link using

- the interleaver of Figure 3.23
- convolutional codes at rates 1/2, and 2/3 and any constraint length
- Viterbi decoding

The resulting data latency is shown in Table 3.2.

Table 3.2: Data Latency

constraint length	rate (sec)	
	1/2	2/3
2	4	4.8
3	6	7.2
4	8	9.6
5	10	12.0
6	12	14.4

If data latency greater than 5 seconds cannot be tolerated, then only the smallest constraint lengths can be used. The codes with constraint length 2 will not perform as well as the codes analyzed earlier, which had constraint length 6. Consequently, we will continue to investigate channel memory under Technical Task No. 2.

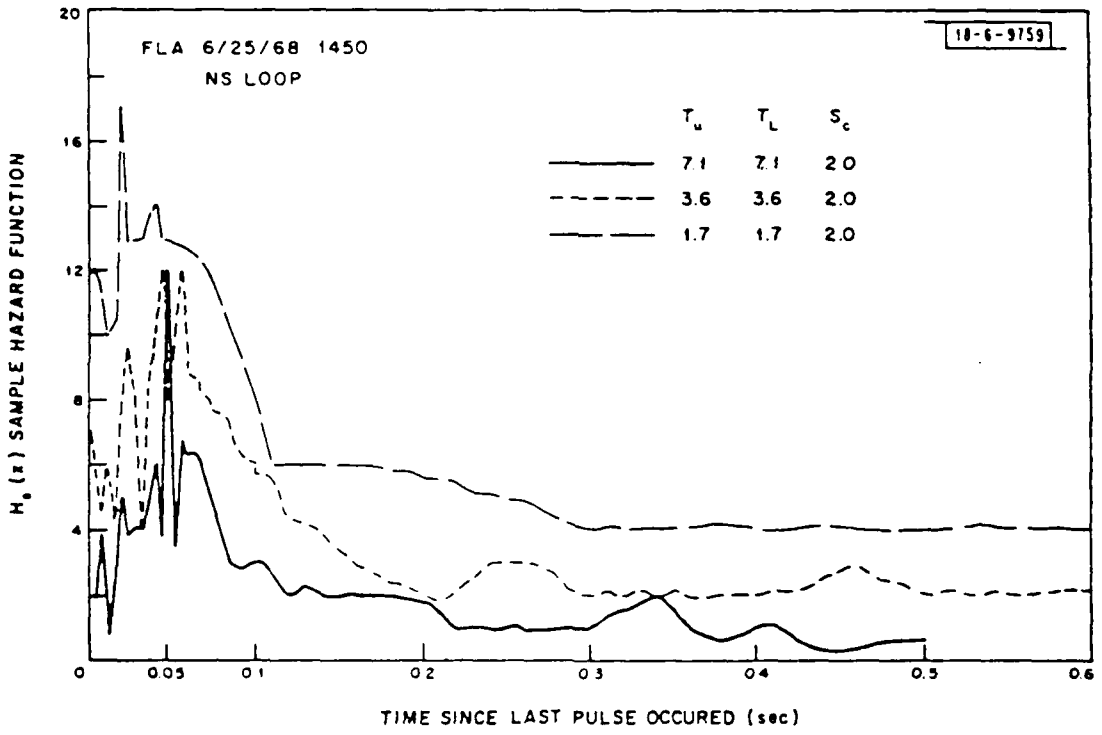

Figure 3.24: Hazard Function of Interburst Interval for Various Criteria (Florida, June 1968)

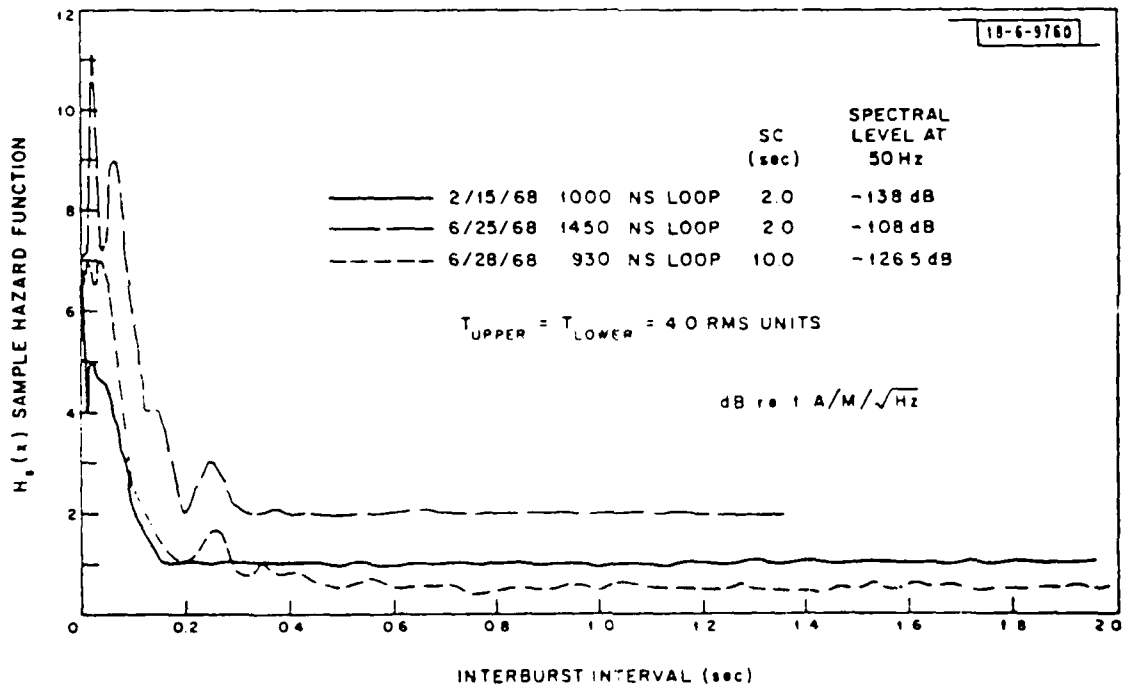

Figure 3.25: Hazard Function of Interburst Interval for Various Florida Data

Bibliography

[1] H. Akima, "A Method of Numerical Representation for the Amplitude Probability Distribution of Atmospheric Radio Noise," U.S. Dept. of Commerce, Office of Telecommunications, OT/TRER 27, 1972

[2] K. Brayer, "Error Correcting Code Performance on HF, Troposcatter, and Satellite Channels," IEEE Trans. on Commun. Tech., vol COM-19, pp 835-848

[3] CCIR, "XIth Plenary Assembly Oslo, Vol II: Propagation," International Telecommunication Union (ITU), Geneva, 1966, pp 42-51

[4] CCIR (International Radio Consultative Committee) Report 322, "World Distribution and Characteristics of Atmospheric Radio Noise," International Telecommunication Union (ITU), Geneva, 1964

[5] CCIR Recommendation 435-3, "Prediction of Sky-Wave Field Strength Between 150 and 1600 kHz," ITU, Geneva, 1978

[6] CCIR Report 575-1, "Methods for Predicting Sky-Wave Field Strengths at Frequencies Between 150 kHz and 1600 kHz," ITU, Geneva, 1978

[7] G.C. Clark and J.B. Cain, "Error Correction Coding for Digital Communication," Plenum, New York, 1981

[8] J.E. Evans, "Preliminary Analysis of ELF Noise," Lincoln Laboratory Technical Note 1969-18, March 1969

[9] S. Gupta, "Short Term Time Characteristics of Atmospheric Radio Noise Above Different Thresholds," IEEE Trans. EMC, vol. EMC-13, No. 4, Nov. 1971

[10] A. Kohlenberg, and G. Forney, "Convolutional Coding for Channels with Memory," IEEE Trans. Info. Theory, vol. IT-14, pp 616-626

[11] E.T. Pierce, "Atmospherics - Their Characteristics at the Source and Propagation," Radio Noise of Terrestrial Origins, Part IV, URSI Record Elsevier Publishing Co., Amsterdam

[12] A.D. Spaulding, "Determination of Error Rates for Narrowband Communication of Binary Coded Messages in Atmospheric Radio Noise," Proceedings of the IEEE, Feb. 1964, pp 220-221

[13] A.D. Spaulding and J.S. Washburn, "Atmospheric Radio Noise: Worldwide Levels and Other Characteristics," National Telecommunications and Information Administration, NTIA Report 85-173

[14] A.J. Viterbi and J.K. Omura, "Principles of Digital Communication and Coding," McGraw-Hill, New York, 1979

[15] S. Pasupathy, "MSK: A Spectrally Efficient Modulation," IEEE Comm. Soc. Mag., Vol. 17, No. 4, pp 14-22, July 1979

[16] S. A. Gronmeyer and A. L. McBride, "MSK and Offset QPSK Modulation," IEEE Trans. on Comm., Vol. COm-24, No. 8, Aug. 1976, pp 809- 819

[17] D.H. Morais and K. Feher, "Bandwidth Efficiency and Probability of Error Performance of MSK and Offset QPSK Systems," IEEE Trans. on Comm., Vol. COM-27, No. 12, Dec. 1, pp 1794-1801.

[18] F.M. Gardner, "Phaselock Techniques," John Wiley and Sons, NY, NY, 1979

[19] J.G. Proakis, "Digital Communications," McGraw-Hill Book Co., NY, NY, 1983.

[20] V. Del Toro, "Electromechanical Devices for Energy Conversion and Control Systems," Prentice-Hall, Englewood Cliffs, NJ 1968.

160 Copies

END

DTIC

8-86